Canadä

Communications Research Centre

MODELLING AND IDENTIFICATION OF THE STRUCTURAL PROPERTIES OF AN ASTROMAST

by

Y. SOUCY AND F. VIGNERON

CRC REPORT NO. 1374

TK
5102.5
C673e
#1374

IC

ernment of Canada
artment of Communications

Gouvernement du Canada
Ministère des Communications

OTTAWA, NOVEMBER 1983

COMMUNICATIONS RESEARCH CENTRE

DEPARTMENT OF COMMUNICATIONS
CANADA

MODELING AND IDENTIFICATION
OF THE
STRUCTURAL PROPERTIES OF AN ASTROMAST

by

Y. Soucy and F. Vigneron

(Space Technology and Applications Branch)

Industry Canada
Library - Queen

AOUT
AUG 2 7 2012

Industrie Canada
Bibliothèque - Queen

CRC REPORT NO. 1374

November 1983
OTTAWA

CAUTION
This information is furnished with the express understanding that:
Proprietary and patent rights will be protected.

COMMUNICATIONS CANADA
CRC
JAN 10 1985
LIBRARY — BIBLIOTHÈQUE

TK
5102.5
C673e
#1374
c.b

DD 5106336
DL 5114660

TABLE OF CONTENTS

- ABSTRACT 1
- 1.0 INTRODUCTION 3
- 2.0 DESCRIPTION OF THE ASTROMAST 5
- 3.0 CALCULATIONS OF DYNAMIC CHARACTERISTICS BY THE FINITE ELEMENT METHOD 9
- 4.0 STRUCTURAL DYNAMIC TEST METHODS AND RESULTS 13
  - 4.1 General Remarks 13
  - 4.2 Modal Parameter Identification Software 13
  - 4.3 Base Excitation with Large Electrodynamic Exciter 18
    - 4.3.1 The Test Configuration 19
    - 4.3.2 Instrumentation 19
    - 4.3.3 Exciter Inputs and Control 23
    - 4.3.4 Modal Parameter Estimation 27
    - 4.3.5 Exploratory Tests 28
      - 4.3.5.1 Effect of Accelerometers 28
      - 4.3.5.2 Non-Linearity of the Astromast 32
    - 4.3.6 Test Results 40
      - 4.3.6.1 Sine Sweep Input 40
      - 4.3.6.2 Random Input 46
  - 4.4 Tests in Air and Vacuum with the Hydraulic Exciter 52
    - 4.4.1 Description of Test Configuration 52
    - 4.4.2 Test Results 52
    - 4.4.3 Discussion 58
  - 4.5 Impact Test in Torsion 63
    - 4.5.1 Test Configuration 64
    - 4.5.2 Test Results 64
  - 4.6 The Step Relaxation Method 69
    - 4.6.1 Concept and Configuration 70
    - 4.6.2 Data Acquisition and Results 76
  - 4.7 Summary of Frequencies on Damping Values From Tests 76
- 5.0 STATIC TESTS IN TORSION AND BENDING 79
  - 5.1 Test Set-Ups and Procedures 79
  - 5.2 Test Results 81
- 6.0 COMPARISON OF EXPERIMENTAL AND THEORETICAL VALUES 87
- 7.0 DISCUSSION AND CONCLUSIONS 91
- 8.0 ACKNOWLEDGEMENTS 92
- 9.0 BIBLIOGRAPHY 93

COMMUNICATIONS CANADA
CRC
JAN 10 1985
LIBRARY – BIBLIOTHÈQUE

ABSTRACT

This report describes analytical modeling and identification of static and dynamic (modal) parameters for an Astromast.

The fundamental bending modes in the X and Y directions, three higher order transverse bending modes, and two modes in torsion, were identified in tests in the frequency range 1.8 to 46 Hz. The associated damping factors range between 1.2 and 8.5 percent. The factors associated with the fundamental bending and torsion modes were found to be the same in vacuum and in air. No single configuration and technique was able to identify all of the modes; techniques involving base excitation with an electrodynamic exciter, base excitation with a hydraulic exciter, impact and step relaxation techniques were needed. The MODAL-PLUS software of the Structural Dynamics Research Corporation was used for parameter identification. It was observed to support impact and step relaxation testing fully, but to have limitations for the base excitation methods.

The experimentally-identified modal frequencies were compared with results produced by a finite element model and a continuum model. With bending and torsional stiffness derived from static tests as input parameters, the continuum model produces torsional and bending frequencies that agree within 25% for first bending and first two torsion modes, and are 40-95% in error for higher modes. It is concluded that a continuum model is acceptable for fundamental modes, but is overly simplistic for higher modes. The finite element model results agree with measured values within 12% for the lowest two modes in bending, but agreement is unsatisfactory in torsion and for the higher bending modes. The modeling deficiencies are believed to be due to an oversimplification in the longeron element modeling.

1.0 INTRODUCTION

A number of space projects during the coming decade will use large lightweight deployable lattice-type structures as masts, beams, or trusses, for antennas, solar arrays, and other structures. This type of structure is not yet in wide use, and consequently there is little published information or experience with actual hardware. This report describes test and modeling experience for a representative structure of this type.

The structure involved is a deployable, coilable, continuous longeron mast, manufactured by Astro Research Corporation under the trade name Astromast. Figures 1 and 2 illustrate the structure. Astromasts of this type are part of the European LSAT satellite to be launched in 1986, and are part of the baseline design of the Canadian MSAT and RADARSAT satellites.

The work described in this report has the following contribution:

- Experience with several modal techniques used to test this particular lightweight structure is described. The operation of the commercially available SDRC MODAL-PLUS software is demonstrated.

- Values of modal damping factors for the Astromast are obtained in air and in vacuum.

- Static tests that determine the overall bending and torsional stiffness are described.

- Two analytical models are described, a finite element model, and a simple equivalent continuum beam model. The degree of accuracy of these types of models is demonstrated by comparing analytically-derived modal frequencies and mode shapes with corresponding measured values.

2.0 DESCRIPTION OF THE ASTROMAST

In 1982, the Dynamics Group of the Space Mechanics Directorate purchased a 7.6 meter Astromast as a candidate large flexible structure for test. In July 1982, during preparation for a static test, one of the longeron bucked at about 1.5 meter from one end. The mast was repaired by removing 2 bays, thus producing two structures with lengths of 1.5 and 6 meters. The tests described in this report were done on the 6 meter Astromast. The main dimensions are given in Figure 3. The Astromast is composed of 42 storeys or bays and has a helical rotation of 93° from one end to the other for reduction of in-space solar-induced thermal deformation. Figure 4 is a close-up showing the longerons, diagonals, and battens. The buckled state of the battens creates the rigidity of the structure by producing compression in the longerons and tension in the diagonals. The diameter of the mast, defined as the diameter of the circle passing through the connectors, is 229 mm. The design bending moment as given by Astro, is 23.7 N-m [1]. The weight of the boom is 0.23 kg/m. Thus the structure has a high stiffness to weight ratio.

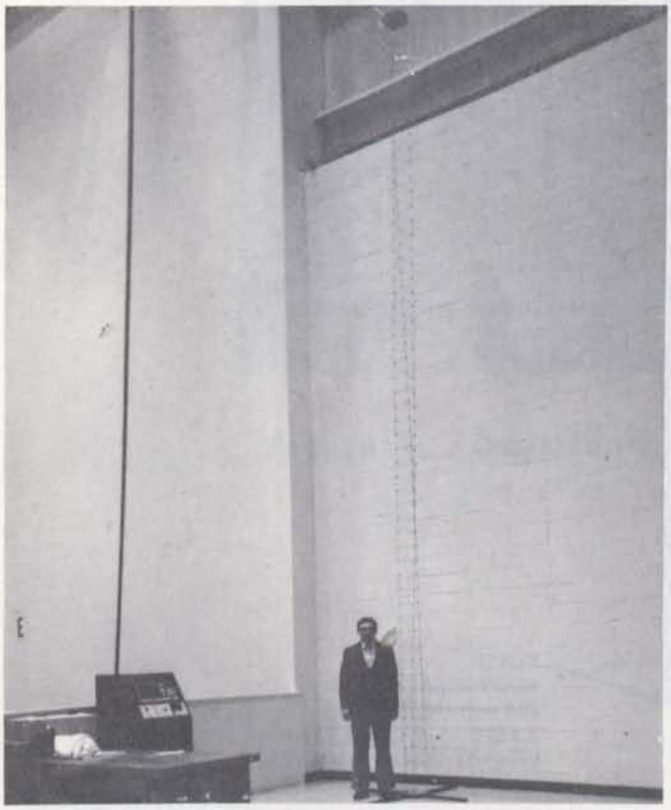

Figure 1. 7.6 Meter CRC Astromast in Fully Deployed State

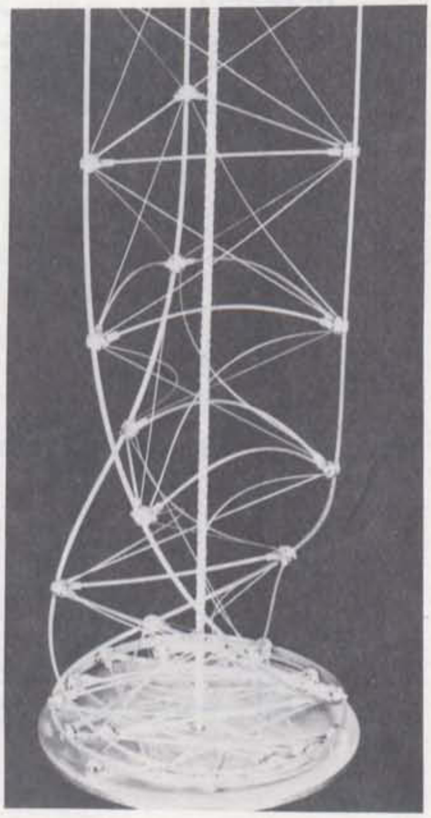

Figure 2. Astromast in Deploying State

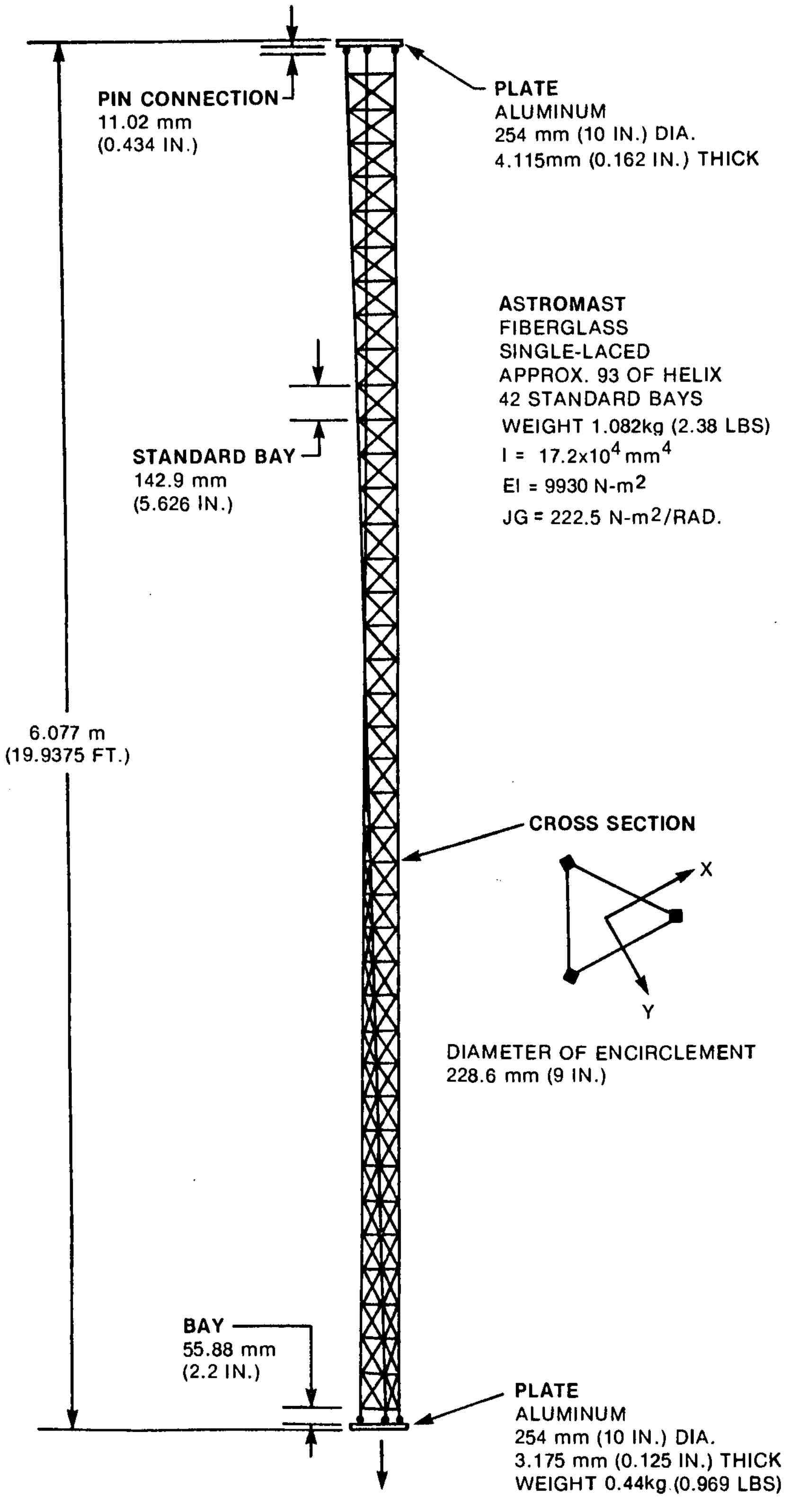

Figure 3. Schematic of the 6 Meter Astromast

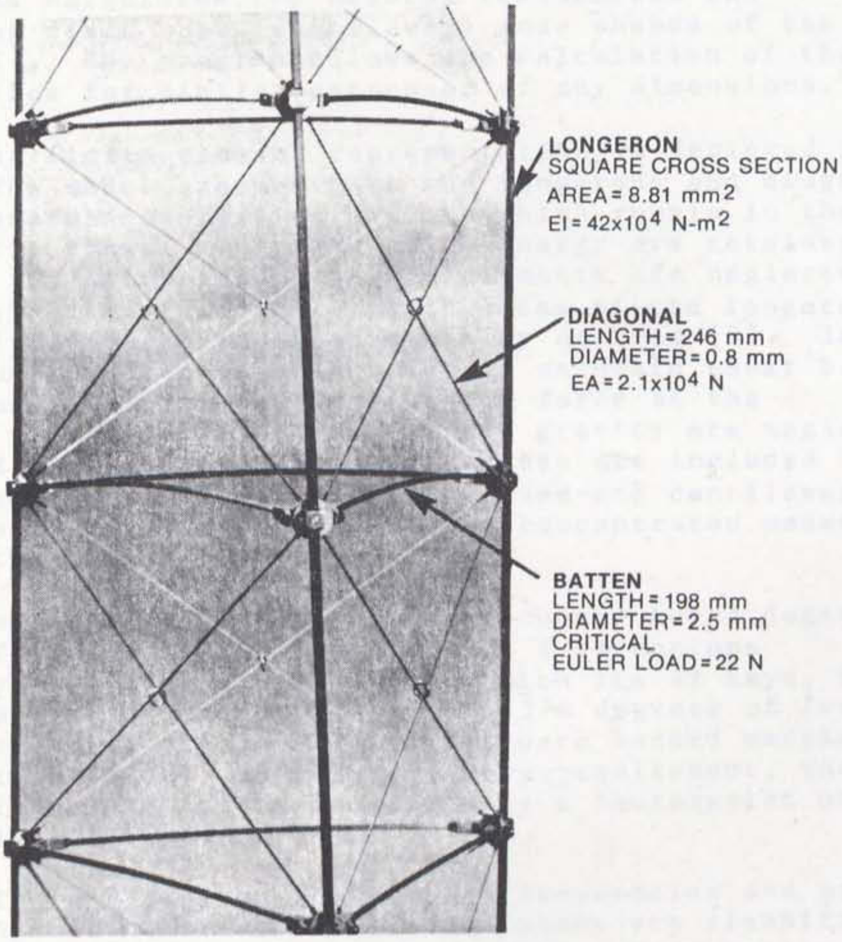

Figure 4. Components of the Astromast

3.0 CALCULATIONS OF DYNAMIC CHARACTERISTICS BY THE FINITE ELEMENT METHOD

A finite element program developed at the Université de Sherbrooke calculates the natural frequencies and corresponding fixed base (cantilever) mode shapes of the Astromast [2]. The program allows the calculation of these characteristics for similar astromast of any dimensions.

The finite element representation is depicted in Figure 5. The model assumes that the longerons and diagonals are axial tension/compression members which remain in their linear elastic range. Only the axial energy are retained, and the bending and twist energy of the elements are neglected. The input values for the axial stiffnesses of the longerons and diagonal elements are experimentally derived [3]. It is further assumed that the battens always maintain their buckled state and thus exert a constant tension force at the connectors. The effects of damping and gravity are neglected. The mass and inertia of only one end plate are included in the modelling, as is consistent with the fixed-end cantilever configuration. The mass is modeled by concentrated masses located at the joints.

The finite element program accounts for 3 degrees of freedom (DOF) per joint in the X, Y and Z directions respectively, or 9 DOF for each bay. With its 42 bays, the 6 meter Astromast is then represented by 378 degrees of freedom. The stiffness matrix is an 378 X 378 square banded matrix with half-band width of 18. To reduce memory requirement, the program replaces the stiffness matrix by a rectangular one with dimensions 378 X 18.

Figure 6 depicts the natural frequencies and mode shapes of the first twelve modes. The modes are classified into three categories: transverse bending - X direction, transverse bending - Y direction, and torsion. It is observed that the bending modes are the same in the X and Y directions. This is explained from simple strength-of-materials beam theory as follows; for any cross-section of the mast, the moment of inertia is the same in all directions, and this implies that the stiffness is the same in the X and Y directions; consequently, the natural frequencies and corresponding mode shapes are the same in two principle directions. The triangles on the structure represent the levels at which the accelerometers were put during the tests described later. Besides looking at the overall deformed shapes, a way to distinguish between bending and torsion modes is to observe that the deformation of the upper triangle is translation for bending and rotation for torsion.

The first five modes appear to be either pure bending or pure torsion. The second and higher torsion modes exhibit a "breathing" characteristic, that is an extension of some battens or sides of triangles. This phenomenon can be explained by the fact that the post-buckled battens admit small axial displacements. The third and higher bending modes have, with different intensity, some coupling with torsion; as is evidenced by a change in shape of the top triangle.

The program also computes extraneous modes that do not exist for the real structure (Figure 7). Five of them appear in the interval 0 to 60 Hz. The model yields these modes because the continuous longerons are modeled by pinned axial elements at each bay with no bending resistance accounted for. The energy associated with the bending of the longerons becomes more significant as the order of the mode increases, and hence the difference between the real structure and the model would be expected to be greater for the higher order modes.

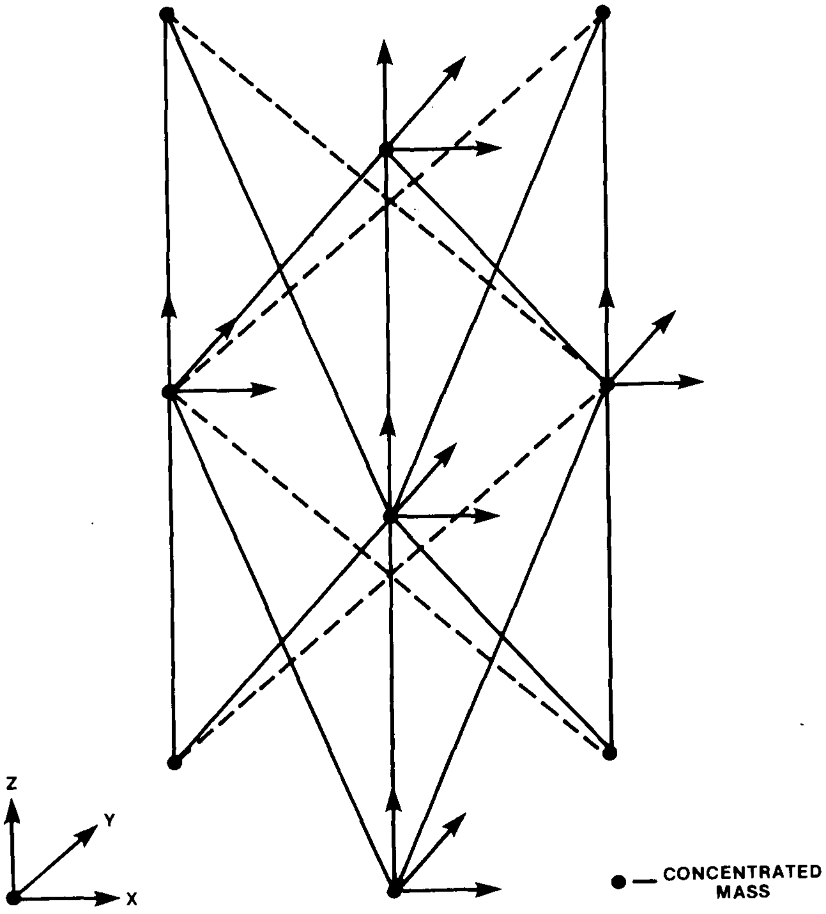

Figure 5. Finite Element Modeling

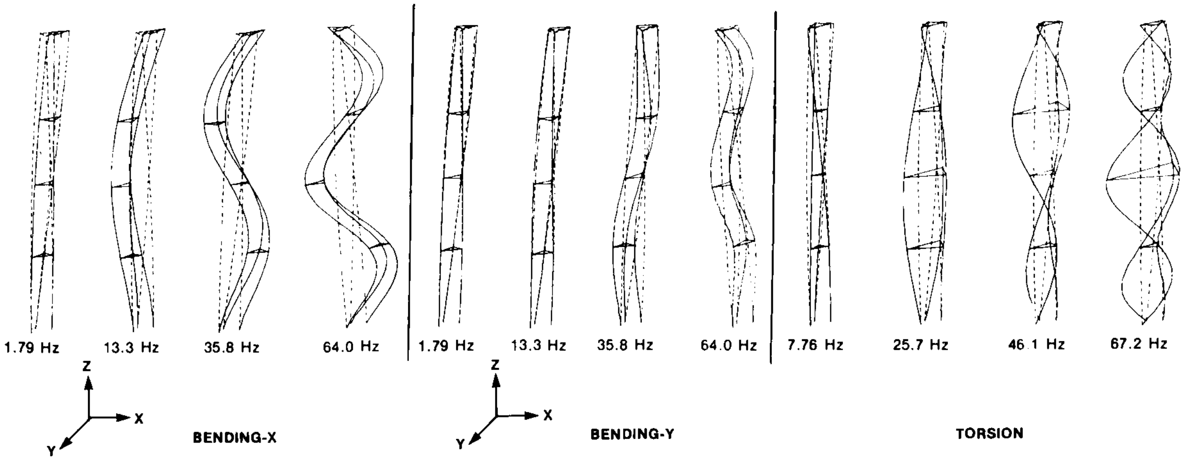

Figure 6. Mode Shapes and Frequencies from Finite Element Program

Figure 7. Example of Extraneous Mode

4.0 STRUCTURAL DYNAMIC TEST METHODS AND RESULTS

4.1 General Remarks

Because the structure is flexible, lightweight, has low damping and a wide range of resonant frequencies of interest, no single test configuration and hardware setup was found capable of providing all of the desired results. As there was a concern that aerodynamic effects might alter damping values, it was felt essential to do some of the tests in a vacuum. Four basic test configurations were ultimately used to obtain the full range of results: (a) tests in air with unidirectional translation input at the base of the structure with an electrodynamic exciter, 5-100 Hz; (b) tests in vacuum and in air similar to (a), but with a hydraulic exciter, 1.0-30 Hz; (c) step relaxation tests, 0 to 10 Hz; (d) impact tests, to confirm a torsion mode at about 30 Hz. Tests with point force excitation (i.e. applied with small portable exciters) were not attempted because impedance mismatch problems were expected to be severe. The test timetable and other information are given in Table 1.

4.2 Modal Parameter Identification Software

The modal parameter identification and associated data acquisition software, namely SDRC's MODAL-PLUS and DATM software, were used for the four test configurations to be described in the later sections and are described briefly in the following. A more complete description is available in Refs. 4 and 5.

During a test in any of the four configurations, the input and output signals are stored on tape in analog form. Modal parameter identification is done subsequently off-line, with the data stored on the tape, using the Gen Rad 2503 system.

The Gen Rad 2503 system is depicted in Figure 8. The system consists of the following sections: a four channel analog data acquisition section; a digital processing section; a data display section; and an analog section to drive an exciter (Reference 6). In the parameter identification mode, the analog data acquisition section is used to acquire data from the tape, in conjunction with DATM which operates in the PDP 11/34. (The exciter control and Gen Rad spectral analysis software (ISAP) is not used in the parameter identification, but will be described in Chapter 4.3.)

TABLE 1 TIME TABLE OF ASTROMAST DYNAMIC TESTS

DATE	ENVIR	EXCITATION DIRECTION	EXCITER	EXCITATION TYPE	COMMENTS	STATUS
Nov 82	Ambient	Transverse At Base	Electrodynamic Shaker	Sine Sweep 5-100 Hz	Accels at 4 levels 6 accels per run	-Freq. & Damping factors obtained by MODAL-PLUS V6
Nov 82	Ambient	Transverse At Base	Electrodynamic Shaker	Random 5-100 Hz	Accels at 4 levels 6 accels per run	-Freq. & Damping factors obtained by MODAL-PLUS V6 -Mode shapes incomplete
Nov 82	Ambient	Transverse At Base	Electrodynamic Shaker	Sine Sweep 5-100 Hz	Effect of cables Accels at tip	-Effect proved
Nov 82	Ambient	Transverse At Base	Hydraulic Shaker	Sine Sweep 1-30 Hz	Accels at tip and mid-span	-Frequencies and approximate damping factors obtained by MODAL-PLUS V6
Nov 82	Ambient	Twist At Base	Hydraulic Shaker	Sine Sweep 1-30 Hz	Accels at tip and mid-span	
Nov 82	Ambient	Transverse At Base	Hydraulic Shaker	Random 1-30 Hz	Accels at tip	
Nov 82	Vacuum	Transverse At Base	Hydraulic Shaker	Sine Sweep 1-30 Hz	Accels at tip amd mid-span	
Jan 83	Ambient	Transverse At Base	Electrodynamic Shaker	Sine Sweep 5-100 Hz Random	Non-linearity	-Effect for sine sweep -No effect for random
Jan 83	Ambient	Transverse At Base	Electrodynamic Shaker	Random	Effect of accels	-Cables have no effect -masses produce slight shift
Jan 83	Ambient	Transverse At Base	Electrodynamic Shaker	Random	Accels at 4 levels 3 accels per run	-Frequencies and damping factors obtained -2nd and 3rd mode shapes obtained
Mar 83	Ambient	2 Tangent Directions	Step Relax.	0-20 Hz	Fundamental bending modes	-modes separated using polyreference
Sep 83	Ambient	Twist	Hammer	Impact test	2 accels and 4 impact locations	-2nd frequency and associated damping factor obtained

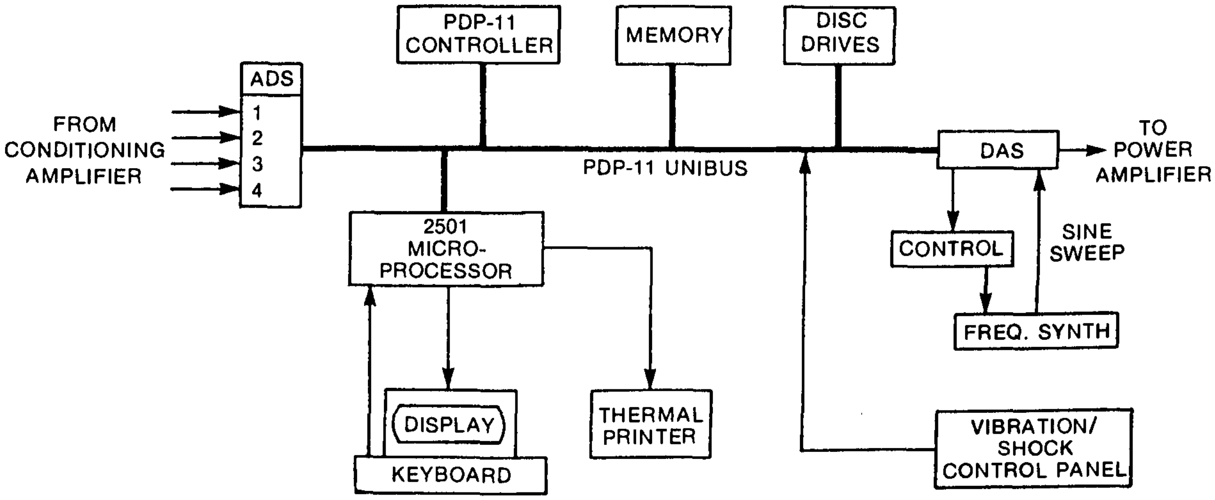

Figure 8. Gen Rad 2503 System

The configuration of the 2503 hardware system allows four input channels simultaneously. One of these channels is chosen by the user as the reference (input) and three others are the responses (output). DATM calculates simultaneously three frequency response functions (FRF's) and their associated coherence functions using Fast Fourier Transform algorithms. For each of the FRF's , the numerator and denominator power spectrum can be obtained. Additional functions and features of DATM follow:

- Setup data files to be used in the storage of acquired frequency response functions (FRF's)
- Zoom capability for higher resolution
- Allow the use of the display screen as limited oscilloscope
- Allow the calibration of data acquisition equipment setup
- Display acquired data using a variety of graphs, grids, line textures, scales and annotations
- Automatically qualifies acquired data with the signal type, measurement point location, direction and sense, date, time and a user specified identification label
- Allow the use of a library of mathematical functions.

DATM stores the calculated frequency response functions in data files accessible to MODAL-PLUS. Other data files which describe the geometry of the structure are also shared by these two softwares.

MODAL-PLUS operates in the PDP 11/34. It contains routines for identification of the modal parameters (natural frequencies, damping coefficients, mode shapes, modal mass, and related parameters) by analysis of the FRF's. The routines are based on the underlying assumption that the system to be identified can be represented by a linear modal model of the form

$$\frac{\bar{x}_j(\omega)}{\bar{f}_k(\omega)} = \bar{H}_{jk}(\omega;\omega_r,\ \zeta_r,\ \alpha_r,\ \psi_{jr}) \qquad (1)$$

where

$$\bar{H}_{jk} = \sum_{r=1}^{n} \frac{\Psi_{jr}\,\Psi_{kr}}{\alpha_r(i\omega+\zeta_r\omega_r-i\omega_r\sqrt{1-\zeta_r^2})} + \frac{\Psi^*_{jr}\,\Psi^*_{kr}}{\alpha^*_r\,(i\omega+\zeta_r\omega_r+i\omega_r\sqrt{1-\zeta_r^2})} \qquad (2)$$

In the above, the f_k are input forces and x_j are response states at discrete points on the structure. The f_k and x_j are both required to correspond directly to measureable quantities (the software can accept measurements of x, $\dot{x}$, or x). $\bar{H}_{jk}(\omega)$ is the Fourier Transform of the unit impulse response function (i.e., the response at location j, to a single unit impulse at location k). The $\{\omega_r, \zeta_r, \alpha_r, \Psi_{jk}\}$ and the order n are the modal parameters to be identified.

By tests and through use of DATM, one acquires measurement of f_k and x_j and then using Eq. (1) constructs experimentally-based $H_{jk}(\omega)$ (in element, column, or full matrix form as appropriate to a particular exercise). Then, using one or more of the routines of MODAL-PLUS, the user obtains the parameters, $(\omega_r, \zeta_r, \alpha_r, \Psi_{jr})$ that result in a curve fit of the analytical $\bar{H}_{jk}$ (transfer function) of Equation (2) to the measurement-based H_{jk} (frequency response function); the corresponding parameters are theidentified modal parameters.

MODAL-PLUS has routines for classical Single-Degree-Of-Freedom (SDOF) curve fits equivalent to the Kennedy-Pancu technique. They are limited to processing data from single-force-input tests. The SDOF routine derives modal frequency and damping from a curve fit of a single scalar element of H represented in the frequency domain, and requires that the modal frequencies be separately spaced. Mode shapes are constructed from the maximum amplitudes of a column of H(ω) at a value of ω equal to the modal frequencies.

The Polyreference Method of MODAL-PLUS is based on the complex exponentials technique. The measurement-based matrix, H(ω), is first converted to the time domain by the inverse Fast Fourier Transform. Then, a time domain equivalent of Eq. (2) is fit to the time domain samples of the measurement-based matrix, H, using a Prony-type algorithm and least squares as described in Reference 7. The Polyreference algorithm is included in Version 7 and later version of MODAL-PLUS.

A Multiple-Degree-Of-Freedom (MDOF) curve fit technique of Version 6 uses the complex exponentials method to curve fit single-input-derived data (i.e., a curve fit of a single element of the H matrix by the complex exponentials method).

In addition to the above capabilities, the features of MODAL-PLUS are:

- Setup data files to be used in the storage of generated data
- Setup the structure geometry data and connectivity specification to be used in the viewing of the deformation patterns of the structure
- Convert geometry data from cylindrical to rectilinear coordinates and/or translate any portion of the geometry
- Display data using a variety of graphs, grids, line textures scales and annotations
- Provide the ability to check the quality and completeness of the modal data base by reconstructing a particular FRF from its mathematical roots (curve fitting)
- Provide the ability to calculate an FRF that has not been measured, allowing the user to validate the process of analysis
- Provide for editing of all data sets and for the updating of storage files
- Convert data taken in radial and tangential directions to their rectilinear components
- Display animated mode shapes from any angle or position in space. Display may be split up into smaller pieces for ease of viewing and may be shown at various speed and scales.
- Split-screen display for simultaneous viewing of multiple modes or multiple views of the same mode.
- Allows use of a library of mathematical functions.

4.3 Base Excitation With Large Electrodynamic Exciter

A number of exploratory and major dynamic tests were done with the Astromast base mounted (fixed-free) to a 178 kN electrodynamic exciter. The lower frequency limit of the exciter was about 5 Hz. The upper limit was set at 100 Hz, this being a reasonable limit of interest for the structure. The second and higher bending modes were expected to be identifiable with this exciter.

The overall configuration is illustrated in Fig. 9. The exciter is operated under digital control to give input the desired excitation waveform at the base of the structure. The base input and the structural deformations are measured with accelerometers. The accelerometer data is acquired and stored on analog tape. A limited number of channels are processed on-line for data screening and vibration control purposes with either the HP 5427A or GEN RAD 2503 system. Parameter identification is done off-line by first reacquiring the data from the tape storage with the GEN RAD 2503 analog-to-digital acquisition system and SDRC DATM acquisition and digital preprocessing software, and then using the SDRC MODAL-PLUS software.

4.3.1 The Test Configuration

The structure is mounted on the slip table of the exciter as shown in Fig. 9. The exciter is a Unholtz-Dickie Model 4000 with a force rating of 178 kN peak sine. Its frequency range is 2 to 2,000 Hz with a practical lower limit of 5 Hz because of control difficulties in the low end. The exciter has a stroke of 2.5 cm peak-to-peak. The slip table, made by KIMBALL, consists of a magnesium slip plate rolling on linear bearings and floating on a thin oil layer in order to minimize friction. Both the shaker and the slip table are fixed to a 363 metric ton seismic mass built under the floor level and serving as a reaction mass. To prevent the reaction force from being transmitted to the foundation of the building, the seismic mass sits on thirty air bags.

Figure 10 shows the mount to fix the mast to the slip plate. Loosening the screws allows rotation and excitation of the structure in any transverse direction.

The scaffold of Figure 11 was found to be the best method of mounting the accelerometers on the Astromast and of supporting their cables to minimize externally-induced damping.

4.3.2 Instrumentation

All measurements were made with ENDEVCO piezoresistive accelerometers (Series 7265), with range of either 10 or 20 g in both tension and compression. These devices have good low frequency response and a range of 0 to 300 Hz at room temperature. Their weight is 6 grams plus 9.2 grams per meter of cables. Each accelerometer was connected to a signal conditioning amplifier that perform three main tasks: supply the accelerometer with a 10 VDC excitation,

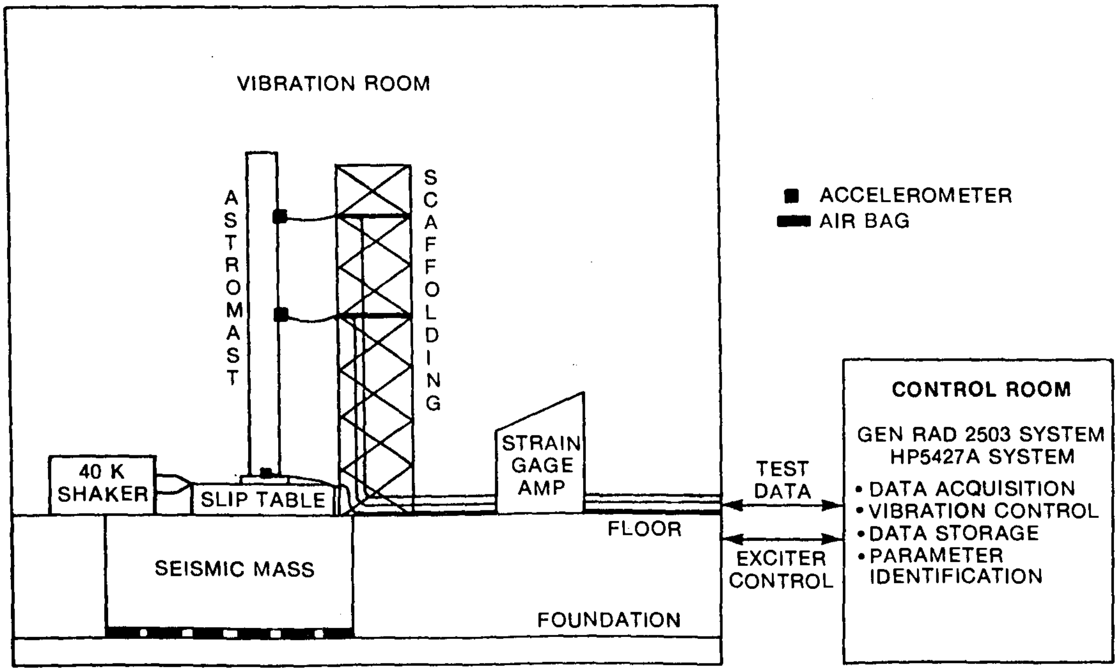

Figure 9. Electrodynamic Exciter Test Configuration

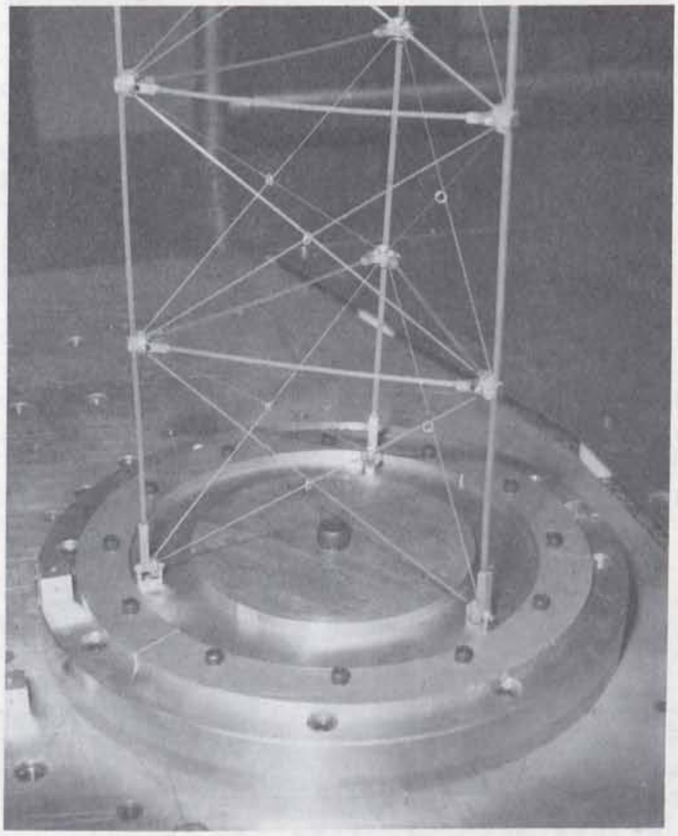

Figure 10. Astromast Mount

Figure 11. Accelerometer Mounting Set-Up

complete and balance the bridge, and amplify the output voltage signal by a factor up to 11,000.

Figure 12 shows the accelerometer locations and directions. A total of 12 response locations were chosen with one on each longeron at four almost equidistant levels. Two accelerometers at each location were used to measure both radial and tangential motions. No accelerometers were pointed in the Z direction since a preliminary test showed the vertical accelerations to be negligible. The input was measured with an accelerometer fixed on the base plate and pointing in the direction of excitation. Because of the small dimensions of the longerons and connectors, the accelermeters could not be put directly on the structure. Aluminum mounts were made which could be attached to the longerons and would allow two accelerometers to be glued at each location (Figure 13).

4.3.3 Exciter Inputs and Control

Two types of base inputs were used for the tests done with the 178 kN exciter: sweep sine, and random (open-loop). The exciter control was implemented with either the HP 5427A system or the Gen Rad 2503 system, depending on system availability.

The HP 5427A system controls the exciter in sweep sine and in open-loop random as depicted in Figure 14 (two other modes are also possible, shock and controlled random).

The swept sine mode (Figure 14a) is a closed-loop configuration: the signals from the control channels are compared to the profile specified by the user and any difference is corrected by a modification of the signal sent to the power amplifier of the exciter. The system can measure on-line in real-time through the use of a multiplexer, amplitude vs. frequency plots for up to 12 channels of which any combination or all can be chosen as control. For frequencies above 1,000 Hz, the limit of measured channels drops to 8. Without the multiplexer, the system allows the use of only four channels. In the tests of this report, one control channel was used and connected to the accelerometer that was fixed on the slip table and bypassed the multiplexer.

In the open-loop random configuration (Figure 14b, the "measurements" or "transfer function" acquisition mode), the HP 5427A system outputs a periodic flat spectrum random noise (pseudo-random) of a bandwidth and amplitude specified by the user. Because of the dynamics of the shaker and the structure under test, the resulting acceleration spectrum may not be flat. This is not a closed-loop configuration since

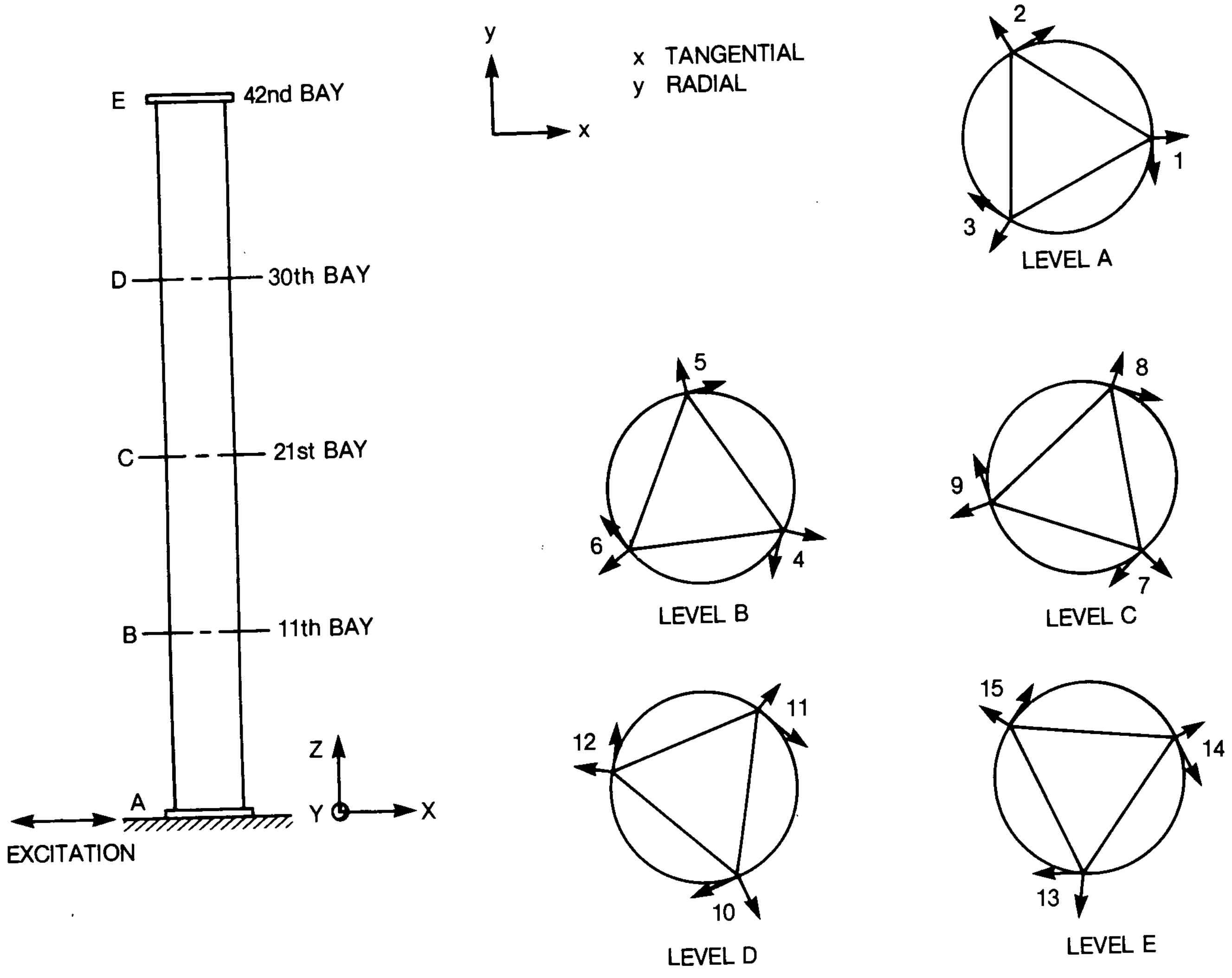

Figure 12. Accelerometer Locations

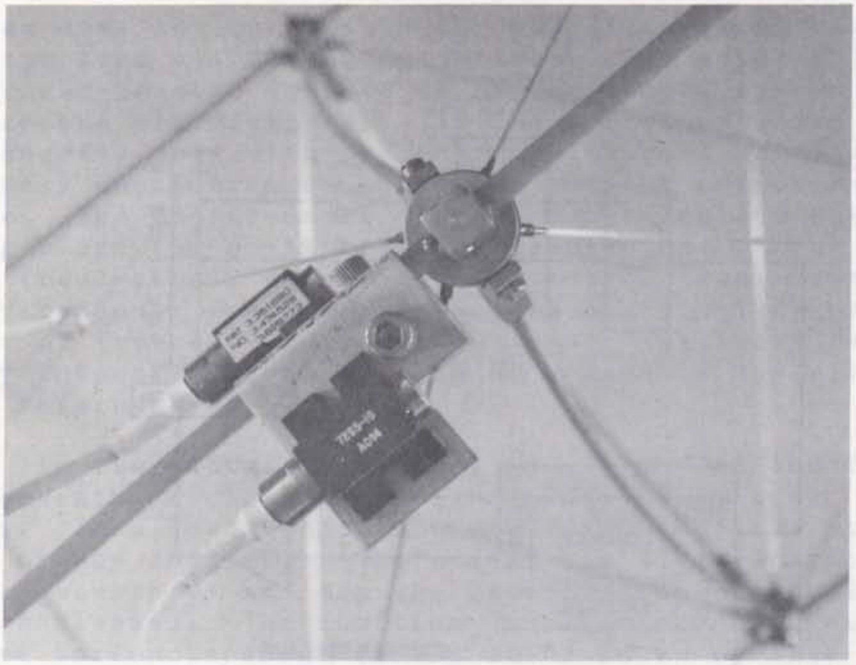

Figure 13(a) Accelerometer Mount (Outer View)

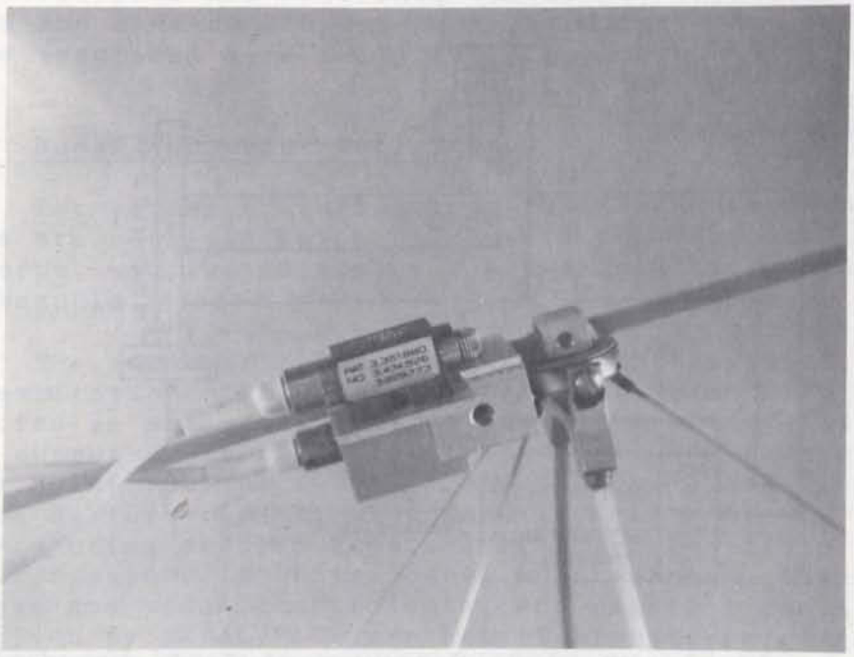

Figure 13(b) Accelerometer Mount (Inner View)

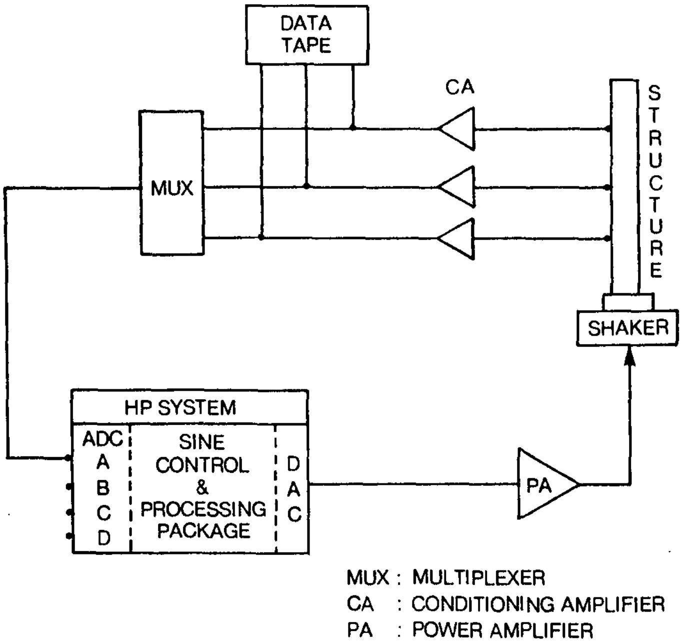

Figure 14(a) HP 5427A Swept Sine Mode

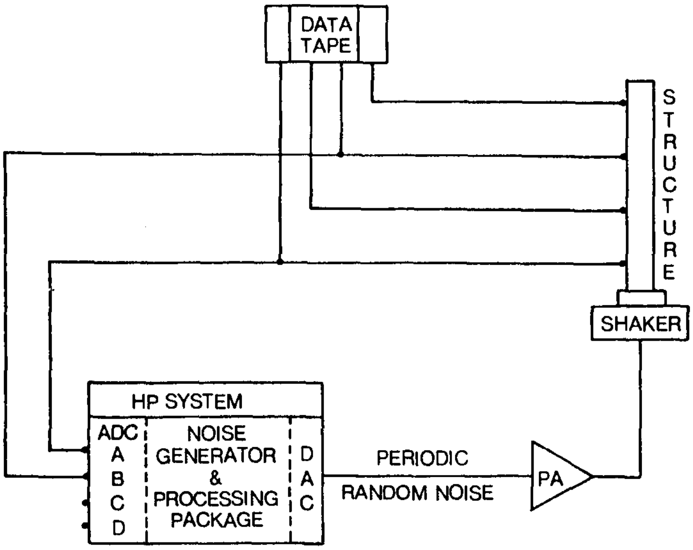

Figure 14(b) HP 5427A Measurement Configuration the system does not compensate for any difference between the control spectrum and the one generated. (An external noise generator can be used instead of having the HP system synthesize the drive signal). In the open loop mode, the system operates only with two channels A and B which are respectively considered as the input and the output on the structure. The measurements package can calculate the following plots for on-line data prescreening: input power spectrum (real-time); output power spectrum (real-time); frequency response function; coherence function; nyquist plot; real part of frequency response function; imaginery part of frequency response function. The HP system is described more fully in Reference 8.

In the vibration control mode, the Gen Rad 2503 system generates a closed loop random and swept sine waveforms. It allows monitoring and display of the average spectrum of any channel. (The system can also generate closed loop shock waveforms and has the capabilities of shock spectrum analysis). The functions are performed through Gen Rad's Time Series Language (TSL), which is an on-line operative software which provides the means of creating, debugging, executing, storing and retrieving the programs of loaded software. TSL can perform the following signal analysis functions for on-line data screening: complex linear spectrum (Fourier transform); auto and cross power spectrum with spectrum averaging; auto and cross correlation function; frequency response and coherence functions; amplitude histogram and time domain waveform averaging. The Gen Rad system is described more fully in Reference 6.

4.3.4 Modal Parameter Estimation

For parameter estimation, the frequency response functions are obtained (with DATM) with the base acceleration as the input, and the astromast mounted accelerometers as the output channels.

The mathematical model of the configuration, Figure 9 (i.e. excitation at the base of the structure, base acceleration as measured input and Astromast accelerations as measured outputs), is slightly different than the model upon which the MODAL-PLUS software is based (Eqs. 1 and 2, Chapter 4.2). The differences are discussed in Reference 9. The modal frequencies deduced from the transfer functions are shown to correspond to "fixed-base" mode shapes. However, the mode shapes and modal coefficients, and possibly the damping factors given by MODAL-PLUS are not rigorously correct. MODAL-PLUS has been used directly herein, with an awareness of these factors.

4.3.5 Exploratory Tests

The tests in this section demonstrate the influence on the FRF's of the accelerometers mass and cables, and the non-linearity of the mast.

4.3.5.1 Effect of Accelerometers

The accelerometers are expected to slightly modify the FRF's for two main reasons. First, the cables contribute to the rigidity and damping of structure. Second, the mass of the accelerometers is significant relative to the lightweight astromast structure. The weight of the Astromast is 1.82 kg while the weight of two accelerometers and their support is about 32 g. The use of 6 accelerometers simultaneously at the same section would correspond to an added concentrated mass of 5 per cent.

To observe the effect of the accelerometer cables, a sine sweep test was performed from 5 to 100 Hz at 0.2 g peak acceleration level. The test was repeated for three different conditions: (1) 6 accelerometers at level E (Figure 12); (2) 2 accelerometers at location 13 (13x and 13y for radial and tangential directions respectively), and (3) 1 accelerometer at either 13x or 13y. For conditions (2) and (3), the accelerometers taken off were replaced by dummy masses having the same weight as the accelerometers and part of their cables, so that any modification of the FRF's would be caused only by the presence of the cables.

Figure 15 shows superimposed Bode diagrams of FRF's for response location 13x. The continuous plot is the frequency response function obtained with one accelerometer on the structure while the dotted plot was measured with the presence of 6 accelerometers. The first peak to the left corresponds to the second bending mode at about 12 Hz; the next peak which is caused by the third bending mode (29 Hz) is perturbed by the presence of what could be a torsion mode. The phases of the two functions are practically the same while there is some meaningful difference in their modulus at the two bending modes.

The same kind of superposition is presented in Figure 16 for response location 13y, which is a tangential accelerometer. The torsion mode at about 34 Hz is much more apparent. The plots overlay very well up to about 30 Hz. For higher frequencies, there is an unacceptable difference.

In order to check the effect of cables on FRF's obtained from random tests, five minute runs were performed at 2g rms level for a frequency range of DC to 100 Hz. For the first run, one accelerometer and its support were fixed on

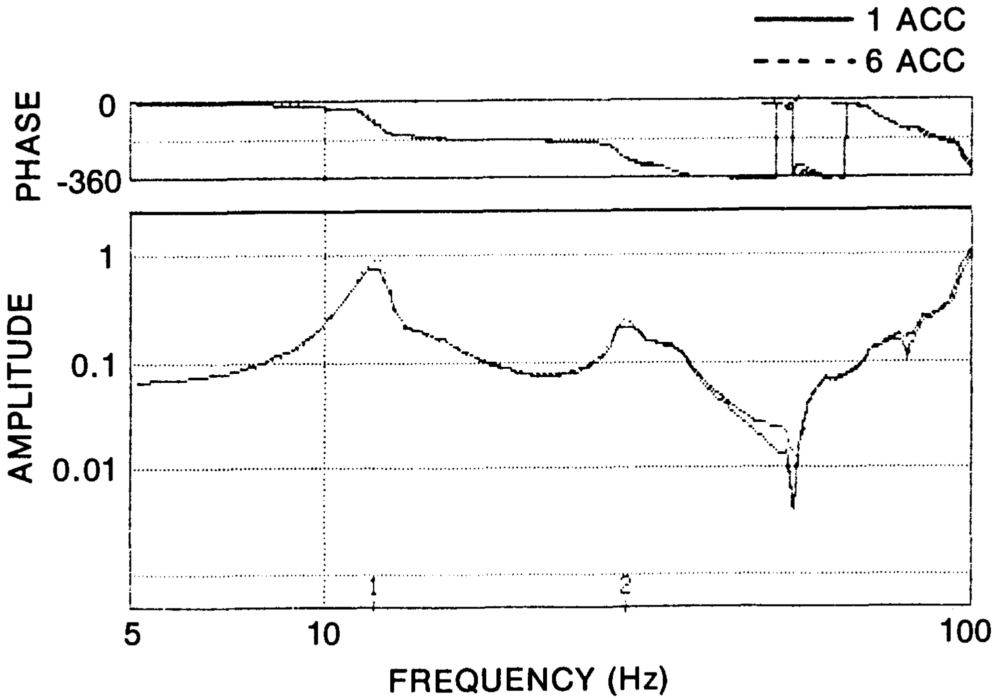

Figure 15. Effect of Accelerometer Cables (Sine Sweep, 13x)

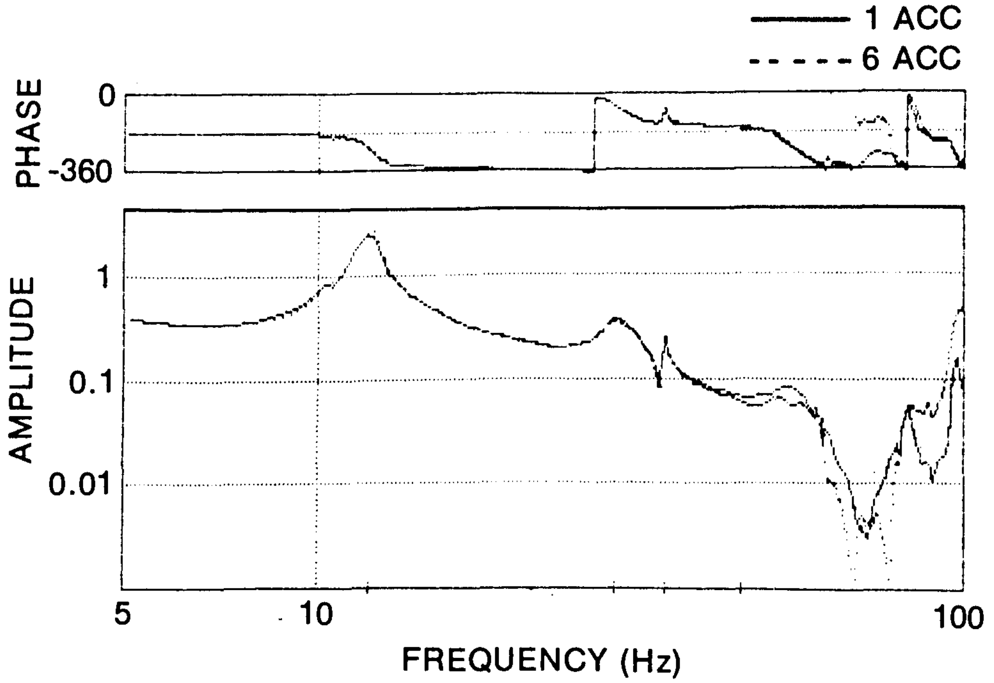

Figure 16. Effect of Accelerometer Cables (Sine Sweep, 13y)

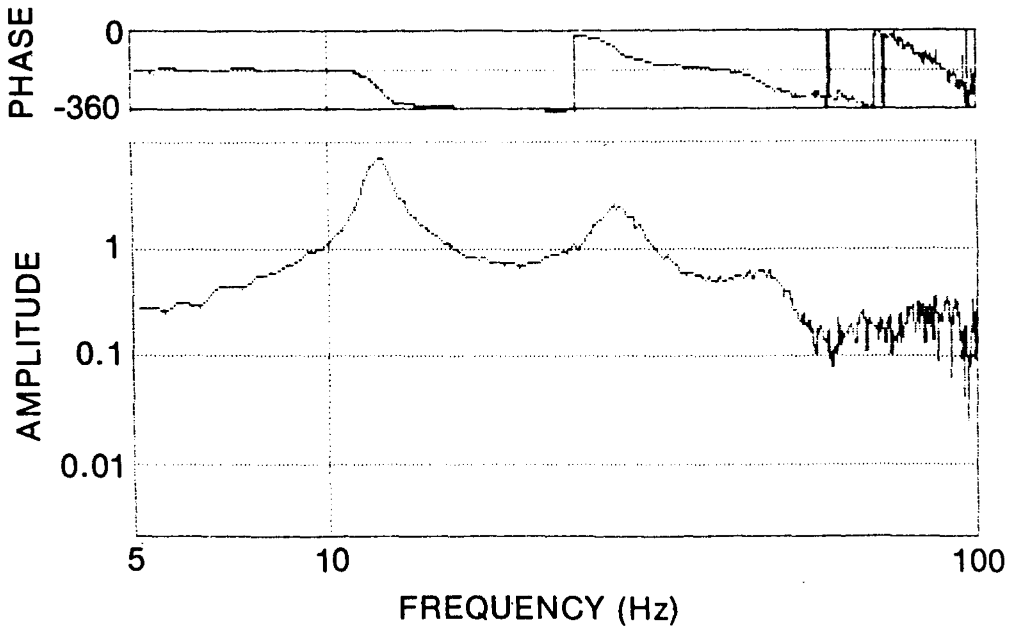

Figure 17. Effect of Accelerometer Cables (Random Burst, 12x)

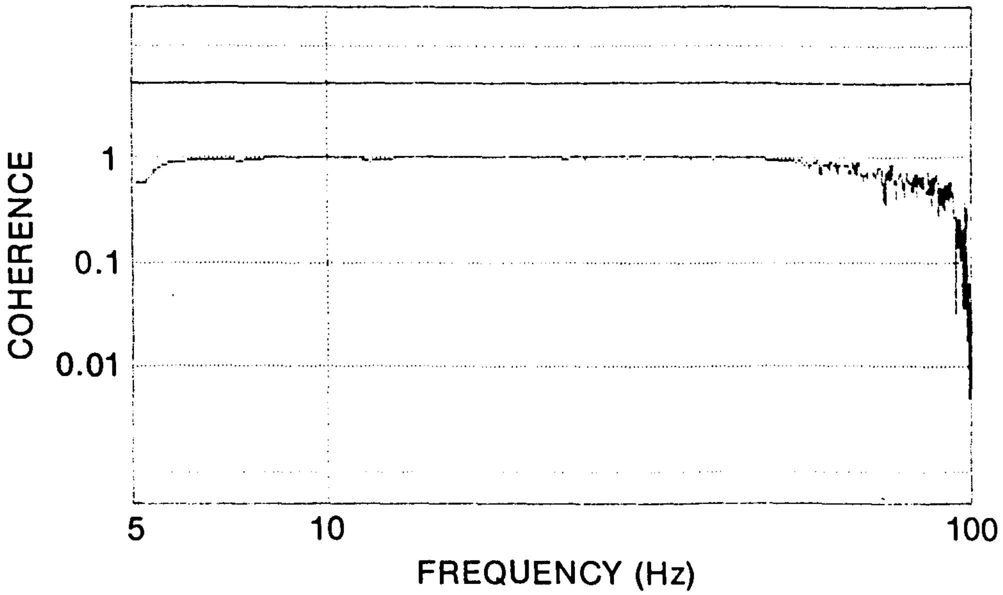

Figure 18. Example of Coherence Function from Test for Effect of Accelerometer Cables (Random Burst, 12x)

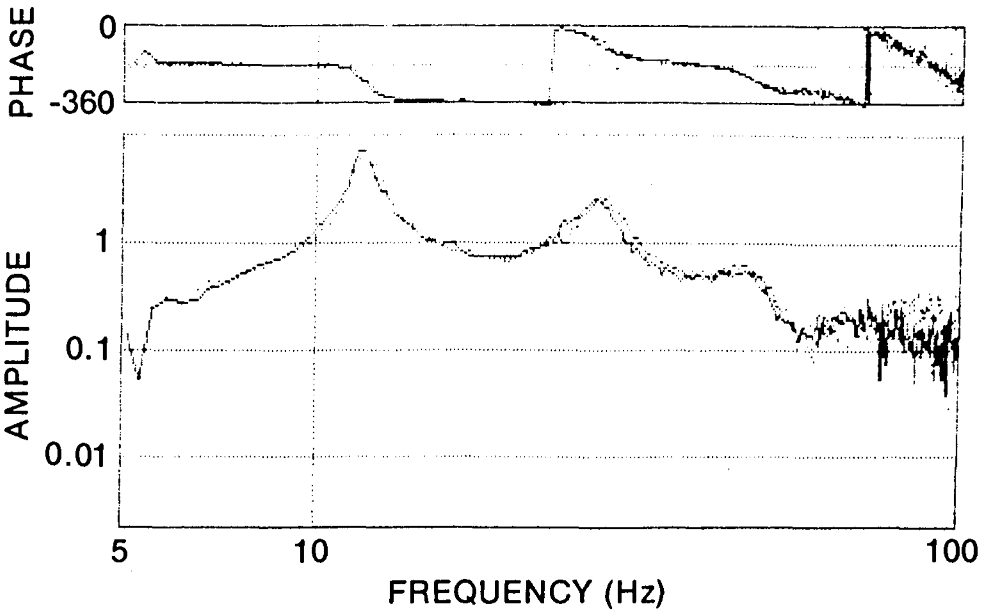

Figure 19. Effect of Accelerometer Masses (Random Burst, 12x)

each longeron, at station D. for the second run, only the response accelerometer at 12x was retained and the two others were replaced by dummy masses. The FRF's obtained from these two runs were identical in phase and modulus up to about 60 Hz (Figure 17).

As shown in Figure 18, the coherence function drops and the FRF's become very noisy for frequencies above 60 Hz. This is due to a lack of energy being transmitted to the structure from the excitation location.

A third random run was performed to check the effect of the mass of the accelerometers. This was done by leaving the accelerometer at location 12x without the other dummy masses at other locations. Figure 19 shows the overlaid FRF's; the continuous and dotted plots are from run 2 and 3 respectively. The peaks corresponding to the second bending mode are the same. For the third bending mode, there is a shift of 0.7% in frequency and 5% in amplitude. For the fourth bending mode, the previous values are doubled. The damping of each of these three modes is practically the same for one or three accelerometers. We conclude that if we are mainly interested in frequencies and damping, the use of three accelerometers simultaneously is acceptable for random test.

4.3.5.2 Non-linearity of the Astromast

The structure was expected to be non-linear before tests were begun. The three main causes of non-linearity follow:

- Freeplay in some connections between longerons and battens
- Buckling of battens which causes local changes in the sectional inertia of the mast (and thus in the effective bending modulus, EI)
- Local buckling of the compressed longerons in the region closed to the fixed end (for higher input force levels)

Sine sweep runs were performed at 0.1, 0.2, 0.3 and 0.4 g levels in order to determine the amount of non-linearity in the structure (the formal tests for determination of modal characteristics of the mast were done at 0.2 g level). One accelerometer was fixed at each of the following response locations: 9x, 12x and 13y. Figures 20 to 22 show, for location 12x, superpositions of frequency response functions obtained from these different test levels.

There is a definite change between 0.1 and 0.2 g levels; while the non-linearity effect seems to stabilize between 0.2 and 0.4 g; at least for the two lower peaks. For frequencies higher than 30 Hz, there is a shift in amplitude and a small shift in frequency.

Figure 23 is a superposition of frequency response functions at 0.1 and 0.2 g levels for response location 9x. Difference in the plots can be seen for lower frequencies. Also, the shift of the third peak is well defined. Figures 24 and 25 are superpositions of FRF's at this location between 0.2, 0.3 and 0.4 g levels. Again, the FRF's do not change significantly between these three levels for frequencies lower than 30 Hz. Superpositions of frequency response functions for location 13y (not shown) exhibit the same characteristics as the above ones.

Random vibration was input at the two different levels 2 and 3 g rms. Accelerometers were positioned at location 9x and 12x. For both locations, the frequency response functions from these two levels were identical for frequencies below 60 Hz, meaning that the results contain no non-linearity distortion. The FRF for location 12x is shown in Figure 26. For frequencies higher than 60 Hz (at the right of the third peak), the signals were too noisy to be meaningful and had a drop in the coherence functions (the reason was explained before). This invariance to different random input levels was expected because random input tends to eliminate, through averaging, any non-linearity of a structure [10].

Before closing this section, two remarks should be made. First, in Table 1 (beginning of Chapter 4), one can see that these 'exploratory' tests were actually performed after the complete sine sweep survey reported in the next section. If they had been done before, the number of accelerometers fixed on the mast for each run and the input level would have been chosen lower in the tests of the next section.

The second remark concerns the coherence functions obtained from the base excitation tests. Any value of the coherence different from 1 can be a sign of poor data, although this is not necessarily the case. Usually, one would expect a drop in the coherence only at anti-resonance (valley in FRF) since the output signal is then at its lowest value and the signal/noise ratio is low. Typical coherence functions for the surveys as well as for the exploratory tests were like the ones of Figure 27 and 28. As one can see, there is a drop in the coherence to about 0.9 for the lower peaks of the frequency response function of the sine sweep data, while only the drop at the first peak is apparent for the random input. The reason for these drops was found only after the

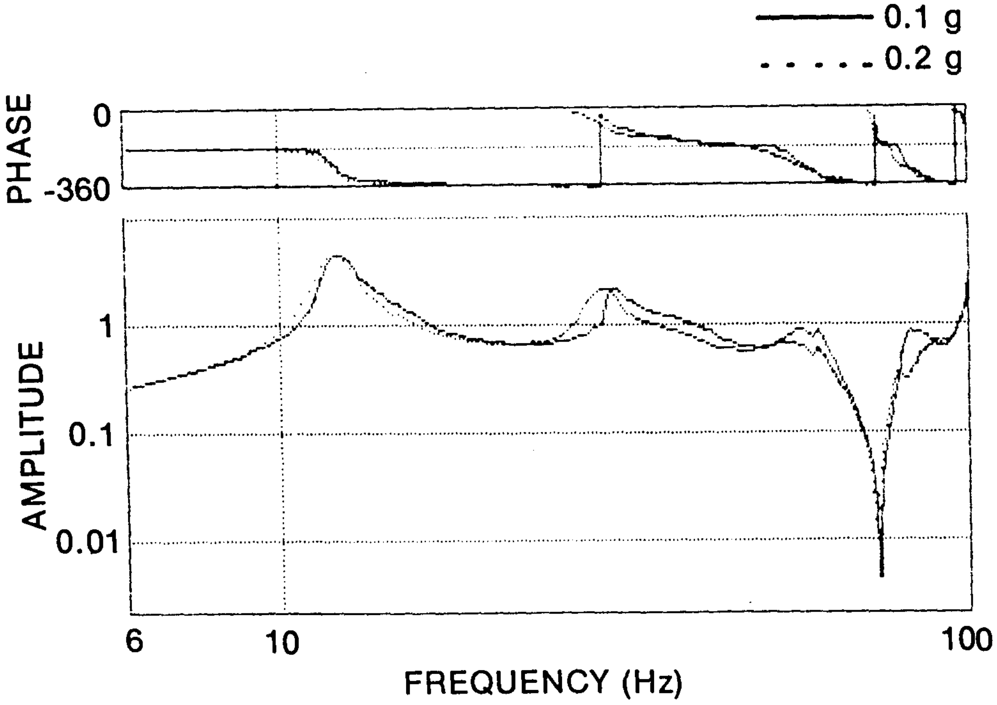

Figure 20. Test for Non-Linearity (Sine Sweep, 0.1 g and 0.2 g, 12x)

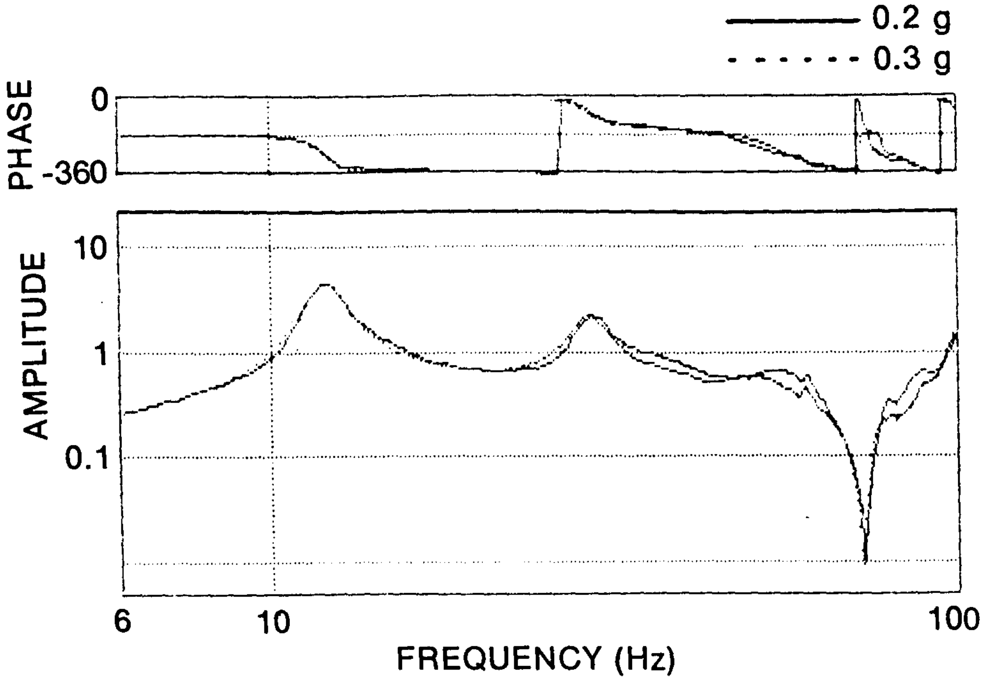

Figure 21. Test for Non-Linearity (Sine Sweep, 0.2 g and 0.3 g, 12x)

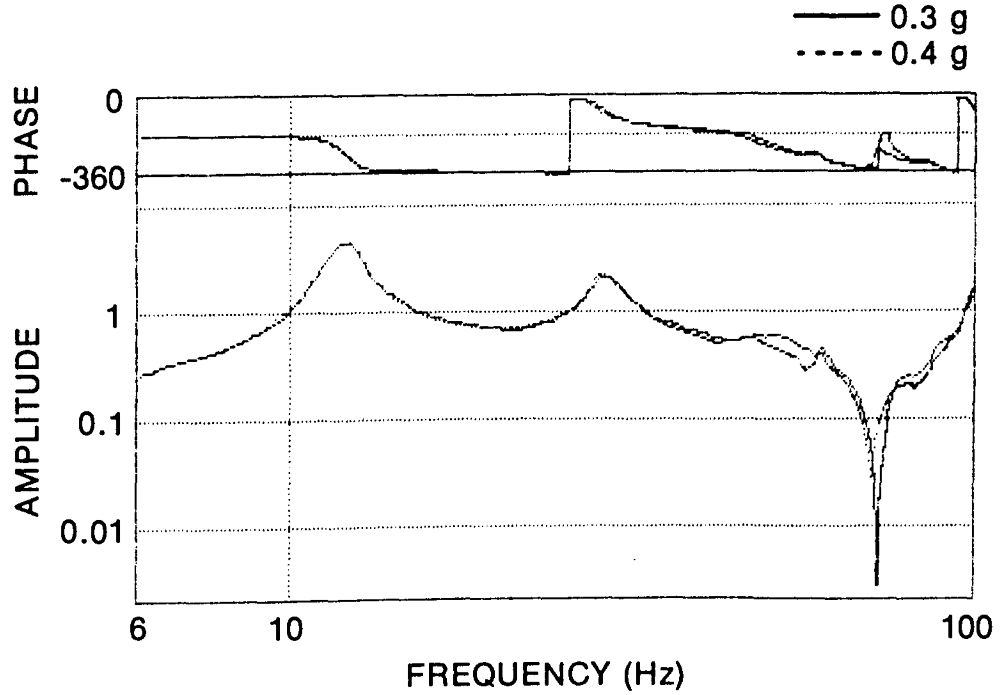

Figure 22. Test for Non-Linearity (Sine Sweep, 0.3 g and 0.4 g, 12x)

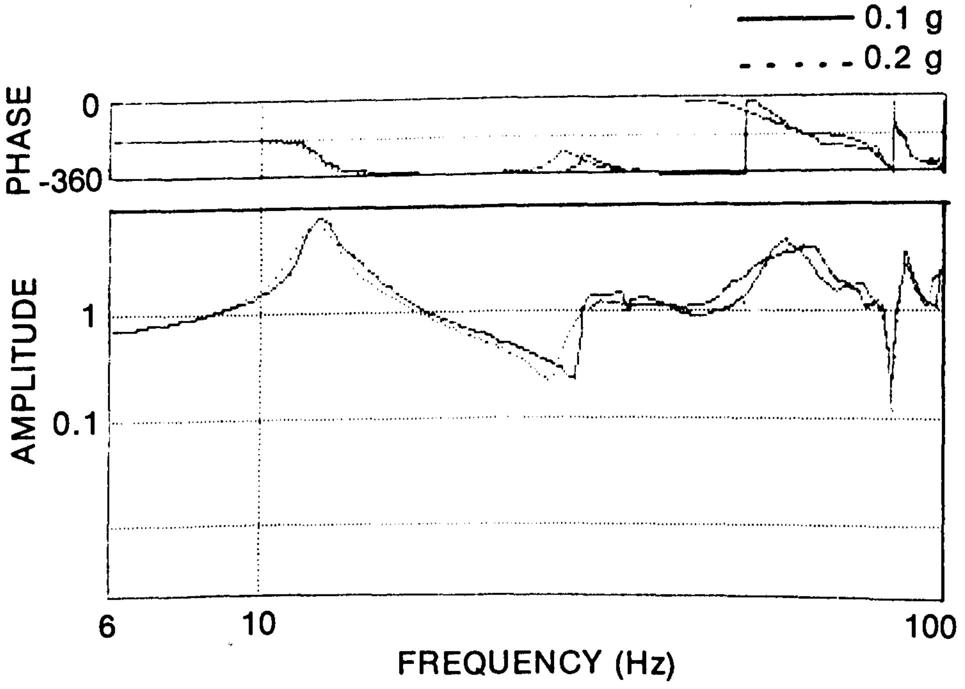

Figure 23. Test for Non-Linearity (Sine Sweep, 0.1 g and 0.2 g, 9x)

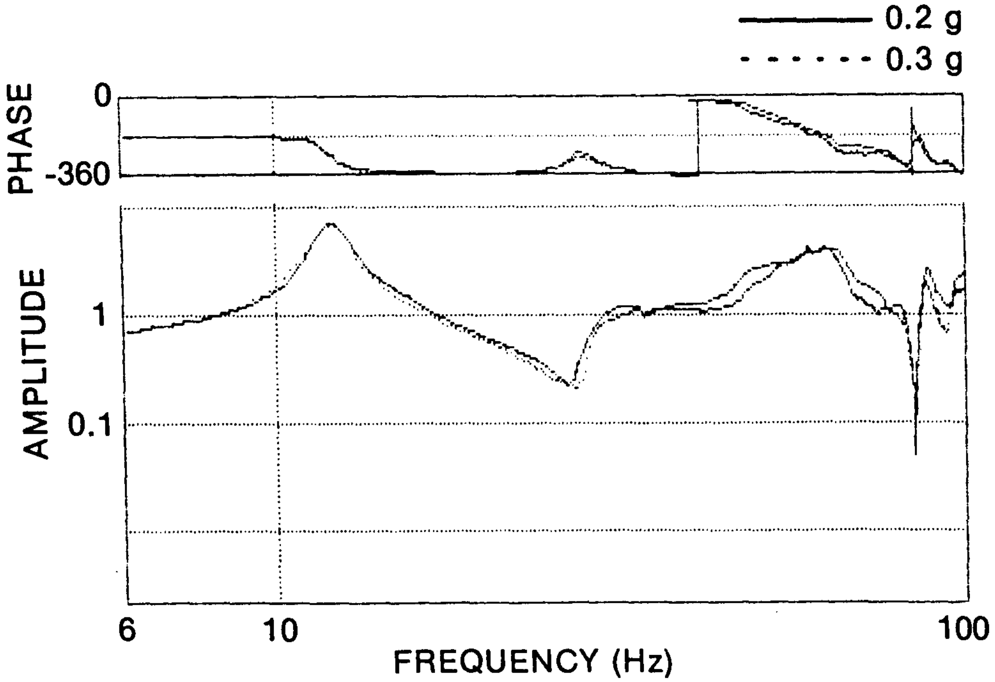

Figure 24. Test for Non-Linearity (Sine Sweep, 0.2 g and 0.3 g, 9x)

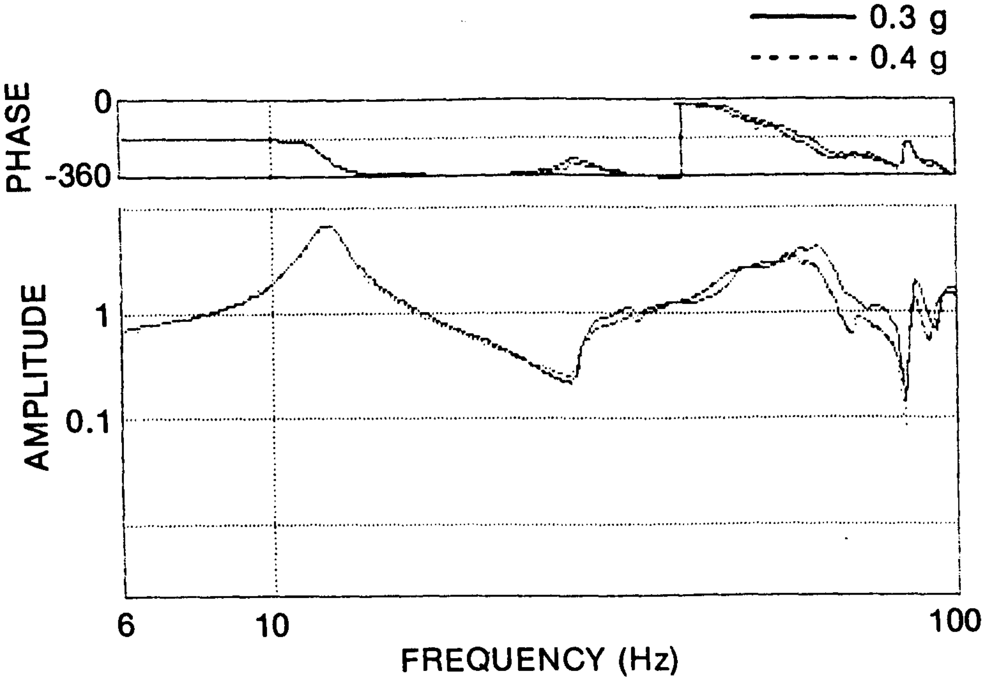

Figure 25. Test for Non-Linearity (Sine Sweep, 0.3 g and 0.4 g, 9x)

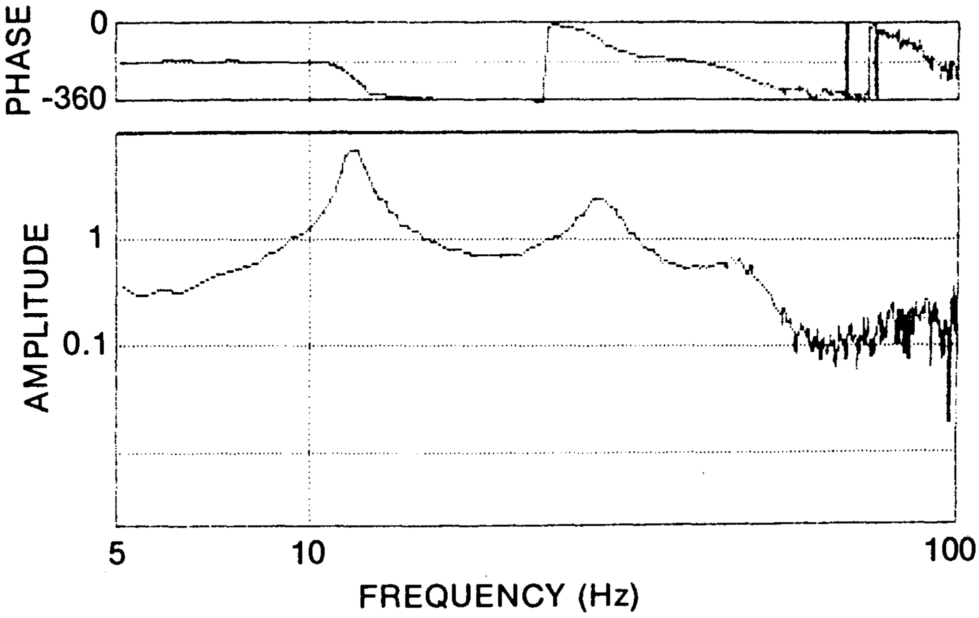

Figure 26. Test for Non-Linearity (Random Burst, 2 g and 3 g RMS, 12x)

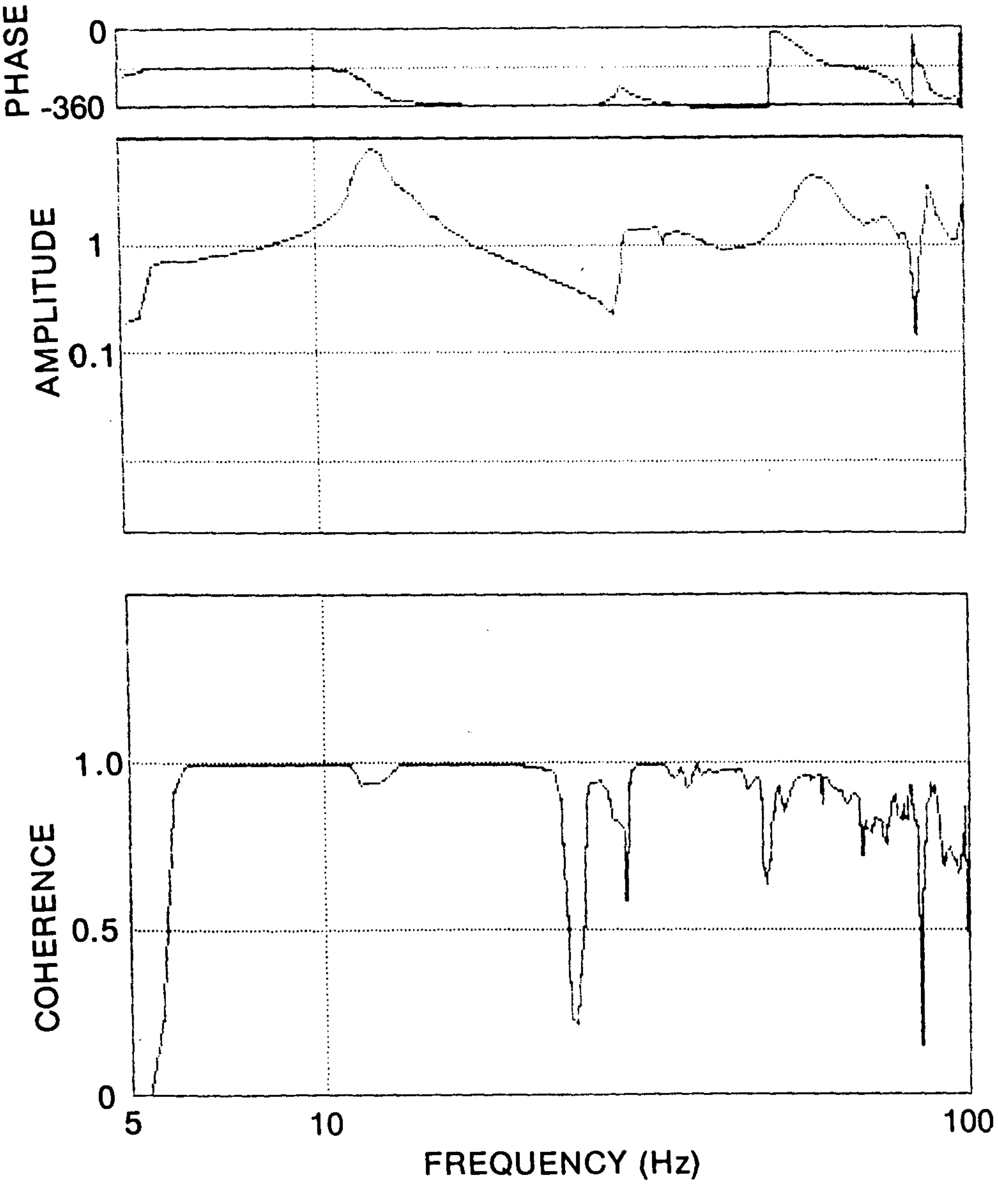

Figure 27. Typical Coherence Function for Sine Sweep

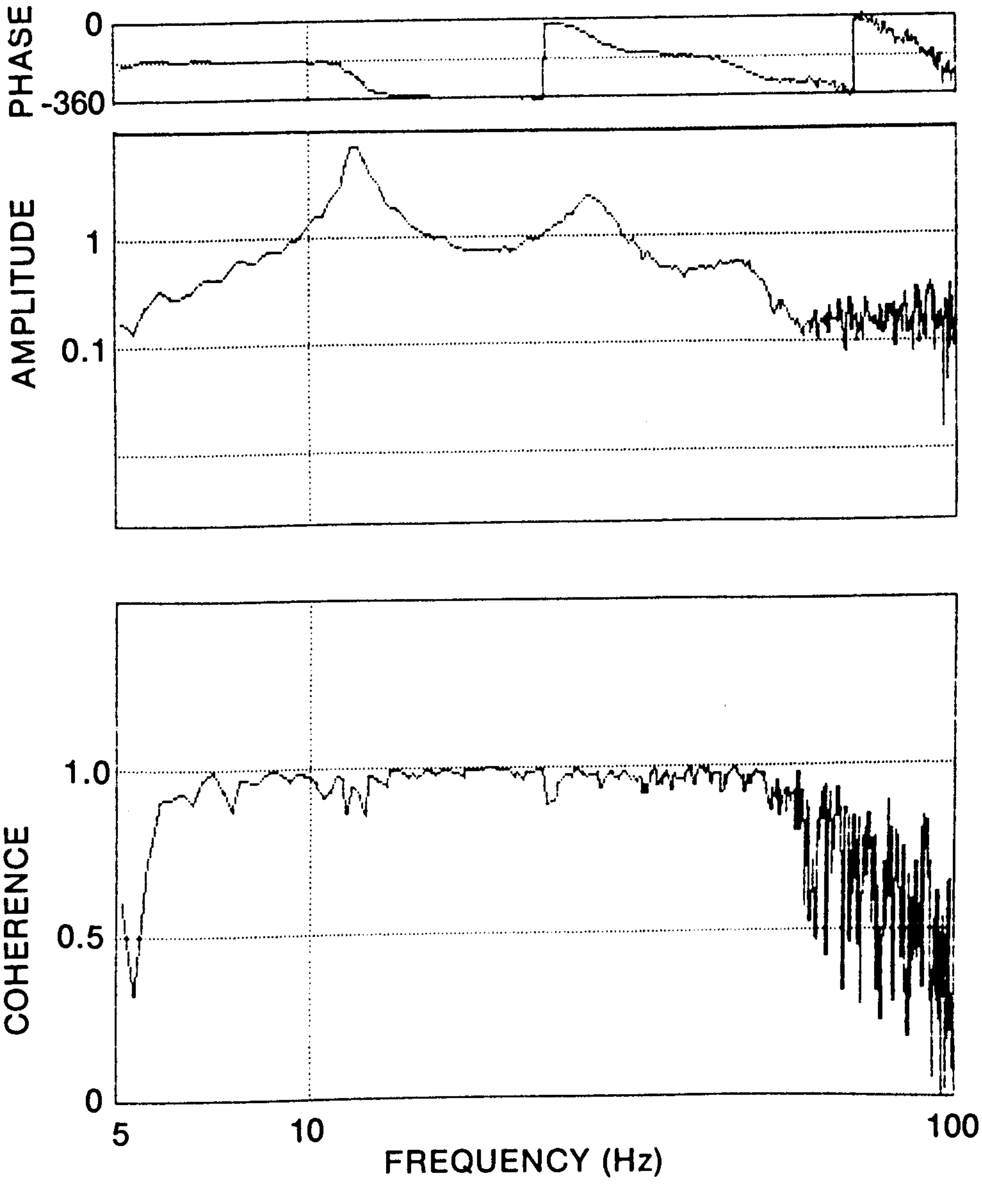

Figure 28. Typical Coherence Function for Random Burst

whole set of tests was completed. The drop is due to a lack of resolution in the calculation of the FRF's, (that is the distance between two adjacent frequency lines is too large). For the maximum frequency of 125 Hz that was used (limit of anti-aliasing filter fixed at 100 Hz), the value of Δf is 0.25 Hz. For both random and sine sweep, the processing was re-done with a resolution about five times higher ($\Delta f = 0.05$ Hz) for two different accelerometers. For the four FRF's, the coherence function became essentially equal to 1. More important, for the random input, there was no difference between the frequency response function from the two different resolutions, while for sine sweep, the first peak region was almost the same. One concludes that, while the coherence functions were not calculated properly in all cases, the frequency response functions were, and hence the FRF-derived modal information is valid.

4.3.6 Test Results

The results from the two test surveys using the 178 kN electro-dynamic shaker follow. These surveys consisted in taking data at the 24 response locations shown previously in Figure 12.

4.3.6.1 Sine Sweep Input

More than one run per survey was needed since not all the accelerometers were mounted on the structure at the same time. For each run, six accelerometers were put at the same level (either B, C, D or E). The complete survey required four runs. The peak value of input acceleration was set at 0.2 g for the frequency range of interest (5-100 Hz). This input level was selected in order to have clean signals without submitting the structure to too high displacement and stress.

In order to make sure that the sweep rate was slow enough to allow resonance to build up, the following equation was used:

$$\theta = \zeta \omega_n \left(\frac{\pi}{\dot{\omega}}\right)^{\frac{1}{2}} \tag{3}$$

where θ is Hop's sweep rate parameter, ζ is the damping ratio, ω_n is the resonant frequency, and $\dot{\omega}$ is the sweep rate.

Reference [11] states that the sweep rate is slow enough if $\theta > 2$. In the present case where the sweep rate was constant throughout the run, only the first resonant frequency (about 12 Hz) had to be checked. The chosen linear sweep rate was such that each run lasted 15 minutes (2-100 Hz).

Figures 29 to 31 are examples of frequency response functions obtained from this survey. They are from accelerometers located at 5x, 9x and 10y. The third bending mode (at about 27 Hz) is not very apparent on the second FRF because the location 9x is close to a node.

As explained previously, this survey was performed before the exploratory tests. From these tests, only the part of the frequency response functions below 30 Hz is expected to be reliable. In fact, with the data taken, only the frequency and damping values of the second bending mode (first peak) have been obtained by averaging more than one estimate. The third mode is contaminated, for most locations, by the presence of a torsion mode created by the effect of too many accelerometers (6) mounted on the structure at the same time.

To obtain resonant frequencies and associated damping ratios, the MODAL-PLUS MDOF algorithm was used to curve fit the experimental frequency response functions. Curve fit results (transfer functions) for the above examples are given in Figures 32 to 34. The first peak can be curve fit relatively well, while the algorithm is unable to calculate a very good fit of the second peak. This shortcoming in curve fitting is likely explained by the presence of non linear effects since the modal analysis theory assumes linearity. This explanation is reasonable since, as has been shown before, the peak at 32-34 Hz is created by the presence of the accelerometers exciting the 2nd mode in torsion.

For the second mode (first peak), 8 of the 24 measurements showed an acceptable coherence function (higher than .85) as well as a good curve fit. An estimate of frequency of the second bending mode was obtained in averaging the value of 17 transfer functions (given in Table 2). The damping ratio was estimated from the 8 good curve fits. For the third mode, in addition of being unable to curve fit, most of the frequencyresponse functions showed an unusual shape for the peak.

These results, as well as the ones to follow, do not account for the mass loading effect due to the relatively high mass of the accelerometers and mounts relative to the mass of the structure. This means that the higher estimates of the resonance frequency from locations with low displacements are more likely better estimates than the lower ones from locations with high displacements.

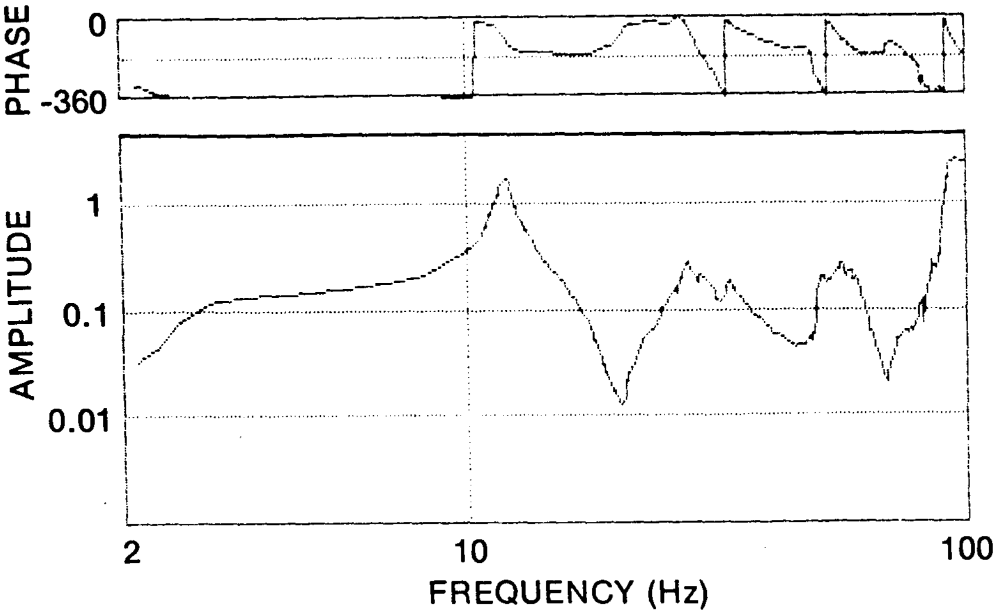

Figure 29. Frequency Response Function (Sine Sweep, 5x)

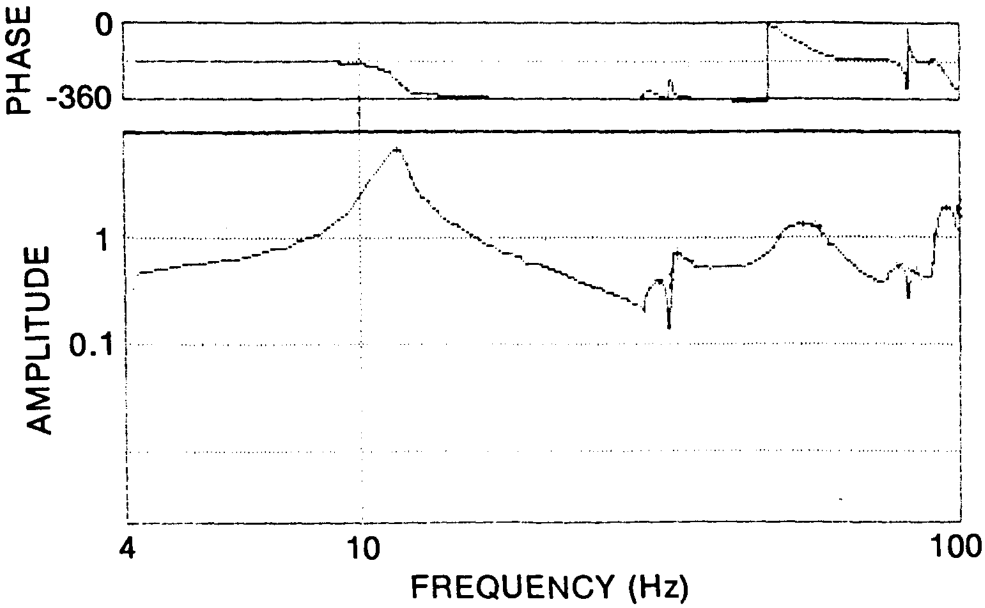

Figure 30. Frequency Response Function (Sine Sweep, 9x)

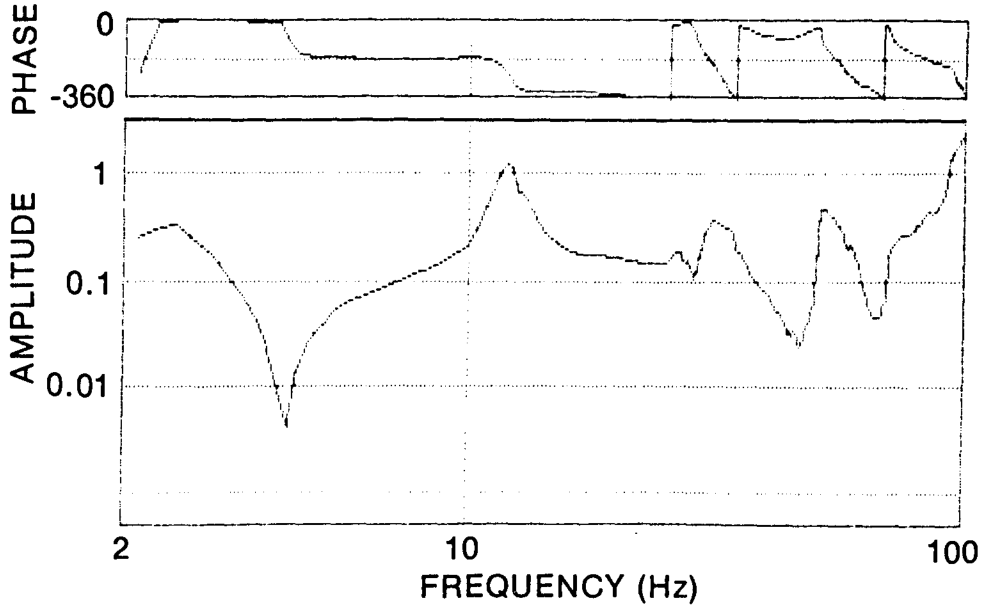

Figure 31. Frequency Response Function (Sine Sweep, 10y)

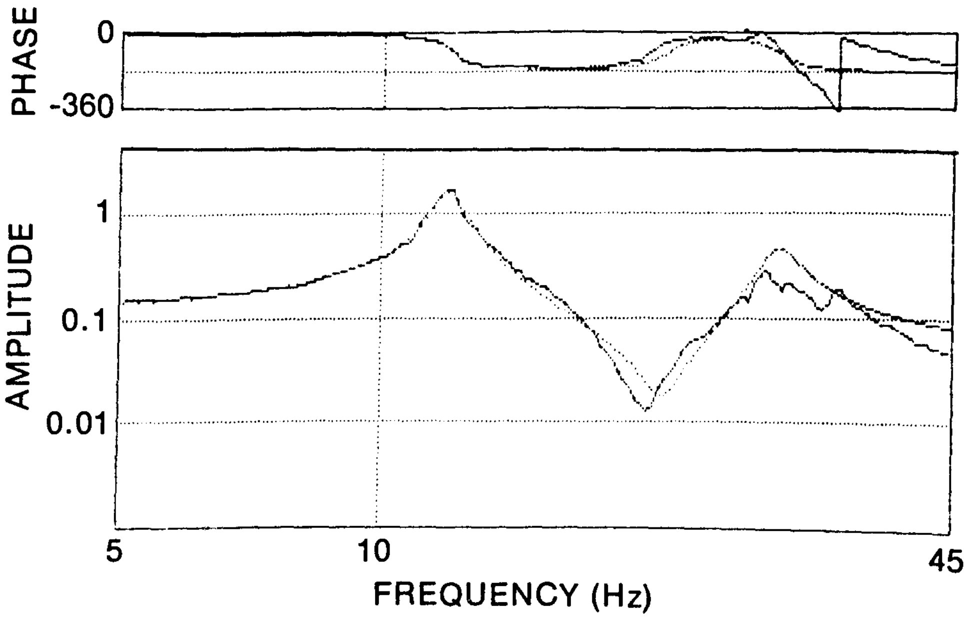

Figure 32. Curve Fit (Sine Sweep, 5x)

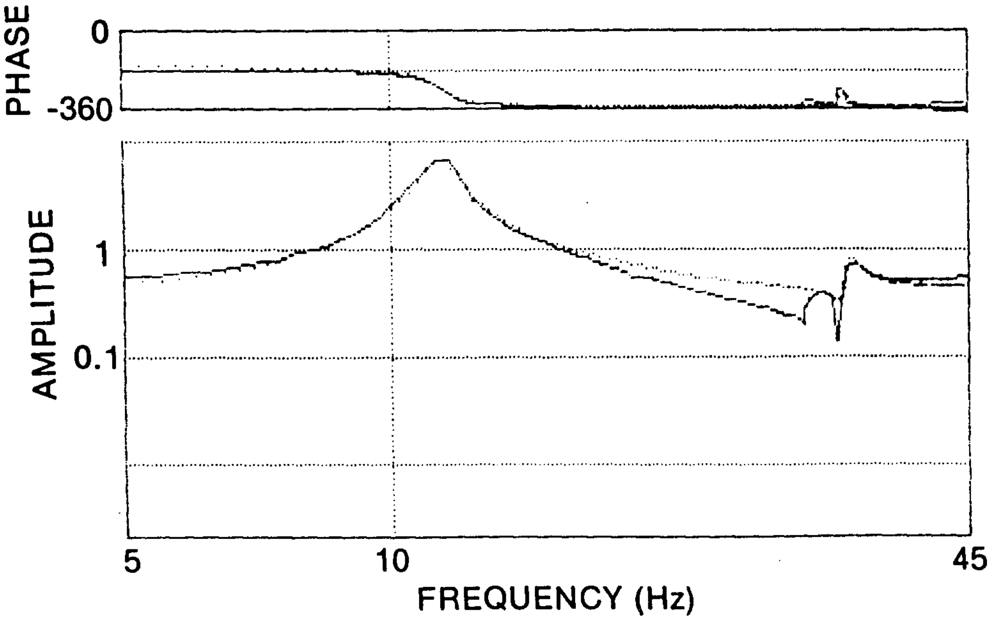

Figure 33. Curve Fit (Sine Sweep, 9x)

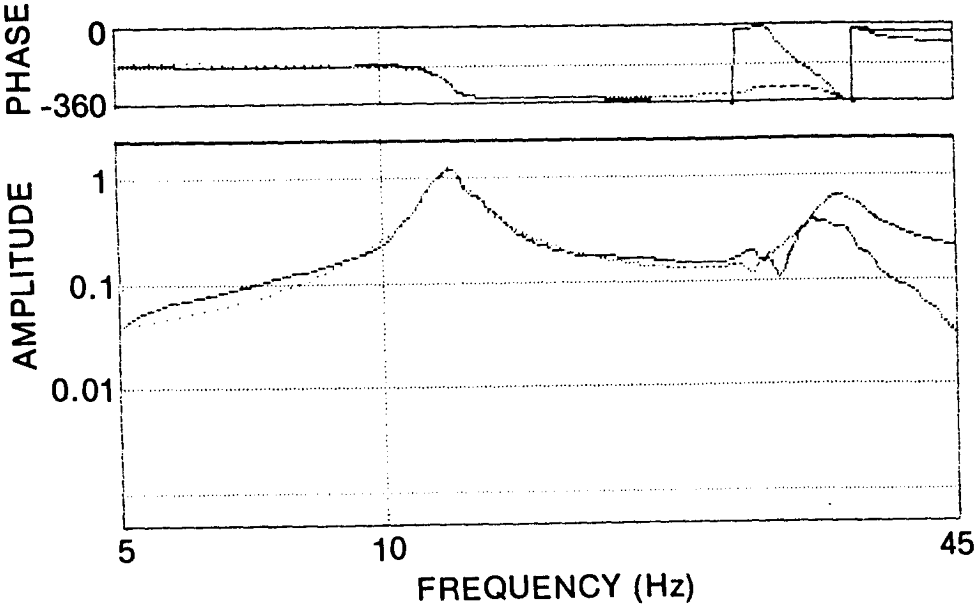

Figure 34. Curve Fit (Sine Sweep, 10y)

TABLE 2 ESTIMATED MODAL PARAMETERS (SINE SWEEP)

CHARACTERISTICS	ESTIMATED VALUE	STANDARD DEVIATION	LOWEST VALUE	HIGHEST VALUE
Resonant Frequency (Hz)	11.8	0.2	11.4	12.1
Damping Ratio (%)	3.7	0.2	3.5	4.1

4.3.6.2 Random Input

This survey was done after the exploratory tests. Thus, it was known that the data would be independent of the input level and that the only effect of the presence of accelerometers, up to three, would be a small shift of the peaks of frequency response functions corresponding to the third and fourth modes. Only three accelerometers were mounted on the structure at each run; they were put on each longeron, at the same level. Eight runs were needed to complete the survey. Each run lasted between three to five minutes. The selected frequency bandwidth was from 0 to 100 Hz. However, the response of the shaker is only reliable above 5 Hz and the signals were too noisy above 60 Hz. The input level was set at 2 g rms.

Figures 35 to 38 are examples of frequency response functions from random input. They are respectively from locations 5y (level B), 8x (level C), 11x (level D) and 14x (level E). For location 5y, all three peaks are quite distinguishable; the same can be said about 11x except the third peak is not well defined. The accelerometer location 8x seems to be close to a node for the third mode (second peak); the same remark was previously made for location 9x. Similarly, accelerometer location 14x seems to be close to a mode for the fourth mode. Generally, as one would expect, these remarks apply for the other five accelerometers at each level.

For these same functions, Figures 39 to 42 show the superposition of the analytical over the experimental plots. The analytical plots are calculated with the MDOF algorithm. Except for location 14x, the experimental and analytical curves match very well at the first peak. The curve fit of the second peak is good except for location 5y. All FRF's corresponding to level B present the same problem of curve fitting one or both slopes of the second peak. As one can see, the ability of fitting third peaks (phase and magnitude) varies with the location. Fortunately, this peak is curve fit with sufficient precision to obtain a good estimate of frequency and damping. The proximity of this peak to the edge of the bandwidth and the associated loss of contribution from higher modes can explain the difficulty of fitting its current slopes.

Table 3 gives the estimated modal parameters (resonant frequency and damping ratio) for the second, third and fourth bending mode, and other relevant information.

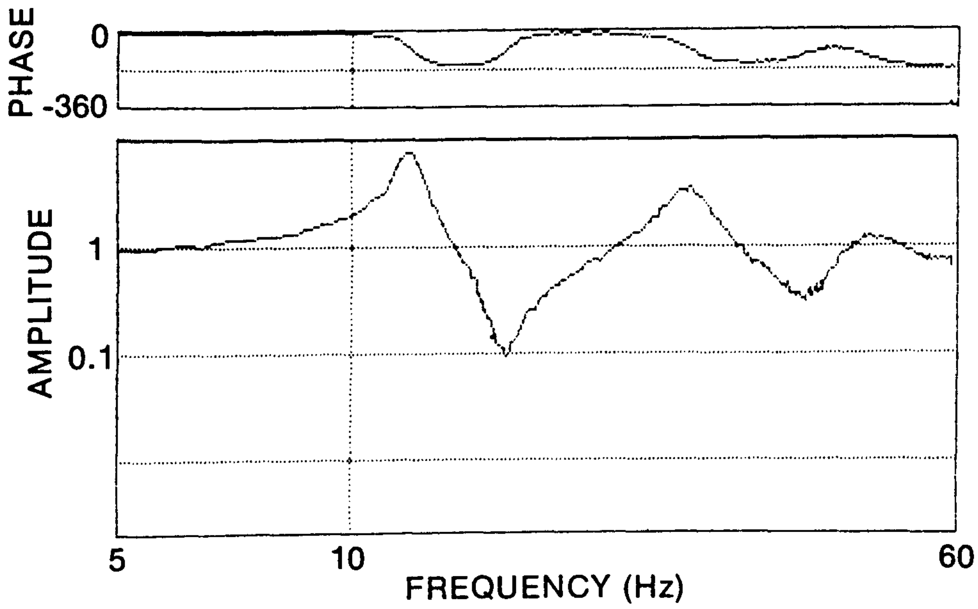

Figure 35. Frequency Response Function (Random Burst, 5y)

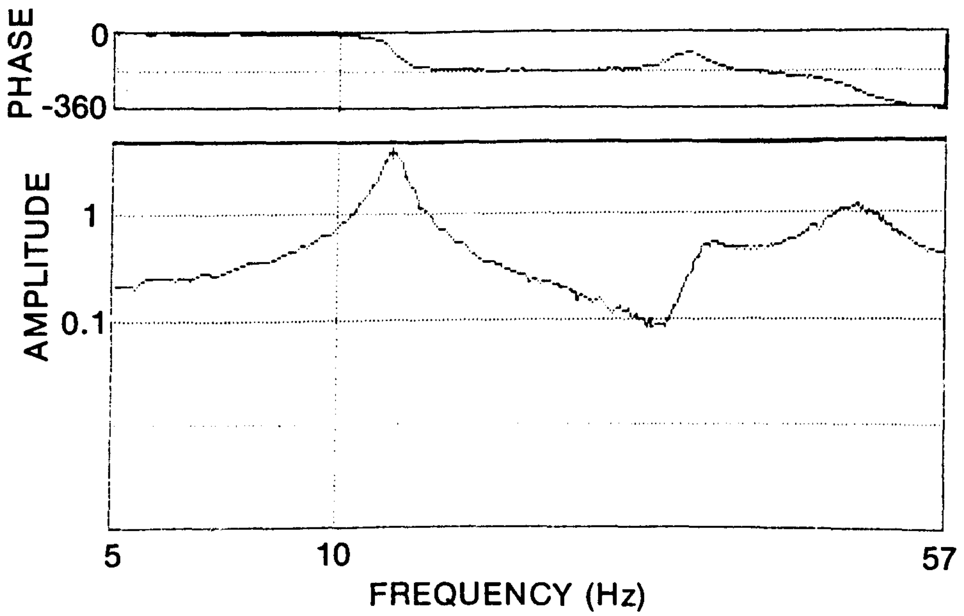

Figure 36. Frequency Response Function (Random Burst, 8x)

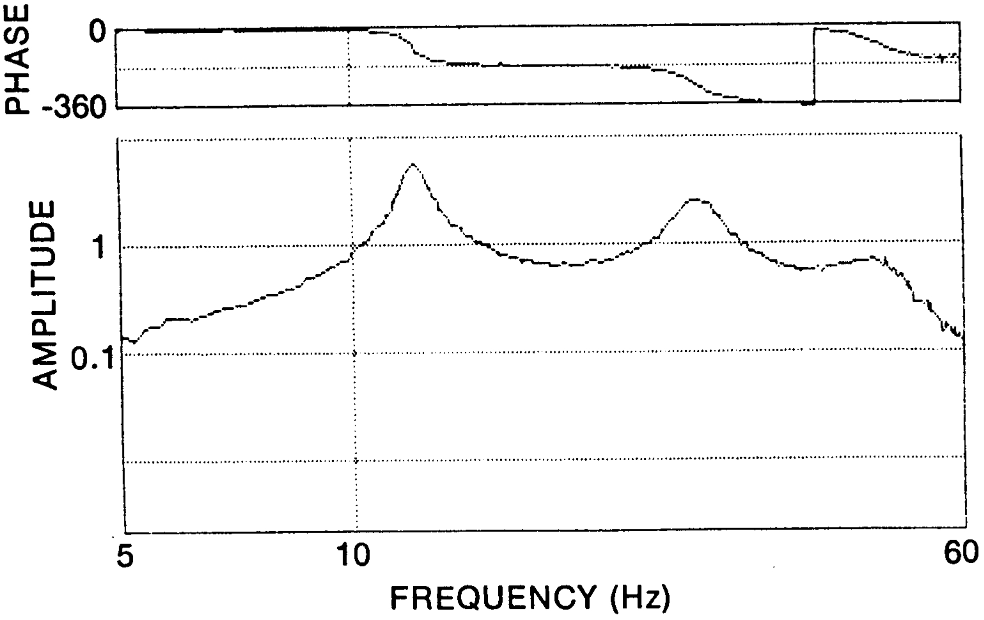

Figure 37. Frequency Response Function (Random Burst, 11x)

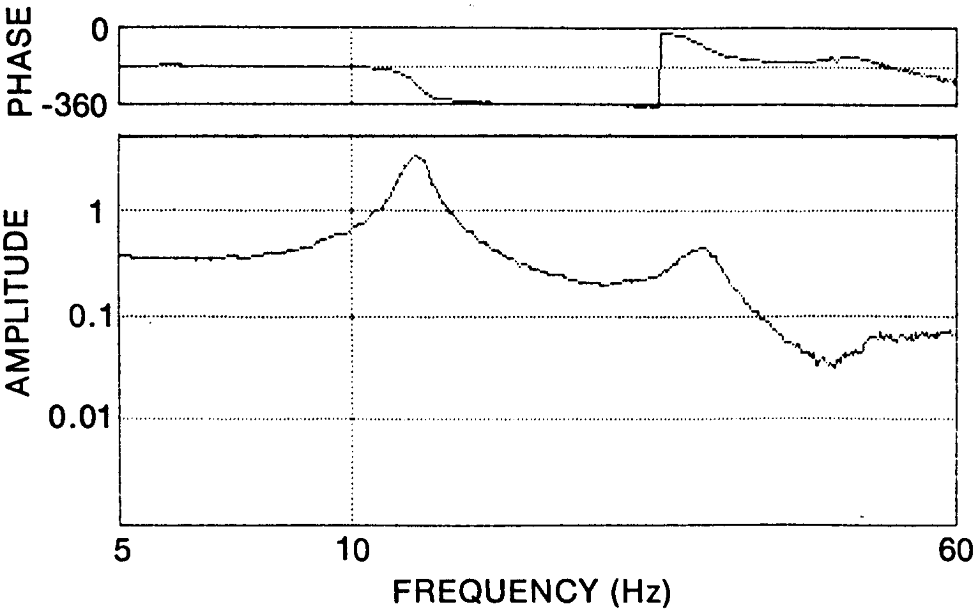

Figure 38. Frequency Response Function (Random Burst, 14x)

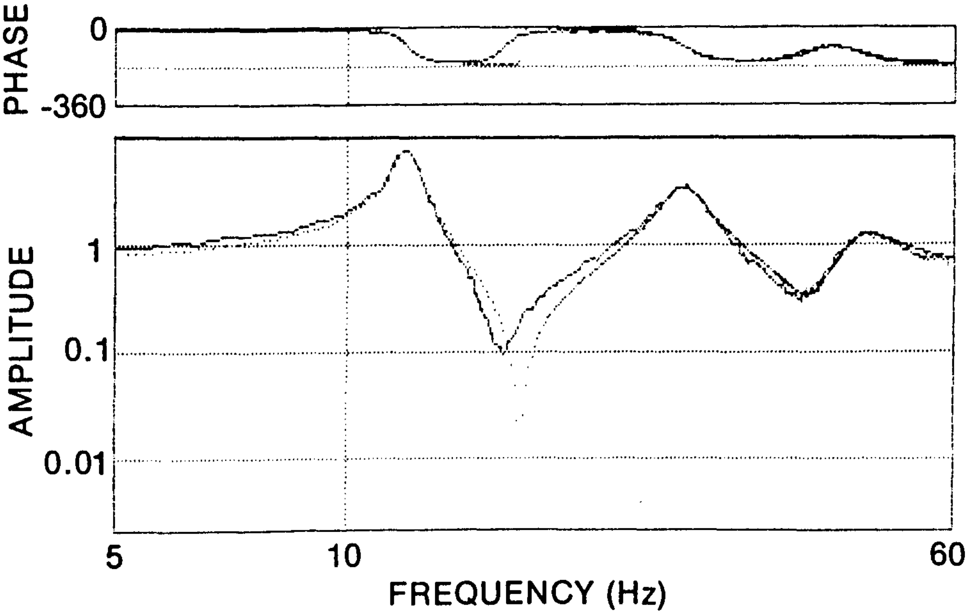

Figure 39. Curve Fit (Random Burst, 5y)

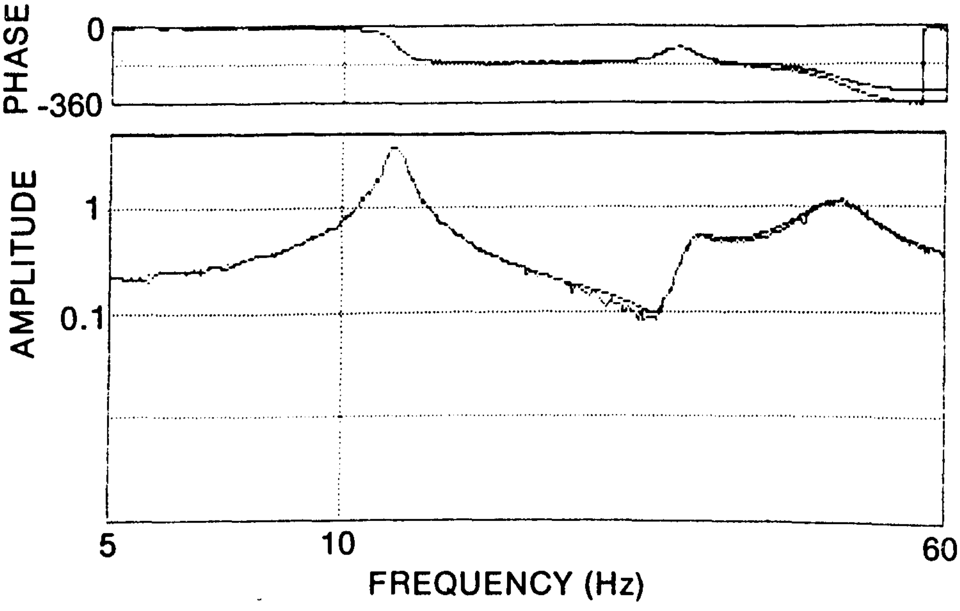

Figure 40. Curve Fit (Random Burst, 8x)

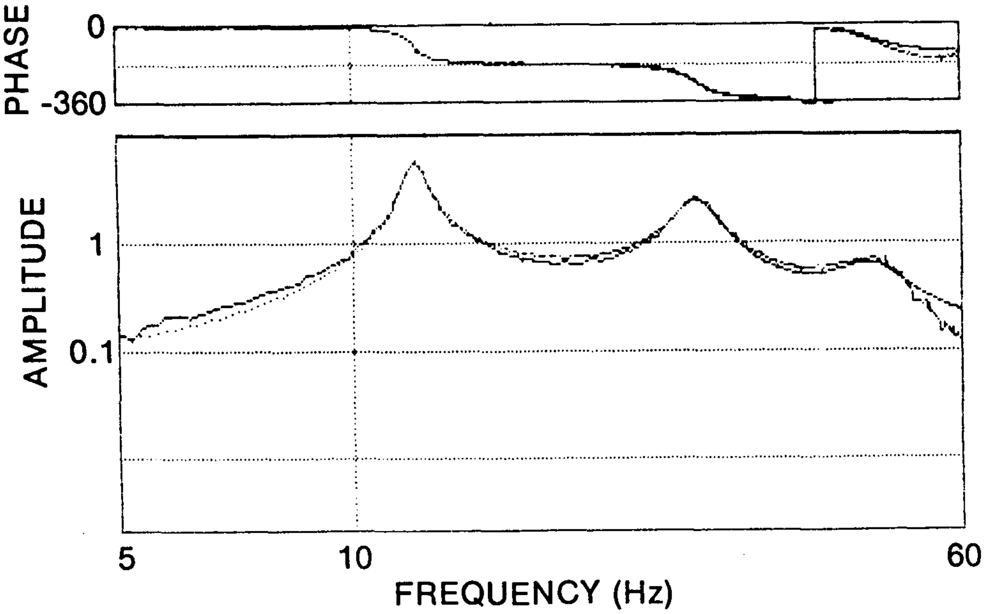

Figure 41. Curve Fit (Random Burst, 11x)

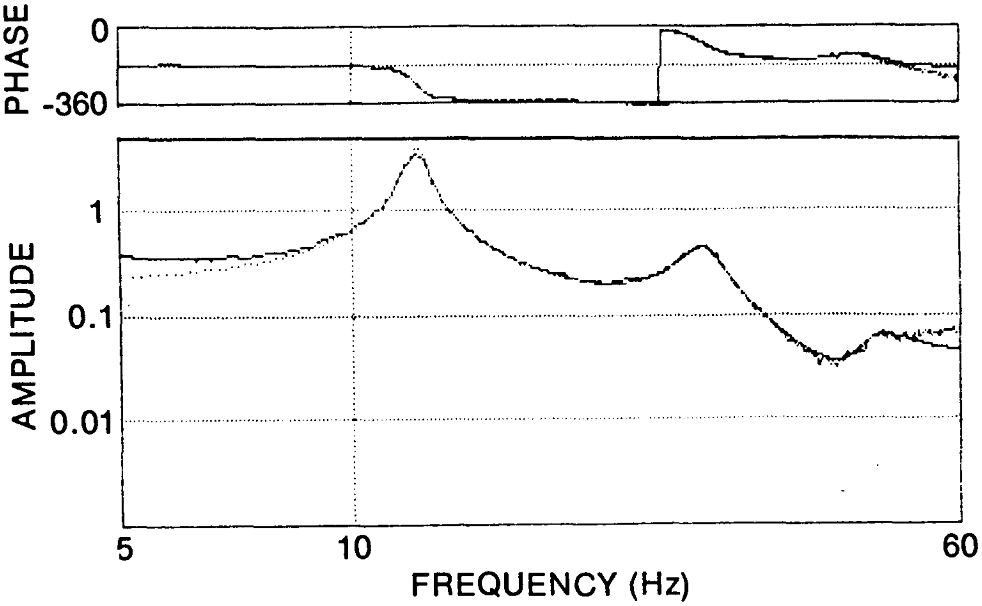

Figure 42. Curve Fit (Random Burst, 14x)

TABLE 3 ESTIMATED MODAL PARAMETERS (RANDOM BURST)

CHARACTERISTICS	ORDER OF BENDING MODE	ESTIMATED VALUE	STANDARD DEVIATION	NUMBER OF SAMPLES	LOWEST VALUE	HIGHEST VALUE
Resonant Frequency (Hz)	2	11.9	0.2	20	11.6	12.3
	3	27.6	0.5	11	27.0	28.4
	4	45.9	1.1	12	44.3	48.0
Damping Ratio (%)	2	3.1	0.2	15	2.7	3.3
	3	5.8	0.2	9	5.4	6.1
	4	8.5	0.7	7	7.5	9.2

4.4 Tests In Air and Vacuum with the Hydraulic Exciter

A hydraulic exciter was used to test the Astromast in the range 1 - 30 Hz. Since the exciter is located inside a vacuum chamber, it was possible to experiment in ambient and in vacuum conditions. The main reason for the tests with the hydraulic exciter was to obtain the properties of the first bending and torsion modes. The first and second natural bending frequencies as well as the first one in torsion were within the frequency range of the exciter.

4.4.1 Description of Test Configuration

A schematic representation of the 3 m x 9 m (10' x 30') vacuum chamber located at DFL is presented in Figure 43. A modified ladder was built and fixed in the chamber to allow the mounting of accelerometers on the mast. Figure 44 is a photograph of the structure in the chamber, looking downward.

The hydraulic exciter (Figure 45) was designed and built by DFL/CRC personnel in mid-seventies for testing a CTS solar array and was refurbished and slightly modified for testing the Astromast. Figure 46 shows the linear/rotational Motion Mount mechanism with the Astromast fixed in linear displacement position.

In this test configuration, the base acceleration is used as the input measurement, and thus the remarks of chapter 4.3.4 concerning the limitations of MODAL-PLUS processing apply also.

4.4.2 Test Results

As an initial check of this configuration, the following two accelerometer locations were instrumented: 26III (longeron 3, 26th bay, x or y direction) and end plate (42nd bay). Because of generally poor quality of the results, a full survey of the structure (24 locations) was eventually discarded.

Except for one run with random input, the driving force profile was a sine sweep for which the linear sweep rate was determined using Equation 3. Because the Astromast is very flexible with a high Q factor for the fundamental bending mode, the input level was very low and varied between the first and second mode. A description of the different runs in the chamber is presented in Table 4.

Figure 47 shows typical frequency response and coherence functions for excitation in linear direction. The

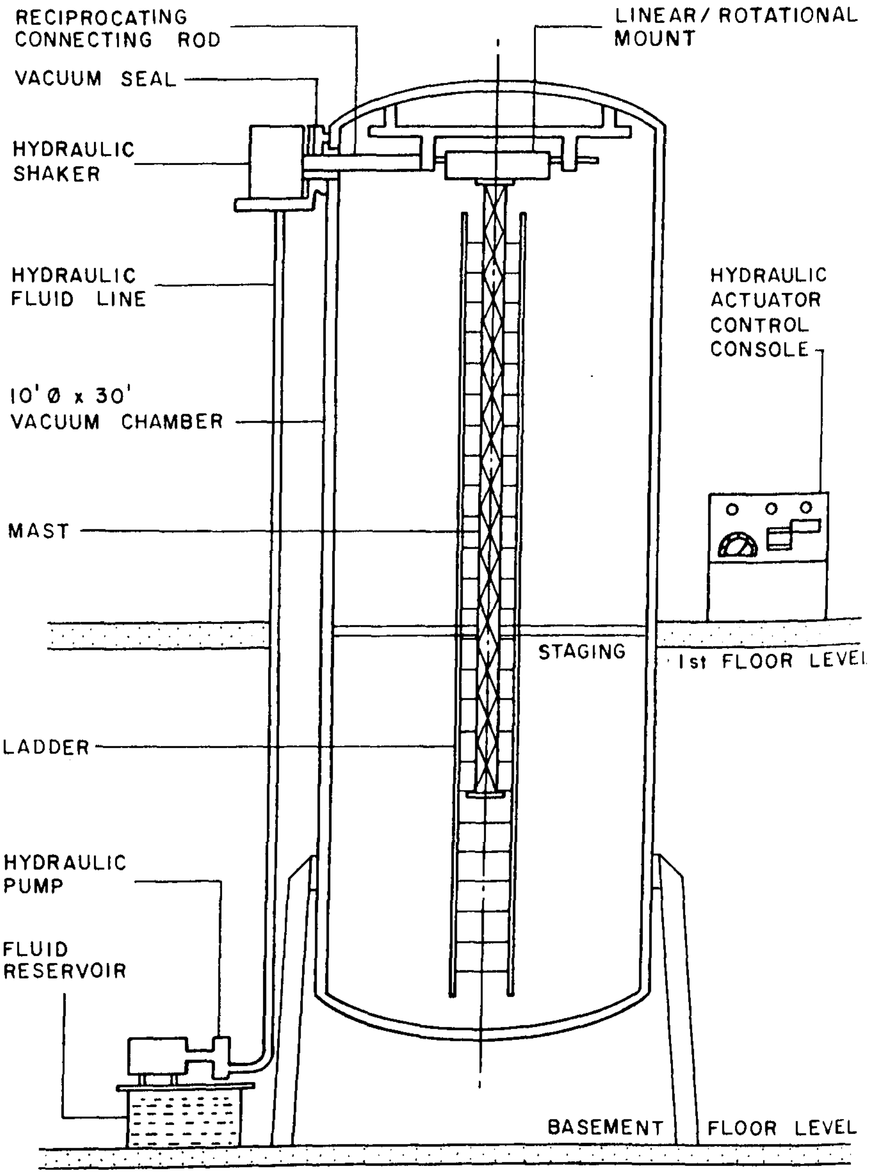

Figure 43. Astromast Vacuum Test Configuration

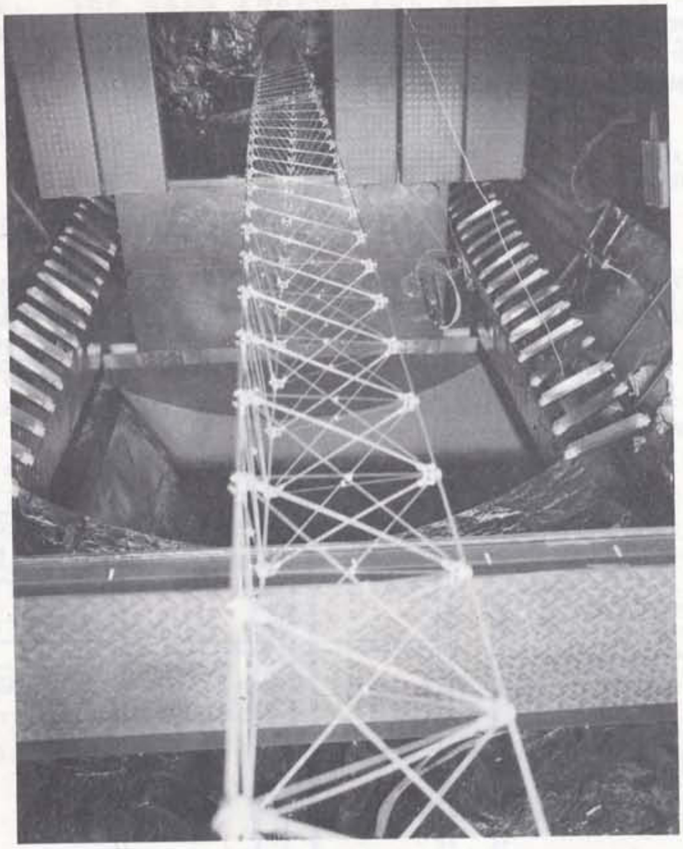

Figure 44. View of the Mast in the Chamber

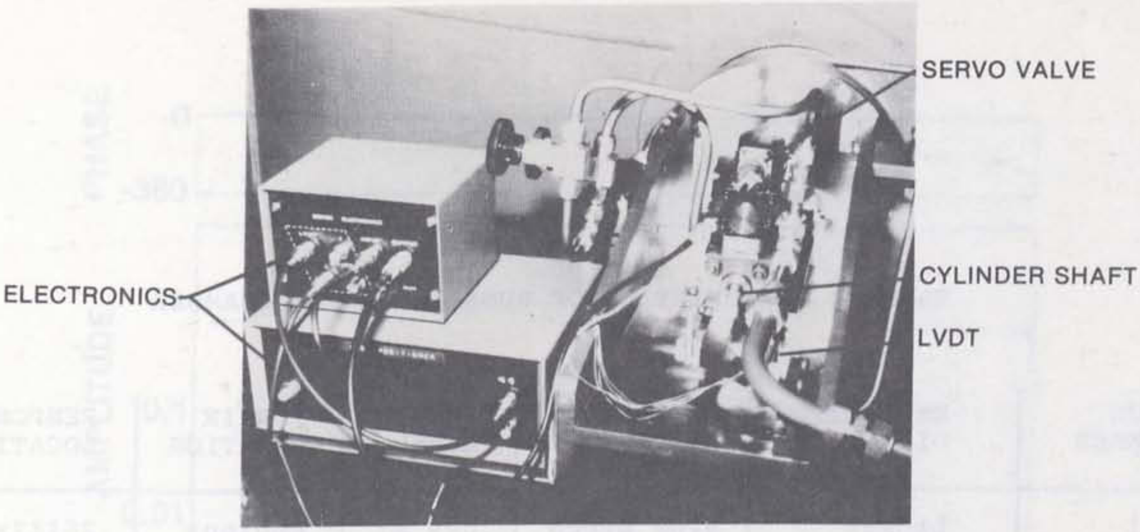

Figure 45. Hydraulic Exciter

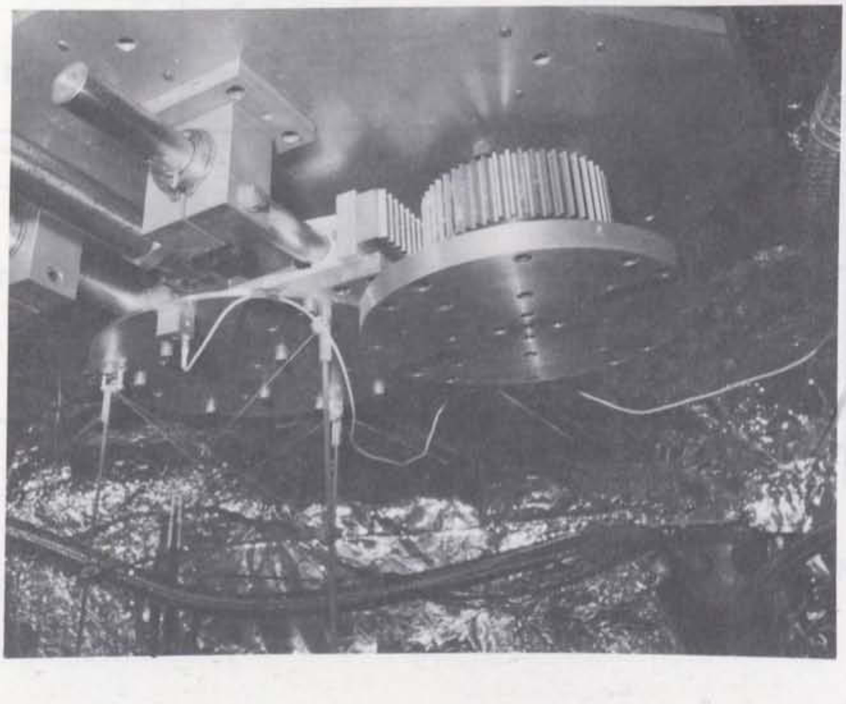

Figure 46. Linear/Rotational Motion Mount Mechanism

TABLE 4 DESCRIPTION OF RUNS IN VACUUM CHAMBER

RUN NUMBER	EXCITATION DIRECTION	EXCITATION TYPE	INPUT LEVEL	ENVIR CONDITION	RESPONSE LOCATION
1	Linear	Sine Sweep	.004 at 1.8 Hz .075 max	Ambient	26IIIx 42x
2	Linear	Sine Sweep	.004 at 1.8 Hz .075 max	Vacuum	26IIIx 42x
3	Rotational	Sine Sweep	.07 at 11 Hz .2 max	Ambient	26IIIy 42y
4	Rotational	Sine Sweep	.07 at 11 Hz .2 max	Vacuum	26IIIy 42y
5	Linear	Sine Sweep	.004 at 1.8 Hz .07 max	Ambient	26IIIx
6	Linear	Random	------	Ambient	42IIIx

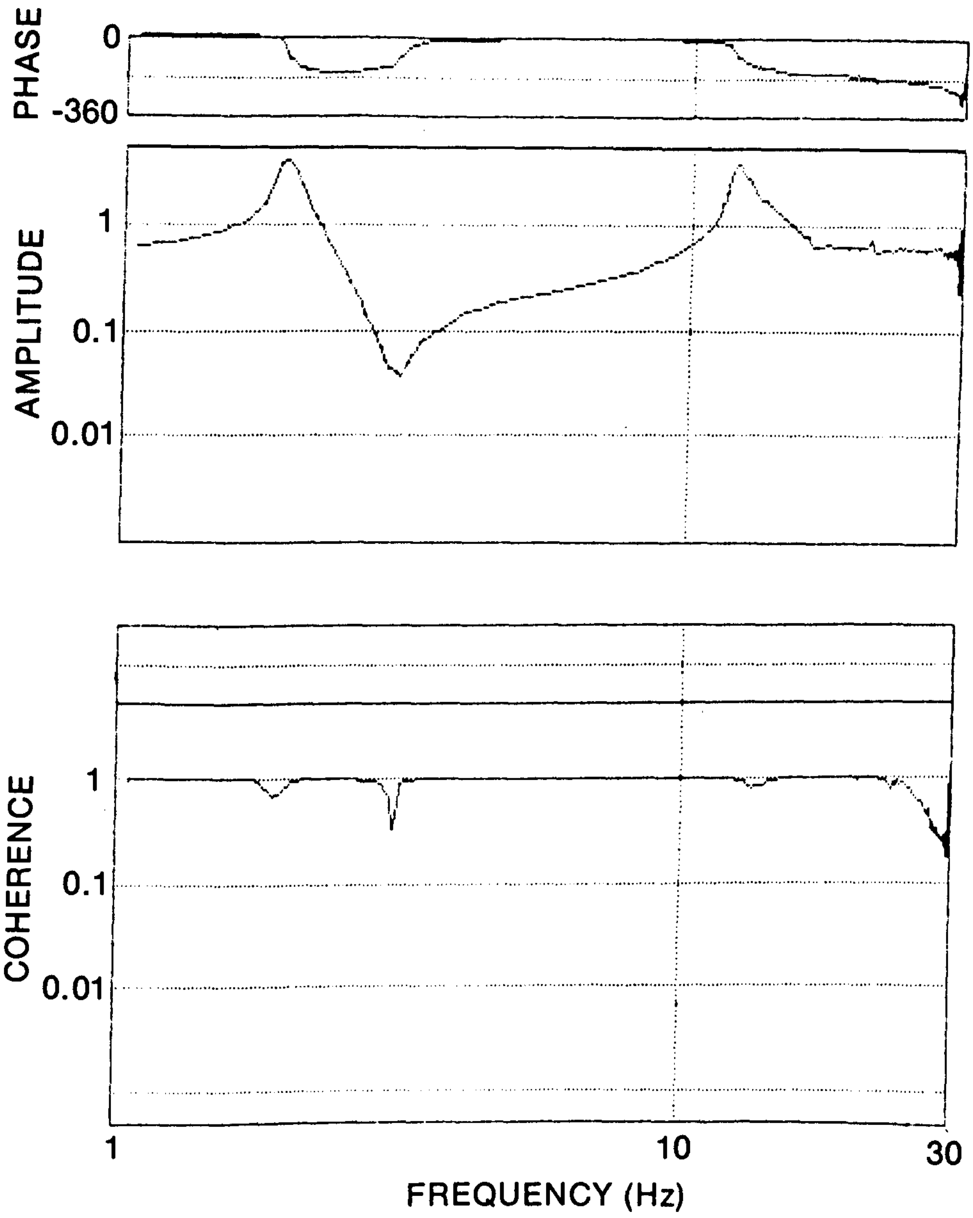

Figure 47. Frequency Response and Coherence Functions (Hydraulic Exciter, Linear Sine Sweep)

first and second modes are respectively located at about 1.9 and 11.8 Hz. The drop in the coherence function at the peaks will be discussed later.

A typical curve fit is given in Figure 48. Except for one case (run number 5), it was not possible to have a good fit of the first mode. For the second mode, some FRF's allowed very good curve fitting. It should be noted that for data taken with the hydraulic exciter, the analytical curves were synthetized from real and pseudo or calculation roots, while only real roots were used to fit data taken with the electrodynamic exciter.

Two runs were performed with rotational sine sweep input. Figure 49 presents an example of frequency response and coherence functions. The peak is located at about 10.3 Hz. It was not possible to get a good curve fit of FRF's.

For bending as well as for torsion modes, there was no significant difference between data taken in ambient and vacuum condition.

Table 5 contains the modal characteristics estimated from data obtained with the hydraulic shaker. As the number of samples indicates, an FRF could often be used to obtain an estimate of the frequencies though not the damping, (either by cursor or analytical curve) even if the curve fitting was not good. The only estimates of damping ratio for the first and second bending modes were obtained with the same frequency response function which was generated by a sine sweep input having a constant g level throughout the frequency range of the first peak. For all other runs, the input level varied within that frequency range. Also, the relatively good fit of the first peak could only be obtained by using an SDOF algorithm (Figure 50). As can be seen, the frequency and damping ratio estimates of the second bending mode agree very well with the values presented before for random excitation with the electrodynamic exciter.

4.4.3 Discussion

The following presents observations made during testing which explain, at least partly, the poor results obtained with the hydraulic exciter.

The main problem was caused by the very high flexibility of the Astromast. To avoid structural damage, the maximum free end displacement of the mast was limited to 2.5 cm. The selection of this value was based on in-house calculations. At the first bending mode (1.8 Hz), this

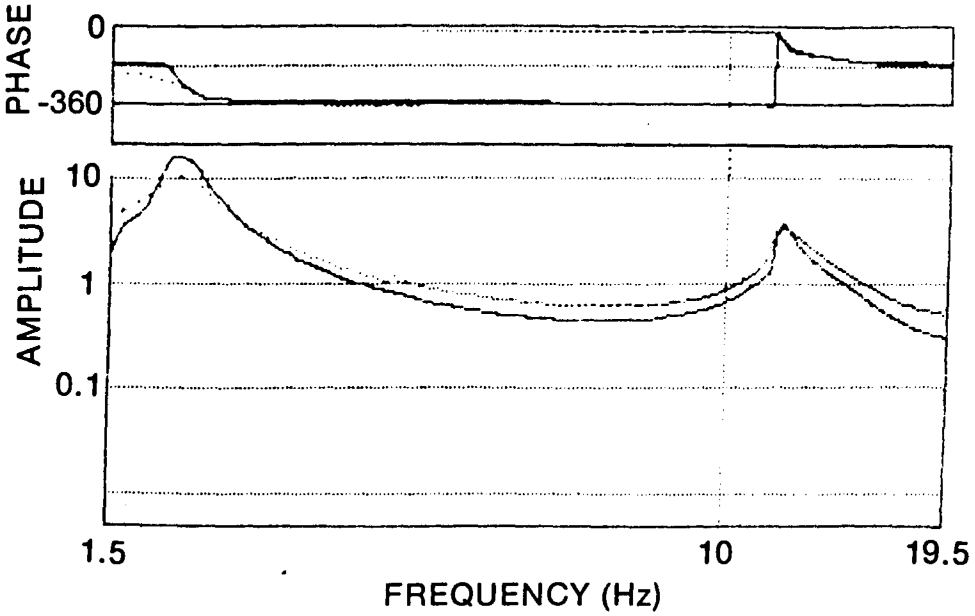

Figure 48. Curve Fit (Hydraulic Exciter, Linear Motion)

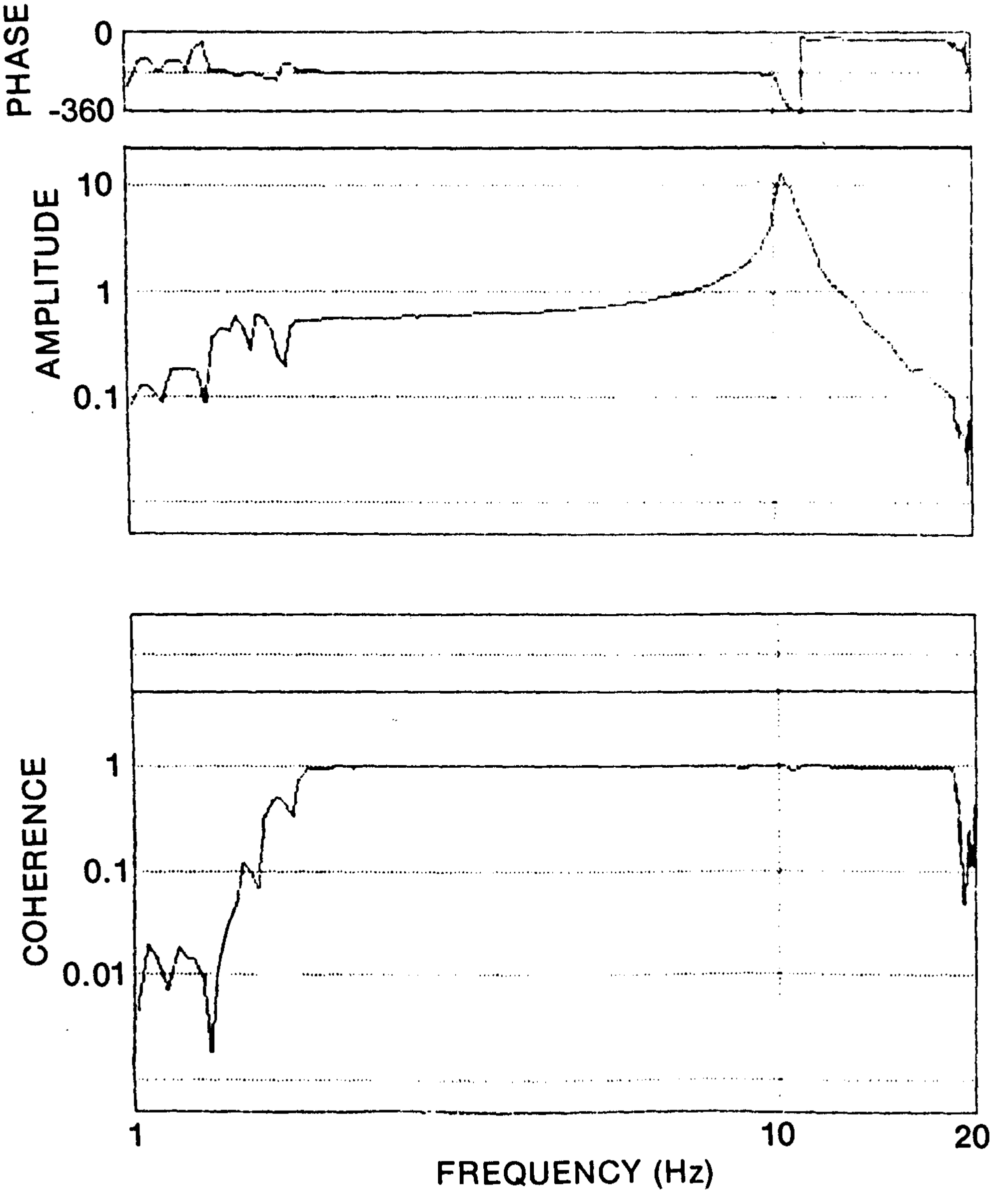

Figure 49. Frequency Response and Coherence Functions (Hydraulic Exciter, Rotational Sine Sweep)

TABLE 5 ESTIMATED MODAL PARAMETERS (HYDRAULIC EXCITER)

MODE	FREQUENCY		DAMPING RATIO	
	ESTIMATE (Hz)	NUMBER OF SAMPLES	ESTIMATE (%)	NUMBER OF SAMPLES
1st Bending	1.94	3	3.5	1
1st Torsion	10.30	4	1.2	2
2nd Bending	11.90	4	3.2	1

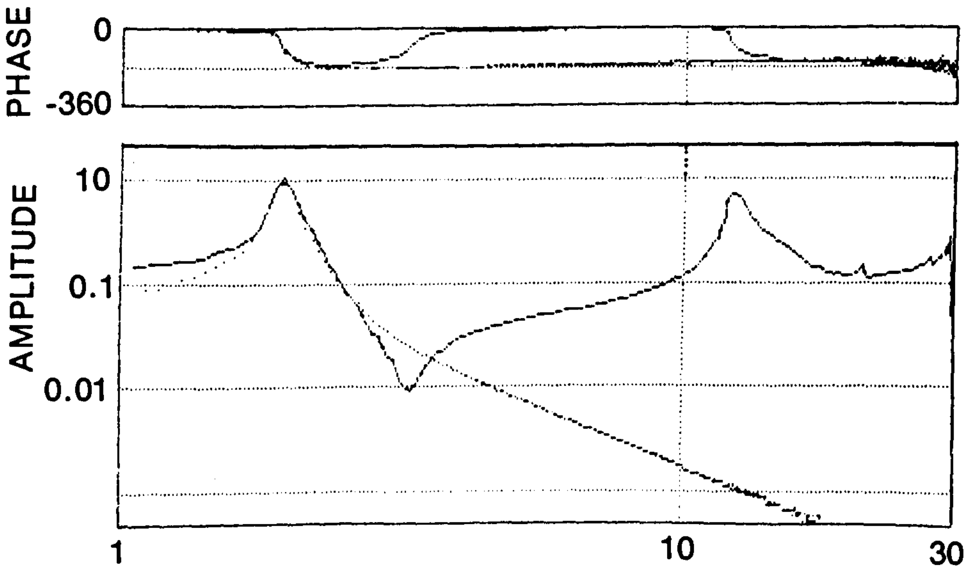

Figure 50. SDOF Curve Fit (Hydraulic Exciter, Linear Motion)

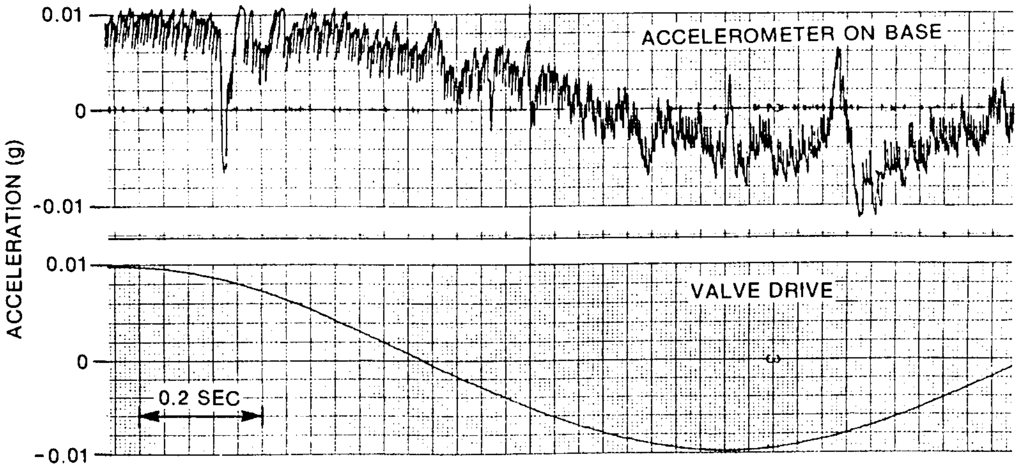

Figure 51. Signals from Hydraulic Exciter at 0.5 Hz

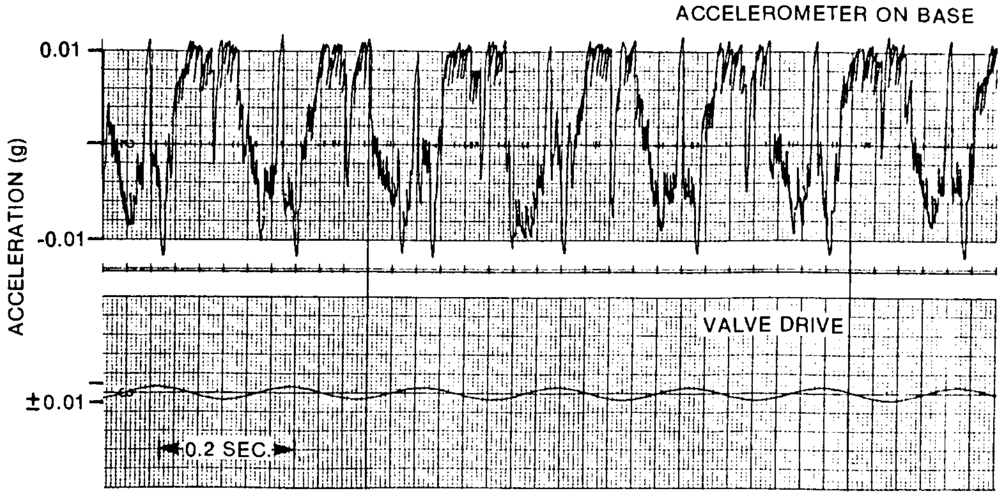

Figure 52. Signals from Hydraulic Exciter at 5 Hz

limited the input peak-to-peak displacement at the very low value of about 1 mm. At such a low input level, the signal transmitted to the mast through the slip table is very noisy. Independent tests were performed to investigate the noise performance of the exciter. Figure 51 contains a sample of two different signals for an 0.01 g sine input at 0.5 Hz. The clean signal (lower trace) is from the valve drive while the top one is the acceleration measured on the slip table. The same signals are shown in Figure 52 for a 0.01g input at a different frequency of 5 Hz. The observed continuous noise is produced by the linear bearings of the slip table, and the spikes are caused by backlash occurring at the ends of the connecting rod located between the slip table and the cylinder shaft.

After the tests with the exciter were done, it was discovered during a static test (to be detailed later in the report) that the mast exhibits a non-linear behaviour at a displacement much below the allowed 2.5 cm. Also, it was observed during step relaxation tests that, for the range of displacement of 2.5 cm, the compressed longeron at the fixed end was buckling along a few bays. The non-linear behaviour, which is incompatible with the linear theory of modal analysis, likely explains part of the problems encountered in curve fitting of the first bending mode.

There is a drop in the coherence function at the peaks, especially the one corresponding to the first bending mode. The resolution in acquiring one FRF was increased in the frequency range of the first peak. As expected, the coherence raised from 0.57 to 0.84. This indicates that the lack of resolution was at least one of the causes of the drop in coherence. However, contrary to what happened when this was done on data taken with the electrodynamic exciter, this increase of resolution modified substantially the shape and amplitude (so damping) of the first peak.

During the initial runs, it was found that the mechanism in the mount which pertains to torsion is very noisy. Thus, additional input noise was transmitted to the mast during rotational excitation. It was found from a later torsional test that the structure was excited into its non-linear region during vibration.

4.5 Impact Test in Torsion

Test using a impact force hammer was performed mainly in order to confirm the first and second torsion modes.

4.5.1 Test Configuration

The Astromast was hung upside down along a structural column at DFL. The top end plate was completely fixed. The lower end of the mast was attached to a fixture which allowed torsion, but had no degree of freedom in translation. This free end in torsion was attached to a linear bearing mechanism that allowed longitudinal (vertical) motion caused by a change in length of the structure while rotating (initially, this configuration was set up for static test in torsion, which will be described later).

A PCB impact hammer (model no. 086A03) was used to excite the structure. A rubber tip was chosen to keep the input energy in the low frequency range. The tip caused the input spectrum to roll off at about 100 Hz. A PCB quartz force transducer (series 208A, 44 N max. force) was incorporated in the head of the hammer to measure the force impacted to the mast.

The input and output channels for DATM were respectively connected to the force transducer and the accelerometers. This configuration of test is modelable directly with Eq (1), and is thus within the scope of operation of MODAL-PLUS.

4.5.2 Test Results

The impact was performed by mounting a very limited number of accelerometers and hitting the structure at many locations. For impact excitation, the fixed response measurements are considered as the references. In the present test, accelerometers were mounted along the tangential direction at the following locations: 9y (level C) and 10y (level D). The mast was hit tangential at four locations: 15y (level E), 12y (level D), 9y (level C) and 6y (level B). Five samples were taken and averaged for each input location.

In general, the quality of data was quite poor. The main reason is the high flexibility of the structure which provokes impedance mismatch and other problems. The frequency response function for input at 15y and response at 10y is shown in Figure 53. The first peak at 11.0 Hz corresponds to the first torsion mode. As can be seen, some problems occur in the phase diagram right after the peak. The second peak located at 33.2 Hz corresponds to the second torsion mode. At this peak, a significant phase shift with respect to that expected (±90°) occurs. The phase shift turned out to be a general problem with frequency response functions obtained with the impact test.

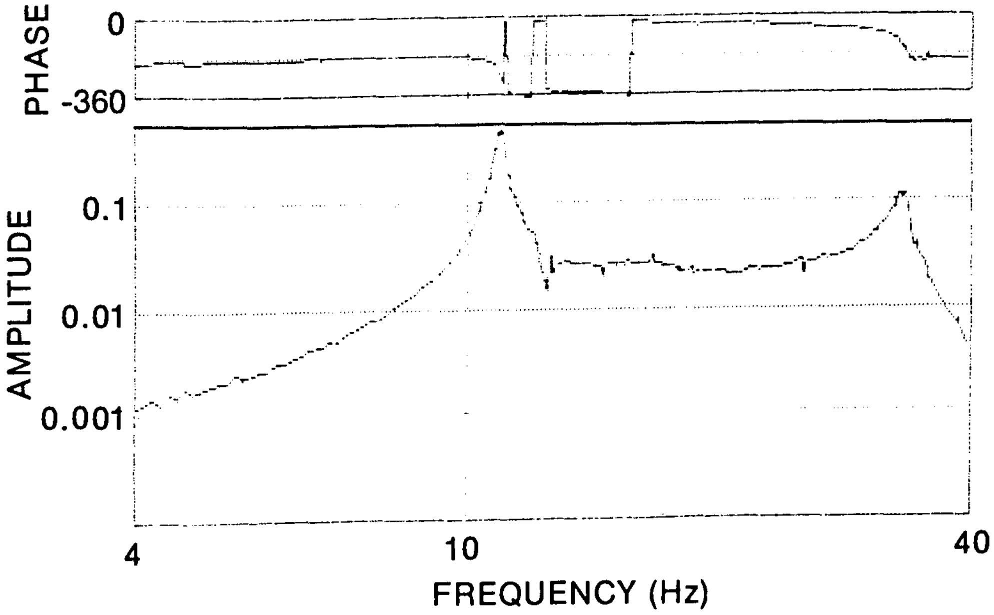

Figure 53. Frequency Response Function (Impact, Input at 15y)

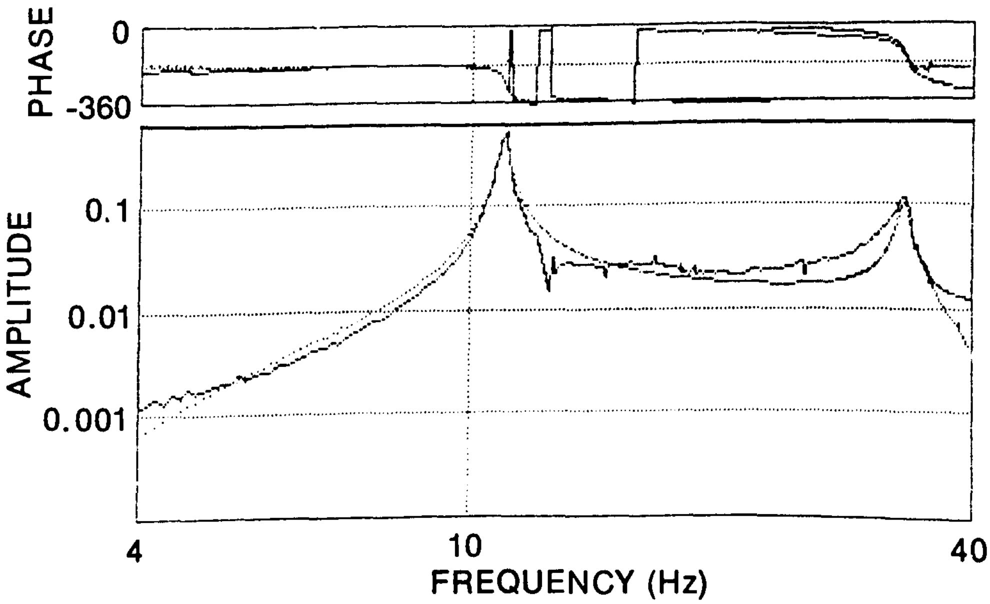

Figure 54. Curve Fit of First Mode (Impact, Input at 15y)

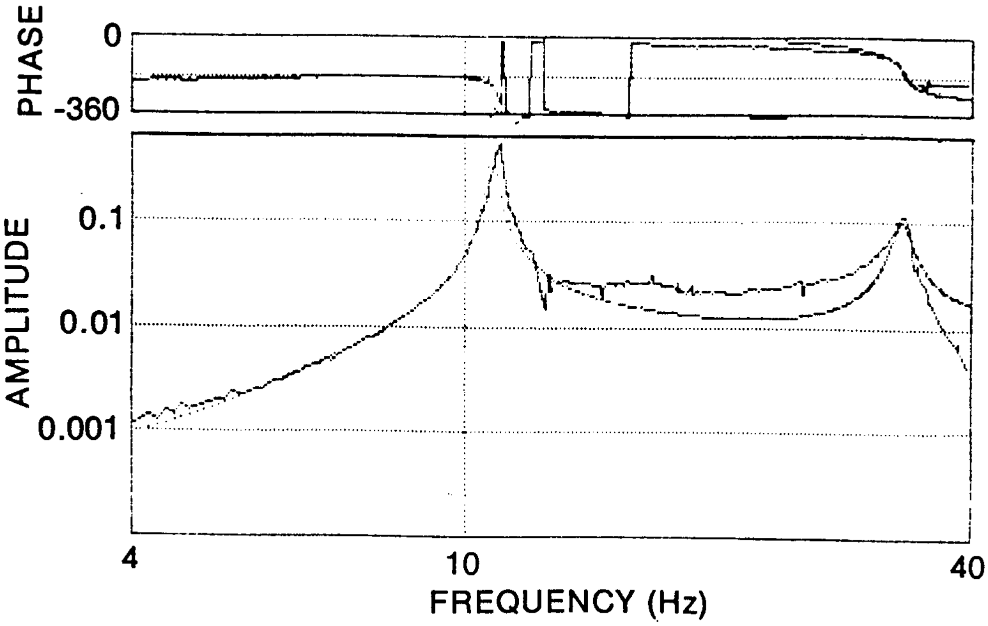

Figure 55. Curve Fit of Second Mode (Impact, Input at 15y)

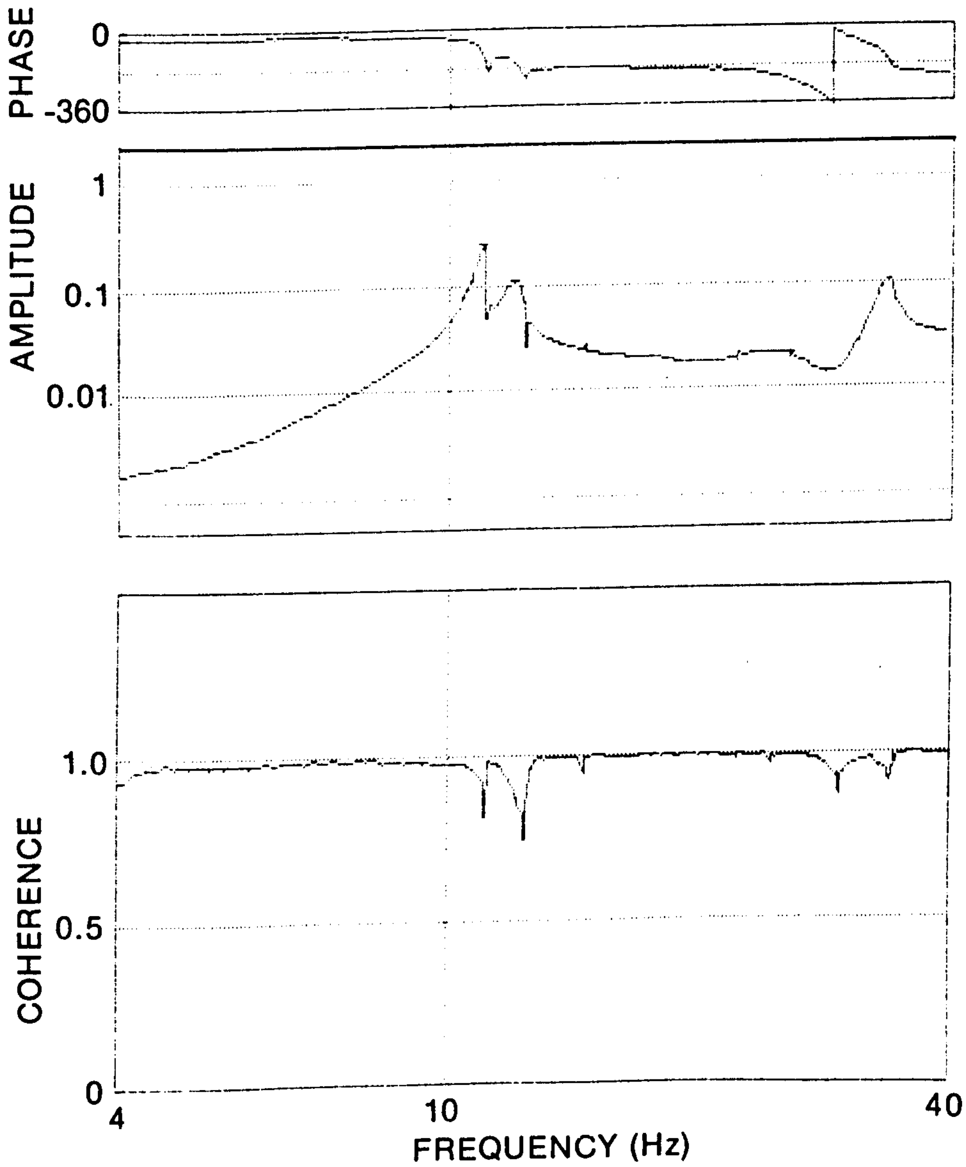

Figure 56. Frequency Response Function (Impact, Input at 12y)

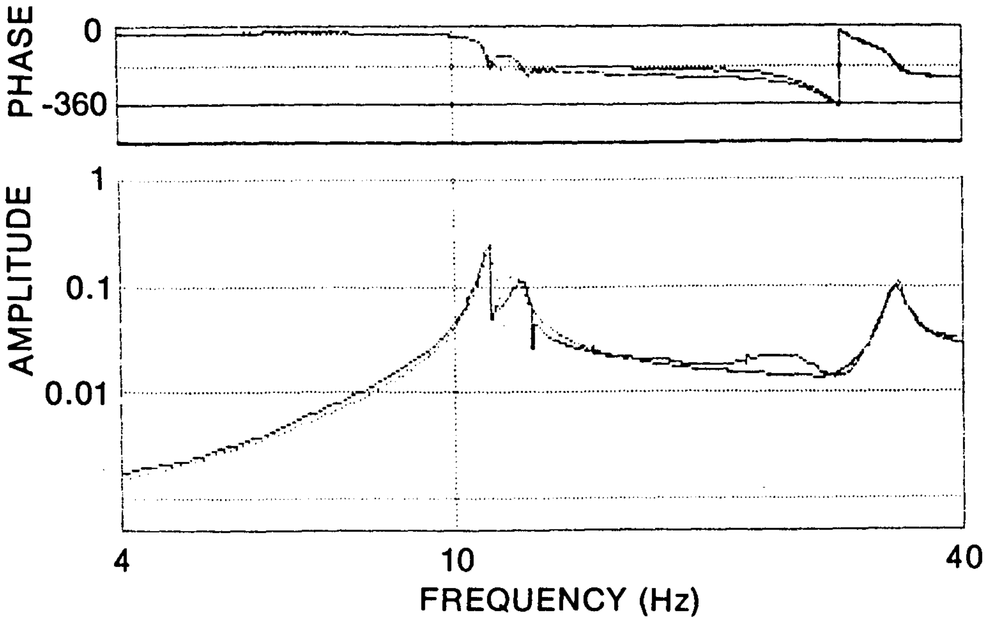

Figure 57. Curve Fit of Second Mode (Impact, Input at 12y)

TABLE 6 ESTIMATED MODAL PARAMETERS (IMPACT TEST)

TORSION MODE	FREQUENCY		DAMPING RATIO	
	ESTIMATE (Hz)	NUMBER OF SAMPLES	ESTIMATE (%)	NUMBER OF SAMPLES
1st	10.9	5	1.3	1
2nd	33.7	6	2.4	3

The curve fit of this FRF is presented in Figure 54. This is the only case for which a good fit of the first peak was possible. The second peak could not be curve fit very well. However, a relatively good fit was obtained by using less roots to generate the analytical curve (Figure 55). The best results were obtained when the mast was impacted at the end plate level.

The following explains how the analytical curves were generated (the technique was the same for all test configurations except for the hydraulic exciter). The roots of the analytical curve that best fit the experimental data are first calculated. At this step, the operator decides the number of roots to be calculated. Next, the pseudo or mathematical roots are identified and eliminated; this identification is done by comparing the roots to previous knowledge of modal characteristics of the structure. The pseudo roots, are usually those having unreasonable values of damping, amplitude and/or phase. Finally, the analytical curve is generated using only the remaining real roots.

Figure 56 shows the frequency response and coherence functions for input located at 12y and response at 9y. A drop in the coherence value can be seen at the peaks; this phenomenon occurred in almost all FRF's. A second peak has emerged at 11.9 Hz and corresponds to the second bending mode. The second torsion mode is apparent at 33.7 Hz. A good curve fit of the second torsion mode was obtained for this FRF (Figure 57). The frequency response function associated with input location 10y was too noisy and of too poor quality to be of any use. This can be explained because the input was at the same level as the response, thereby causing a lot of noise to be transmitted through the three battens.

Table 6 presents dynamic characteristics of the first two torsion modes as obtained with impact test. The very small number of samples used to evaluate damping ratios is a result of the generally poor curve fits.

4.6 The Step Relaxation Method

The previously-described tests did not obtain parameters satisfactorily for frequencies below about 2 Hz due to input noise problems or lack of control of the exciter. To obtain the low frequency parameters, the Step Relaxation technique described herein was implemented. This chapter outlines the technique and main results; additional detail on some aspects is available in Reference 9 and 12.

4.6.1 Concept and Configuration

For Step Relaxation, the input excitation is achieved by initially applying a single force to deform the structure statically at one or more restraining boundary points, and then releasing the force suddenly. The response accelerations at a number of points and the initial force are measured before, during release, and after release as the structure oscillates freely and damps to a motionless state.

The equations that model the system are not directly in the form of Eqs (1) and (2). However, with appropriate mathematical manipulation, the model can be represented as [9]

$$\frac{\dot{a}_j(\omega)}{\bar{\dot{f}}_k(\omega)} = \omega^2 \bar{H}_{jk}(\omega;\ \omega_r,\ \zeta_r,\ \alpha_r\ \ \psi_{jr}) \qquad (4)$$

Hence, a measurement-based impulse response function can be constructed from the Fourier transforms of the derivatives of the accelerometers and force measurements. The various curve fit routines of MODAL-PLUS can then be used to fit the analytical H of Equation (2) to the measurement-derived H, and so identify the parameters.

The SDRC software was modified by SDRC (Dr. Gordon Mutch) in collaboration with the authors for this exercise [12]. Figure 58 illustrates the functions of the software. First, the experimental setup, is configured to apply the force, f_1, to the structure. The force is applied and released (upper chain). The response, a_i and f_1 are acquired, and digitized. They are then differentiated using simple difference algorithm, to obtain $\dot{f}_1$ and $\dot{a}_i$. The Fast Fournier_Transform routines then are used to construct the column, $\bar{\dot{a}}_i(w)/\bar{\dot{f}}_1(\omega)$, which from Eq.(4) is a measurement-based representation of the column, $\omega^2 \bar{H}_{i1}(\omega)$. f_1 may be reapplied several times, the acquisition/preprocessing repeated, and the resulting multiplesamples of $\omega^2 \bar{H}_{i1}(\omega)$ averaged. With reconfiguration of the experimental setup, other single forces, f_k, can be applied sequentially, and the preprocessing repeated to obtain additional columns, $\omega^2 \bar{H}_{ik}(\omega)$ (second chain). At this stage, the graphs of elements of the matrix can be screened visually, and linearity (reciprocity) can be checked. The polyreference software of MODAL-PLUS is then invoked; i.e. the $\omega^2 \bar{H}(\omega)$ matrix is then converted to the time domain, H(t), and the complex expontials technique is used to identify the modal parameters.

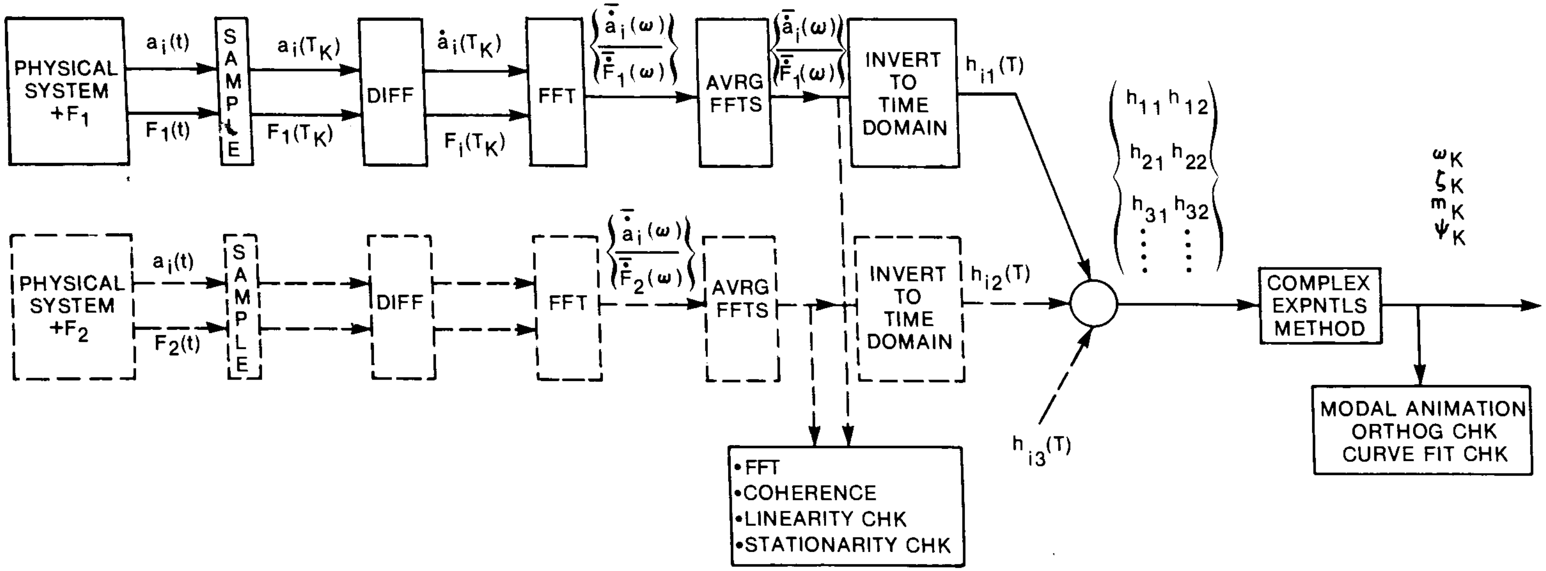

Figure 58. Functional Diagram of the Software for Step Relaxation

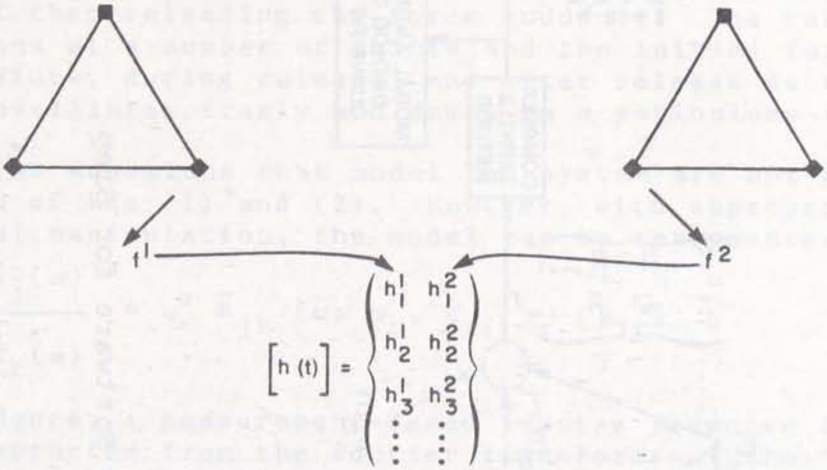

Figure 59. Configurations of Forces f^1 and f^2

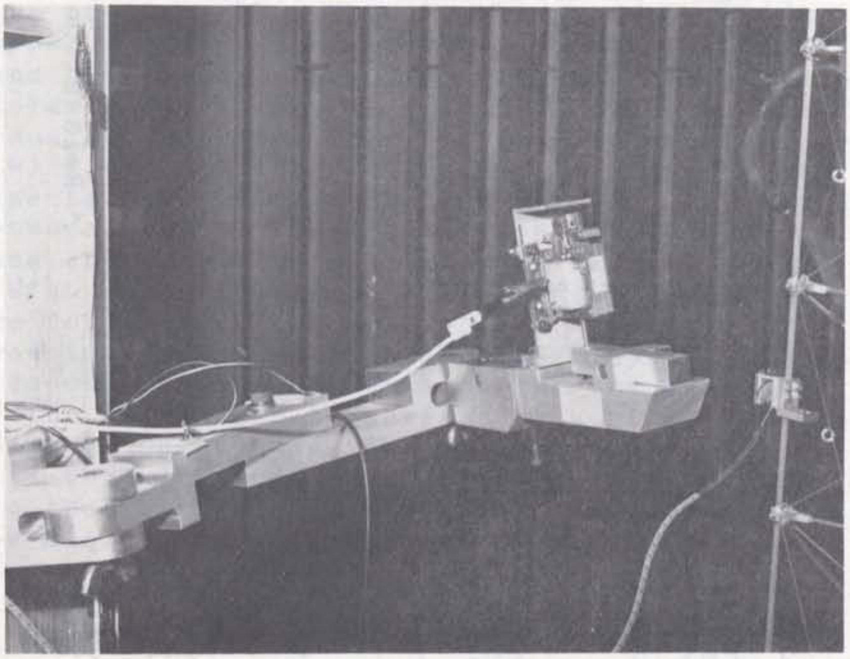

Figure 60. The Force Application - Release System

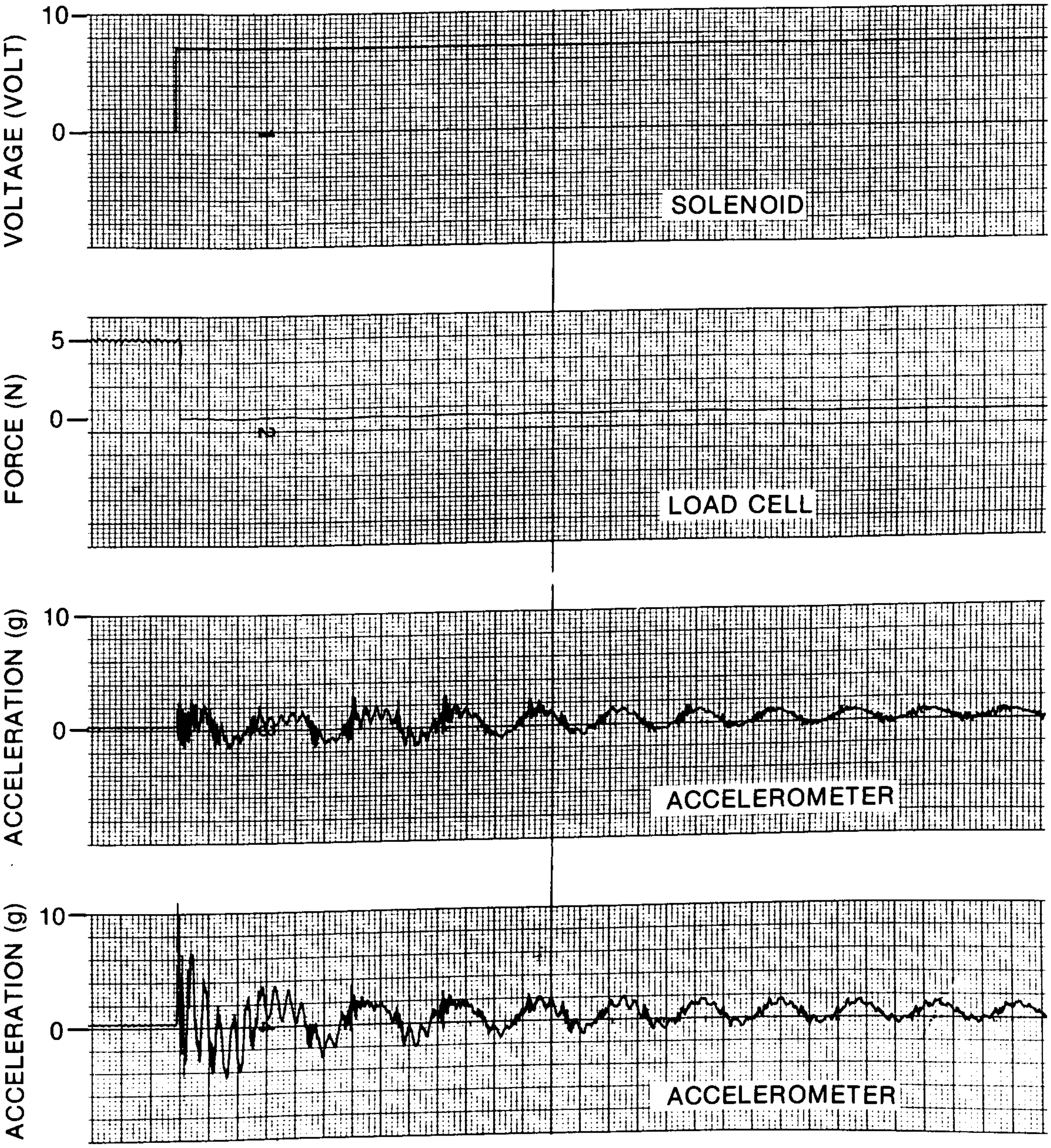

Figure 61. Strip Chart Taken During a Typical Release

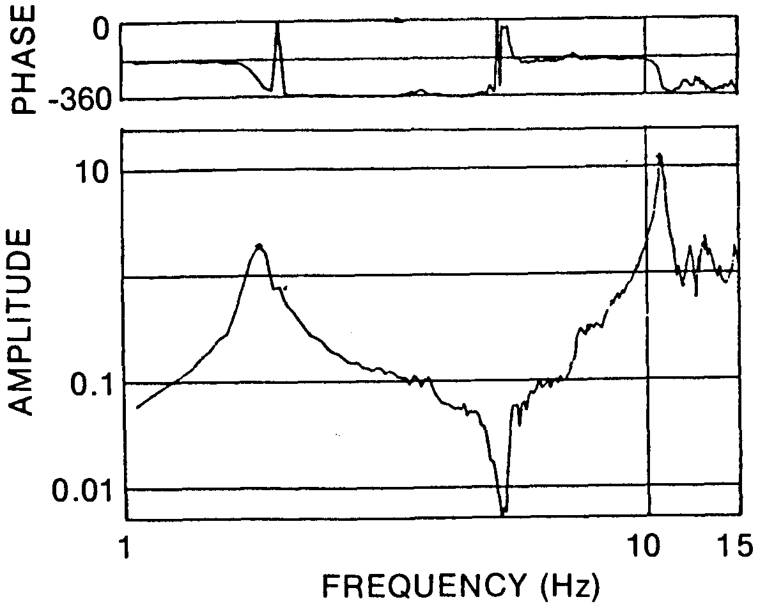

Figure 62. $\bar{\dot{a}}_i(\omega)/\bar{\dot{f}}_i(\omega)$ Average of Three Load Releases

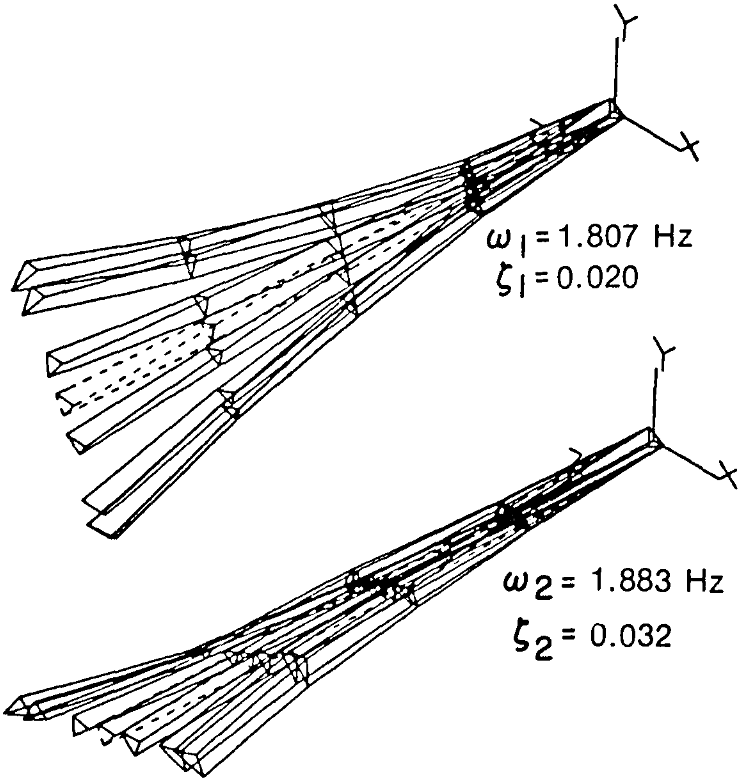

Figure 63. Animation of the First Two Modes

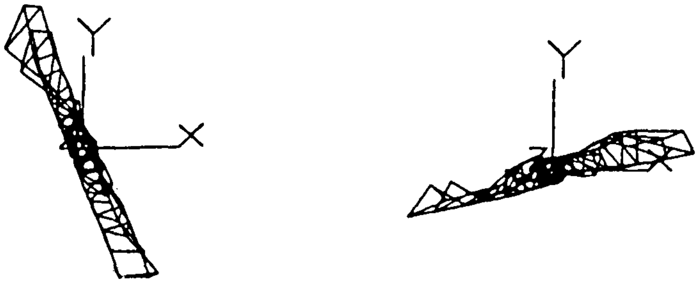

ω_1 = 1.807 Hz

ω_2 = 1.883 Hz

Figure 64. End View of the First Two Modes, Showing Orthogonality

4.6.2 Data Acquisition and Results

Data was acquired for the two configurations of force depicted in Figure 59. The configurations create data containing information on torsion and X and Y transverse bending deformations. An apparatus, shown in Figure 60, for release of the load using a solenoid-activated release mechanism was designed. The load cell made from a strain gaged U section is also shown in Figure 60.

Response accelerometers were mounted at the locations depicted in Figure 12. The accelerometers were limited to two per test run in order to avoid cable and mass loading effects leading to nonstationary problems. A strip chart taken during a typical release is shown in Figure 61. A typical element of H(ω) is shown in Figure 62.

The first bending modes in the X and Y directions were jointly identified successfully, and are depicted in Figure 63. The results demonstrate the ability of the complex exponentials technique to separate two very closely-spaced modes. The damping factors are noted to be slightly different, and further the two modes are seen to be orthogonal to each other (Figure 64).

The technique in its state of development reported herein was not able to identify the next cluster of three closely-spaced modes in a stable conclusive manner. These modes are the first torsion and second X and Y bending modes, known to be approximately 11 - 12 Hz and evidenced in Figure 62.

4.7 Summary of Frequencies and Damping Values from Tests

To conclude this chapter, the results obtained from the four different excitation techniques are compared, and, the best estimates of modal parameters (frequency and damping) associated with the excited modes are chosen. The four different techniques (electrodynamic shaker, hydraulic shaker, step relaxation and impact hammer) led to four bending and two torsion modes.

The estimates of parameters for the first bending modes obtained from the hydraulic exciter and step relaxation agree relatively well with an average difference of less than five percent. Data associated with the first torsion mode, either obtained with the hydraulic exciter or the hammer, are quite poor even though the agreement between the two techniques is quite high (especially for frequency). Estimation of frequency and damping of the second bending mode was obtained from three different types of excitation (random burst and sine sweep with electrodynamic exciter, and hydraulic exciter). There is an almost perfect agreement for the frequency value while the damping estimate of the random electrodynamic tests is the best. The parameter estimation of the other modes were obtained with only one type of excitation.

Table 7 shows the best estimates of frequency and damping values for these modes. The numbers in the quality of estimation columns have the following significance: 1 - very good; 2 - good; 3 - fair; 4 - poor. This quality number is based on different factors: number of samples, standard deviation, type of excitation and frequency (re: preliminary tests), additional checks. Although this kind of qualification is subjective, the relative quality of estimates from different techniques is consistent.

TABLE 7 BEST TEST ESTIMATES OF FREQUENCY AND DAMPING VALUES

ORDER AND TYPE OF MODE	SET-UP	FREQUENCY		DAMPING RATIO	
		ESTIMATED VALUE (Hz)	QUALITY OF ESTIMATION	ESTIMATED VALUE (%)	QUALITY OF ESTIMATION
1st Bending	Step Relaxation	1.81 1.88	1 1	2.0 3.2	1 1
1st Torsion	Hydraulic Shaker (Sine Sweep)	10.3	3	1.2	4
2nd Bending	Electrodynamic Shaker (Random)	11.9	1	3.1	1
3rd Bending	Electrodynamic Shaker (Random	27.6	2	5.8	2
2nd Torsion	Impact	33.7	3	2.4	3
4th Bending	Electrodynamic Shaker (Random)	45.9	2	8.5	3

5.0 STATIC TESTS IN TORSION AND BENDING

An extensive static test was performed on the Astromast to determine the stiffness in bending and torsion, the limits of linearity, and information on static structural hysteresis.

5.1 Test Set-ups and Procedures

The Astromast was hung upside down from a column in the DFL. Figure 65 shows the set-up for torsion loading. The angular displacement was measured by a high precision rotary transducer which produced a voltage as output (100 mv/degree). The transducer was connected to the mast through two shafts which were joined with a mechanism that was designed to allow longitudinal movement without lateral displacement. The mechanism was composed of a flexible coupling attached to a linear bearing. The torque was produced by weights attached to a string which pulled the structure horizontally through a pulley.

The mast was loaded and unloaded in increments by adding and removing weights. Careful manipulation avoided errors caused by impact. The Astromast is designed with a 93° helix angle, and the torque was applied in the same direction as the twist (torsion) and in the opposite direction (torsion C) to verify that the stiffness was the same. Several sets having different maximum load were taken: for torsion, the maximum weights were 2000, 200, 150 and 100 grams while an extra set with a maximum of 250 grams was added for torsion C. The first set (2000 g) was aimed at determining a value for the limit of linearity. For averaging purposes and to increase reliability of data, at least three samples were obtained for each set.

In bending configuration, the mast was suspended as a cantilever and was completely free to move at the lower end (Figure 66). A laser system was used to measure linear displacements along the force direction. The readout presented displacement directly in inches. The string was attached to the centre of the end plate and went around a pulley which, to allow potential small movement in perpendicular direction, was mounted on a linear bearing moving along a hardened steel shaft.

The mast was pulled in three different directions since it appeared reasonable to believe that the rigidity of the structure would be slightly variable with direction. Different sets were performed, in each direction, with maximum loads of 400, 300, 200, 150, 100 and 65 grams. As for torsion, at least three samples were taken for each set.

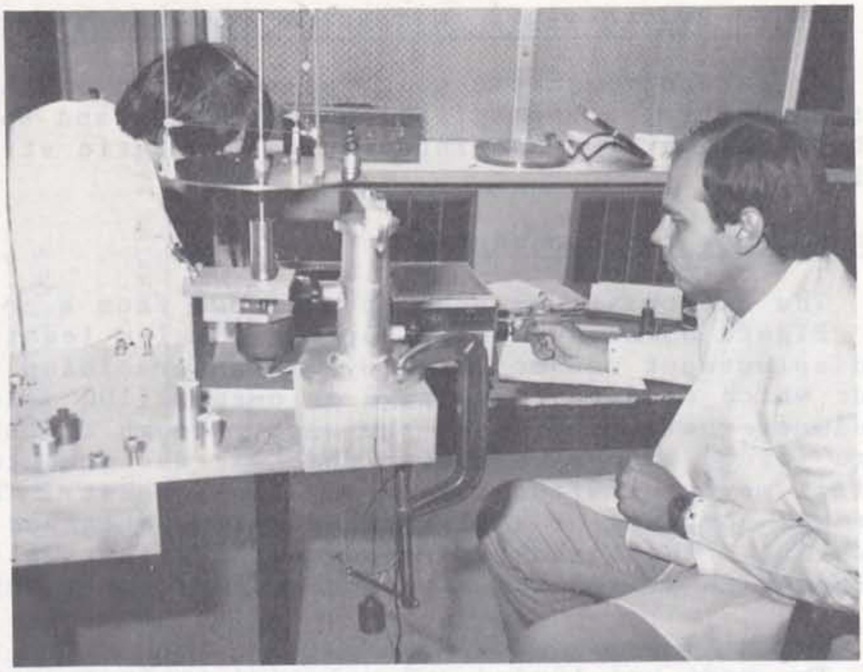

Figure 65. Static Set-Up For Torsional Loading

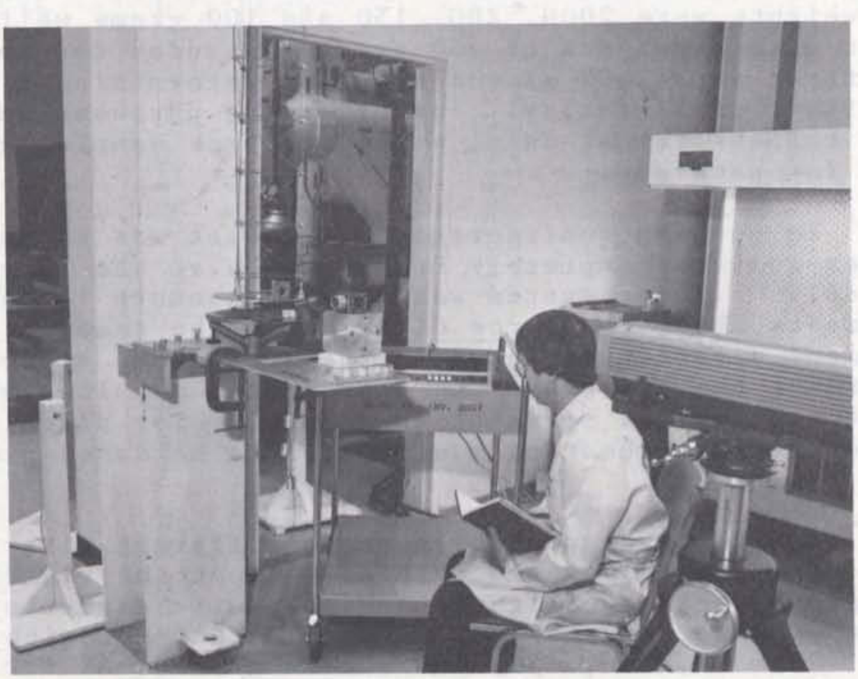

Figure 66. Static Set-Up For Lateral Loading

5.2 Test Results

Figures 67 and 68 are examples of torsional loading-unloading curves. Each sample contains between seven and eleven points in each direction; this is more than enough to obtain a valid estimation of an individual slope. The six samples with the maximum mass of 2000 g showed the limit of linearity as being 200 g for torsion and 250 g for torsion C. The remaining samples confirmed this estimation by producing straight lines for the loading part of the curves. Explanations will be given later on the significance of the results for the unloading portion of the curves.

The results are given in Table 8. Each of the 22 samples have very consistent points as shown by their coefficient of correlation being between 0.9997 and 0.9999 (the value is 1.0 for a perfect straight line). Torsional stiffness GJ/L is given by the equation.

$$GJ/L = FR/\phi \qquad (5)$$

where G is the shear modulus, J is polar mement of inertia, L is length of the mast, ϕ is angle of twist, F is force, and R is distance between F and the central axis.

Within the constant R, the stiffness corresponds to the slope of the load vs displacement plot. As the standard deviations show, the values given by the samples are very consistent with each other. From the results, one can conclude that torsional stiffness in the structural twist direction is the same as the one in the inverse direction; the only change is a slight difference in the limit of linearity.

Examples of loading-unloading curves for static bending are given in Figures 69 and 70. The limit of linearity, which corresponds to the end of the initial straight line turned out to be much lower than expected. It varies with the direction of the load and from one sample to another. Figure 70 is a good example of what happens in the loading part of many curves: two almost parallel straight lines are connected together by a short intermediate curve. Conservative values for limits of linearity would be 100 g (8 mm) from 0° angle, 50 g for 90° and 55 g for 180°. Maximum displacement of a cantilever beam is given by

$$\delta = \frac{FL^3}{3EI} \qquad (6)$$

from which the flexural rigidity EI is obtained:

$$EI = \frac{FL^3}{3\delta} \qquad (7)$$

Thus, the rigidity is given by the slope of the initial line of the load-displacement graph multiplied by the constant ($L^3/3$).

The results of the static test in bending are presented in table 9. Although these samples do not fall on a straight line perfectly, they are very valid data with coefficients of correlation between 0.9960 and 0.9999. The standard deviations show the consistency between the estimates of EI of different samples. The lowest rigidity is measured when the load is applied with an angle of 0°. This result is reasonable because the compressive stress in a longeron is then maximum since there is only one such member near the fixed plate, when the bending moment is maximum, in a state of compression.

In these tests, significant friction was present in the bearing of the loading mechanism, and one cannot attribute the observed hysteresis solely to the astromast.

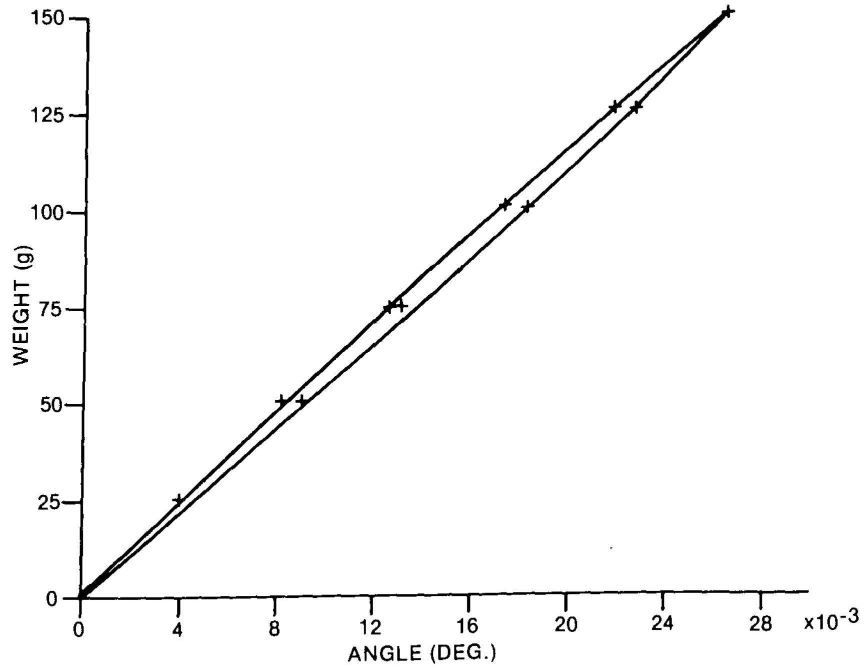

Figure 67. Example of Curve for Static Torsion

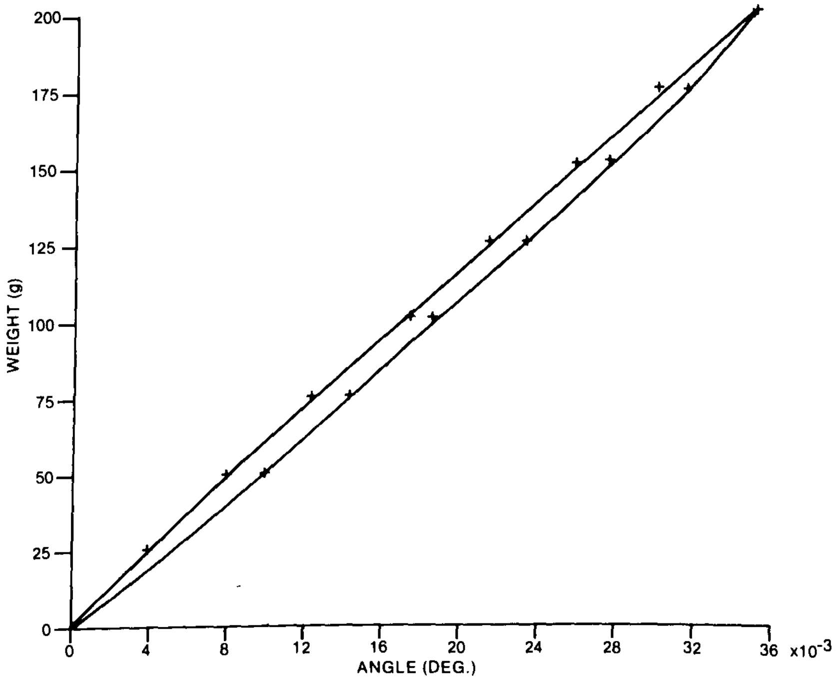

Figure 68. Example of Curve for Static Torsion C

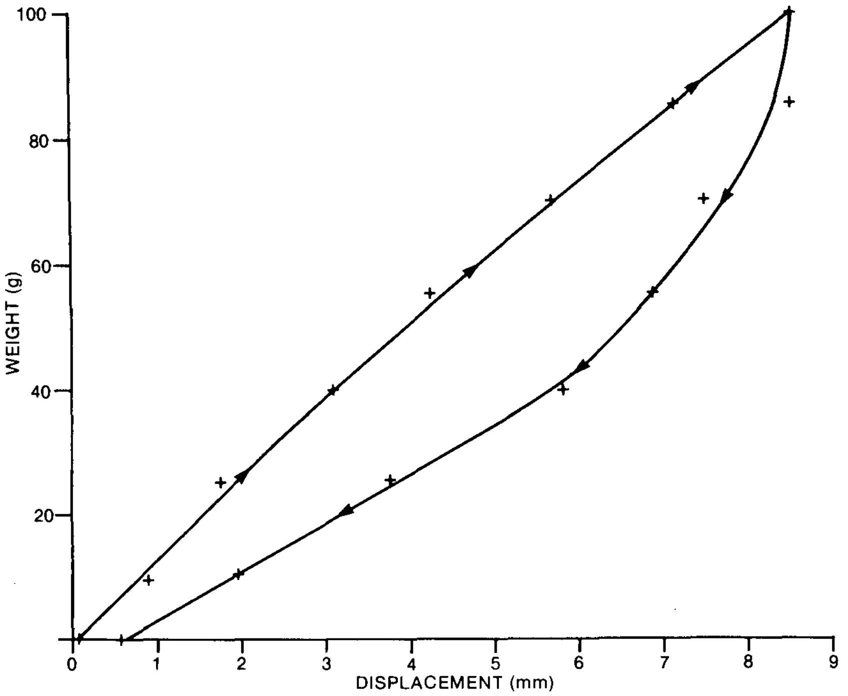

Figure 69. Example of Curve For Static Bending (θ=0°)

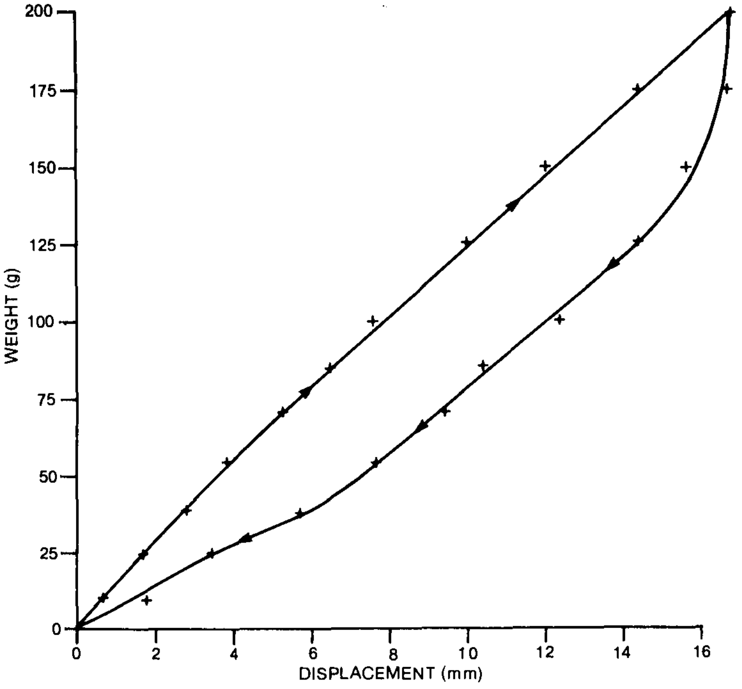

Figure 70. Example fo Curve For Static Bending (θ=90°)

TABLE 8 EXPERIMENTAL TORSIONAL STIFFNESS

DIRECTION	ESTIMATED GJ/L (N-m/degree)	STANDARD DEVIATION	NUMBER OF SAMPLES	MINIMUM VALUE OF GJ/L	MAXIMUM VALUE OF GJ/L
TORSION	0.642	0.010	9	0.631	0.658
TORSION C	0.636	0.016	13	0.612	0.662

TABLE 9 EXPERIMENTAL BENDING STIFFNESS

DIRECTION	ESTIMATED EI (x10^3 N-m^2)	STANDARD DEVIATION (x10^3 N-m^2)	NUMBER OF SAMPLES	MINIMUM VALUE (x10^3 N-m^2)	MAXIMUM VALUE (x10^3 N-m^2)
0°	9.33	0.46	21	8.61	10.22
90°	10.22	0.37	18	9.39	10.65
180°	10.30	0.60	18	9.10	11.19
AVERAGE	9.93	0.66	57	8.61	11.19

6.0 COMPARISON OF EXPERIMENTAL AND THEORETICAL VALUES

In this chapter, the experimental values of frequency are compared with calculated values obtained with two different models of the Astromast.

The first model is based on a finite element method (FEM) and was described in chapter 3. Table 10 shows the values of the main physical parameters input to the program. The longitudinal modulus of elasticity for the longerons and diagonals were measured from dynamic tests performed on available samples [2,3]. Because of their importance, the masses of the different components were evaluated very precisely at CRC. They were determined by carefully conducted weighings of the individual components and the total structure.

The second model of the Astromast is based on a continuous representation [13]. The mast was treated as slender uniform, cantilevered beam with a tip mass undergoing transverse flexural and torsional oscillations. Masses are the same as for the FEM. The flexural rigidity and the torsional stiffness needed in the model were obtained experimentally from the static tests described in the Chapter 5.

The calculated frequencies from both models are compared with the experimental values in Table 11 (the experimental values are regarded as correct and not in question). The FEM gives better agreement for bending modes than the continum model while the opposite holds for the torsion modes. The FEM produces good values for the first two bending frequencies. The continuum model calculates good approximations of the first two torsion and the first bending modes, but higher modes are in substantial error. All frequencies from the continuum model are higher than the measured values. This is likely due to the fact that such a model is more constrained than the physical system.

The general lack of agreement between the frequencies obtained from the FEM and the measured frequencies implies that the present model has some shortcomings. As it was explained in Chapter 3, the flexural as well as the torsional energy in the longerons was neglected, to save processing time and computer memory. The rationale was based on preliminary calculations which showed that the compression, tension axial energy in the longerous due to the overall bending of the mast was dominant. After further considerations, it seems that the addition of longeron flexural and torsional energies would slightly improve the model. However, the neglection of these energies is not likely to be among the main causes of the discrepancy which, at this stage, are not obvious.

The continuum model can account for gravity by treating it as an axial force. Its effect on bending frequencies is shown in Table 12. One can see that gravity has almost negligible effect on the present structure. These numbers also establish the compatibility between the experimental values for the second bending frequency obtained with the electrodynamic and hydraulic exciters.

Sensitivity analyses were also performed using the continuum model [13]. The stiffness and density of the boom, and the tip mass were the variable parameters; they were varied by ∓ 10%. For the first three bending modes, the frequency changed by 5% when the stiffness was varied. The sensitivity to boom density increase with the order of the frequency (5% variation for the third mode). The influence of tip mass decreases with the order of the frequency (3% variation for the first mode).

TABLE 10 PARAMETERS FOR FINITE ELEMENT METHOD

PARAMETER	MEASURED VALUE
EA OF DIAGONAL	21800 N
EA OF LONGERON	370000 N
WEIGHT OF FREE TIP	467 g
TOTAL WEIGHT OF THE BOOM	1082 g

TABLE 11 COMPARISON OF EXPERIMENTAL AND THEORETICAL FREQUENCIES

ORDER AND TYPE OF MODE	FREQUENCY (Hz)				
	EXPERIMENTAL	FEM		CONTINUUM MODEL	
		VALUE	% ERROR	VALUE	% ERROR
1st Bending	1.85	1.79	3	2.16	16
1st Torsion	10.3	7.76	25	12.2	18
2nd Bending	11.9	13.3	12	17.4	46
3rd Bending	27.6	35.8	30	52.9	92
2nd Torsion	33.7	25.7	24	41.6	23
4th Bending	45.9	64.0	39	---	---

TABLE 12 EFFECT OF GRAVITY ON BENDING FREQUENCIES

GRAVITY $(m\text{-}s^{-2})$	FREQUENCY (Hz)		
	1	2	3
-9.81	2.15	17.39	52.84
0	2.16	17.40	52.86
9.81	2.17	17.42	52.87

7.0 DISCUSSION AND CONCLUSIONS

Modal parameters of the Astromast were obtained from modal testing. It was possible to determine the fundamental bending modes in the X and Y directions at 1.81 and 1.88 Hz respectively, bending modes at 11.9, 27.6, and 45.9 Hz, and the first two torsion modes at 10.3 and 33.7 Hz. The values of damping ratios were between 1.2 and 8.5 percent.

Due to the high flexibility and fragile nature of the mast, no single type of excitation was able to derive the results. The following test configurations were used: electrodynamic exciter (linear sine sweep and random), hydraulic exciter (linear and torsional sine sweep), step relaxation and impact (torsion).

The structure behaves non-linearly for frequencies higher than 30 Hz and thus requires random excitation in that region. Because of the low damping and light weight of the mast, the accelerometers' masses and cables proved to have a definite effect on the results. Their number was limited to two or three at the same time on the structure.

The high flexibility of the mast caused limitations in the use of electrodynamic or hydraulic base excitation. The first bending mode could not be obtained because it required an input level too low. Random excitation turned out useless for frequencies higher than 60 Hz due to the high energy dissipation in the structure preventing sufficient accelerometer excitations.

The base excitation techniques used frequently in the space industry are compatible with SDRC's standard data acquisition and processing algorithms (DATM and MODAL-PLUS) for determination of modal frequencies. However, there is an inaccuracy with respect to modal coefficients which generate mode shapes, and possibly with respect to modal damping.

Frequency response functions of the first bending and torsion modes showed no significant differences between runs performed in ambient and vacuum conditions.

Step Relaxation proved to be an excellent technique for exciting the low frequency fundamental bending modes. The advantage of this technique is to allow the input of a good amount of noise-free energy at low frequencies. With data from two force inputs at two different locations, it was possible to separate the two closely spaced fundamental bending modes of frequency 1.81 and 1.88 Hz along the two transverse principal axes.

The experimental frequencies were compared to theoretical values obtained from a finite element model (FEM) and a continuum model. Rigidities of the structure input to the continuum model were measured during a static test. The FEM is more in agreement with the experimental values than the continuum model for bending modes while the reverse is true for torsion. The values from the FEM and tests agrees within 5 and 8% for the first two bending modes.

The results of the finite element model, especially for torsion modes, possibly might be improved by adding the contribution of flexural and torsional energy to the longerons.

8.0 ACKNOWLEDGEMENTS

The authors wish to acknowledge the technical support provided by David Florida Laboratory, and in particular Mr. Tom Steele, in setting up the instrumentation, acquiring and recording dynamic test data, processing some of these data and giving practical useful advice. Mr. John Giurgevitch of Ottawa Mouldcraft made vital contributions in designing and machining the various pieces of hardware, and in assisting in the tests. Mr. Ted Williams refurbished the hydraulic exciters, and also assisted in design of specialized equipment. Dr. Ken Lips calculated the theoretical frequencies of the mast treated as a continuum beam.

9.0 BIBLIOGRAPHY

1. "Astromast for Space Applications", ARC-B-004, Astro Research Corportation, Carpinteria, California, August 1978.

2. Massoud, M., Bêliveau, J.-G., and Bourassa, P., "Méthode d'identification pour la détermination des caractéristiques structurelles d'une sous-structure d'un satellite", Contractor Report, DOC-CR-SP-82-019, Space Technology & Application Branch, Department of Communications, Ottawa, Canada, March 1982.

3. Massoud, M., Bêliveau, J.-G., Bourassa, P., Lauzier, C. and Doyon, P., "Méthode d'identification pour la détermination" des caractéristiques structurelles d'une sous-structure d'un satellite", Partie B: Etude paramétrique par estimation baysienne, Contractor Report, DOC-CR-SP-83-009, Space Technology & Application Branch, Department of Communications, Ottawa, Canada, March 1983.

4. "User Manual for MODAL-PLUS 7.0", General Electric CAE International Inc., Rockville, Maryland, 1982.

5. "User Manual for DATM 7.0", General Electric CAE International Inc., Rockville, Maryland, 1982.

6. "System Description and Operation - 2500 Series Systems", Gen Rad Inc., Santa Clara, California, 1981.

7. Vold, H., Kundrat, J., Rocklin, G.T. and Russel, R., "A Multi-Input Modal Estimation Algorithm for Mini-Computers", SAE Technical Paper Series (820194), 1982.

8. "Operating Manual - 5427A Digital Vibration Control System", Hewlett-Packard Co., Santa Clara, California, 1980.

9. Vigneron, F.R., "Comparison of Test Configurations for Modal Parameter Identification", Tech. Memo No. DSM-29, Communications Research Centre, Ottawa, May.

10. Richardson, M., "Modal Analysis Using Digital Test Systems", Reprinted from Seminar on Understanding Digital Control and Analysis in Vibration Test Systems, The Shock and Vibration Information Center, Naval Research Laboratory, Washington, D.C.

11. Hok, G., "Responses of Linear Resonant System to Excitation of a Frequency Varying Linearly with Time", Journal of Applied Physics, Vol. 19, August 1948, pp. 242-250.

12. Mutch, G., Vigneron, F.R. and Vold, H., "The Dynamic Analysis of a Space Lattice Structure Via the Use of Step Relaxation Testing", Proc. 2nd International Modal Analysis Conference, Orlando, Florida, February 6-9, 1984.

13. Lips, K.W., "Astromast Modal Characteristics Derived from a Continuum Model", Memo #CRC 5440-2, Internal Communication, Communications Research Centre, Ottawa, August 8, 1983.

SOUCY, YVAN.
--Modeling and identification of
the structural...

TK
5102.5
C673e
#1374

DATE DUE
DATE DE RETOUR

LOWE-MARTIN No. 1137

CRC LIBRARY/BIBLIOTHEQUE CRC
TK5102.5 C673e #1374 c. b
Soucy, Yvan.
and identification of the

INDUSTRY CANADA / INDUSTRIE CANADA
209011